Estimates of the local contribution to trace plutonium in soils from Blelham Tarn and Windermere

A thesis submitted following the requirements of Lancaster University for the degree of Doctor of Philosophy

by

Argaia Madina

February 2025

ACKNOWLEDGEMENTS

I would like to express my special thanks and gratitude to my supervisor, Prof. Malcolm Joyce, for their able guidance and advice throughout my PhD. I appreciated all the support that you gave to me. I am also very thankful to those who helped me and guided me to make such a project, including Dr Christopher Tighe and Richard Wilbraham. I also thank my reviewers Prof Sarah Green and Prof James Taylor, for giving their continuous feedback on the annual reports.

I would like to thank the Engineering research group at Lancaster University for the helpful discussions and support, as well as the National Trust and National Heritage.

I sincerely wish to thank Dr Chantal Nobs and Callum Grove at the Culham Centre for Fusion Energy, for their guidance and support with gamma spectrometry. I also want to thank Stephen Chappell and all the staff at the radiation laboratory at Liverpool University, for their help with spectral analysis.

I am greatly thankful for the cooperation and help from the Chemistry lab staff at Lancaster University, and Dr Jennifer Readman at the University of Central Lancashire, for their help with XRD analysis.

I want to say a massive thank you to Dr Marcus Christl of ETH Zürich and the staff there for carrying out AMS measurements. I would like to acknowledge the experimental officer in the Engineering department at Lancaster University Patrick Collins and Southampton University for their support in the refractory measurements; without them, I would not have been able to complete this research.

I want to give a large thank you to my husband, who has sacrificed a lot for me to do this PhD, especially since we have four children. He was the main supporter for me and my kids, whether inside or outside the house. I am very lucky and happy to spend the rest of my life with you.

Finally, words are not sufficient to express my gratitude to my family members for supporting me, as without their encouragement and support I would have not reached this stage.

ABSTRACT

The assessment of trace environmental actinide quantities in Blelham Tarn and Fell Foot samples is described. This research comprises the assessment of trace quantities of americium and plutonium in soil samples taken in the environments surrounding these two lakes in the English Lake District, using broad-energy, High-Resolution Gamma-ray Spectroscopy (HRGS) and compact Accelerator Mass Spectrometry (AMS). It targets the concentration of trace radioactivity, mass abundance and isotopic fraction in soils and aims to discern the global and local proportions that constitute this quantity.

The γ-ray spectrometry studies indicate that the ^{241}Am (and hence ^{241}Pu) content in Lake District samples studied in this research is consistent with the prior art [1]. The average ^{240}Pu/^{239}Pu ratio (0.181 ± 0.002) measured in this research is observed to be consistent with the global fallout average reported in several previous studies, such as the global fallout average [2], and with that, the sediments in Lake Ontario [3].

The average ^{244}Pu/^{239}Pu ratio for the Blelham Tarn and Fell Foot data, not measured previously for Lake District samples [4], has been compared with data from Erie Lake, Salzburg, the Enewetak and Bikar atolls samples to estimate the local contribution to trace plutonium deposited ($F_{L_{239}}$ / %), from the atmosphere at these sites [4] [5] [6] [7], respectively. Further Analysis of this local contribution, derived in terms of its ^{244}Pu/^{239}Pu and accounting for (18 ± 13) at % of the majority isotope ^{239}Pu for the combined data from both sites, indicates that it has a ^{240}Pu/^{239}Pu ratio of (0.21 ± 0.08) consistent with the prior measurement of samples from the Irish Sea [5]. In addition, this suggests that the local material deposition is more consistent with reprocessed Magnox materials rather than fallout from either the Windscale or Chernobyl accidents, notwithstanding significant

uncertainties and the potential for a shortfall in assessment due to the resistance of the refractory component in fallout residues.

The dependence with depth of trace environmental plutonium measured in this research is observed to be consistent with the trend that combines the phenomena of convection and dispersion, as per the Convection-Dispersion Equation (CDE). Using the CDE for a single deposition (the traditional application of the CDE) yields a deposition period consistent with the peak fallout from nuclear weapons tests in 1963. Using a modified version of the CDE comprising two deposition components, each with time spans distinct from one another, yields timescales for the local distribution of approximately (30± 12) years and for the global fallout component of approximately (57 ±10) years, consistent with the era of permitted discharges at Sellafield and peak global fallout, respectively.

Finally, a consideration of the potential for there to be a refractory-based reserve that is resilient to some preparatory processes has been explored and the implications for this work considered.

DECLARATION

Lancaster University

Faculty of Science and Technology

Engineering Department

I, Argaia Madina, declare that this thesis is my own work and has not been submitted in substantially the same form towards the award of a degree or other qualification. Acknowledgement is made in the text of assistance received and all major sources of information are properly referenced. I confirm that I have read and understood the publication Guidance on Writing Technical Reports published by the Department.

Signed ………………………………………………………….

Date ……………………………………………………………

LIST OF FIGURES

LIST OF TABLES

LIST OF CONTENTS

CHAPTER 1: INTRODUCTION

CHAPTER 2: BACKGROUND

CHAPTER 3: EXPERIMENTAL METHODS

CHAPTER 4: RESULTS

CHAPTER 5: DISCUSSION

CHAPTER 6: Optimising the extraction of the refractory component

CHAPTER 7: CONCLUSION AND FUTURE WORK

CHAPTER 1: INTRODUCTION

1.1 Introduction

Environmental radioactivity in the soils associated with marshland, like the catchment areas near large bodies of water such as the lakes that make up the English Lake District in Cumbria, UK, have been subject to scientific inquiry via either alpha- (α-particle) or high-resolution, gamma-ray (γ-ray) spectroscopy from time to time [1]. This thesis concerns trace actinide analysis of americium and plutonium of soil samples taken in the environments of two such lakes utilising broad-energy, high-resolution γ-ray spectroscopy (HRGS) and accelerator mass spectrometry (AMS). It targets the concentration of trace radioactivity in soils and aims to discern the local and global contributions to the anthropogenic proportion of these activities. These measurements identify the levels of trace plutonium in the natural environment at less than 500 fg/g, for comparison with the prior art whilst enabling a comparison of HRGS and AMS.

The English Lake District is in the county of Cumbria, a few hours north of London in the UK (see Figure. 1). It is recognised by UNESCO [8] as a world heritage site and comprises of many lakes and rivers, with a number that has been subject to prior analyses of trace actinides through high-resolution, γ-ray spectroscopy and α-particle evaluation [8]. Some areas of the English Lake District have been subject to widespread agricultural development but are otherwise undeveloped industrially. It thus offers a unique opportunity to examine trace radioactivity in an indigenous habitat that is somewhat undisturbed, with which to inform whether the greater part of the deposited radioactivity derives anthropogenically as a global contribution (predominantly from nuclear weapons tests) or locally from accidental and permitted discharges from the nearly industrial nuclear complexes such at Sellafield [9].

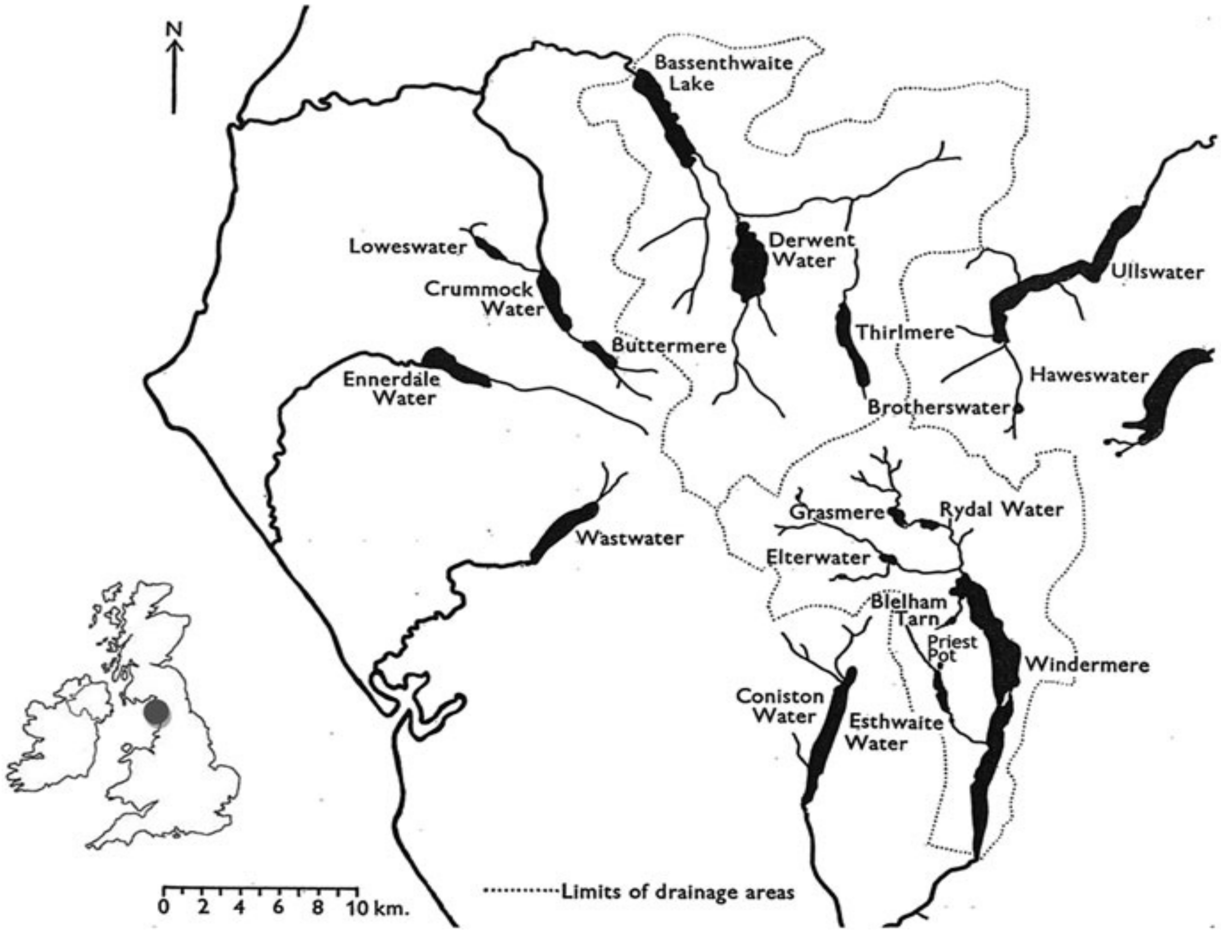

Figure 1: Lake District map in the UK [10]

Environmental radioactivity measurement can be necessary to determine the proportion of radioactivity emerging from natural sources that incorporates deposition of activity from natural sources from the air etc. and that from the Earth emerging from radionuclides resident in rocks, water, and silt. Besides natural sources, radioactivity in the environment includes anthropogenic components, for example, those that derive from industrial nuclear facilities and activities, for example, Sellafield [1].

The Lake District comprises of extensive uplands at critical elevations (the greatest 978 m in altitude), which are known to have also been subject to activity from, for example, the Chernobyl disaster in 1986 and atmospheric weapons tests, especially those near to the arctic circle peaking in 1963. Sellafield is geographically close (~15 km) and was the site of both authorised and accidental radioactive releases to the environment (air, earthbound and marine) in the past. It was also the site of the Windscale fire, in 1957, which resulted in radioactivity being dispersed to the environment, especially locally [1].

1.2 Research Objectives

The research described in this thesis evaluates and discusses trace environmental plutonium and americium arising in soil cores gathered from the Lake District, at Blelham Tarn and Lake Windermere (at Fell Foot). It addresses the goal to estimate deposited actinide concentrations associated with these elements via Broad-Energy Germanium detector (BEGe), for HRGS (at the University of Liverpool and the Culham Centre for Fusion Energy) and AMS (at ETH Zürich). This research follows a comprehensive analysis procedure to determine trace radioactivity in soil samples from these locations.

The specific activity for ^{241}Am has been derived with the BEGe detector systems at the Central Teaching Hub (CTL) at the University of Liverpool, UK, and those at the Culham Centre for Fusion Energy (ADRIANA) laboratory near Abingdon, UK. AMS has been used to quantify the femtogram-per-gram abundance and corresponding isotope ratios of Pu using the TANDY AMS system at ETH Zürich and Lancaster University [11].

The ^{241}Am data have been used to infer the ^{241}Pu activity based on several lifetime scenarios [6]. The portfolios of these two isotopes are compared with the prior data of Michel et al. published 20 years ago [1], albeit of the lakebed sediments. This thesis addresses the goals of this investigation once more, to determine the stability or otherwise of this inventory at Blelham, considering the effects of the cessation of atmospheric weapon testing, industrial nuclear accidents (particularly Windscale and Chernobyl), the variance between two nearby places in terms of distinctions in land type and the potential for there to be discernible, distinctly local, and global components such as the potential effects of climate change (i.e., environmental behaviour).

1.3 Summary of the Objectives

The objectives of the research described in this thesis were as follows:

- To measure ^{241}Am and ^{241}Pu activities (Bq/g) using HRGS for samples from Blelham Tarn and Lake Windermere (the latter at Fell Foot).
- To compare these measurements with the prior art concerning plutonium and americium records for sediment cores in Blelham Tarn (Michel et al., 2002 [1]), and to determine if what is known about Blelham Tarn is the same for other lakes, such as Windermere, in this case.
- To use and present a novel signal-to-noise ratio method in the lower-energy scatter region to determine the optimum proportion to subtract to achieve the best signal-to-noise ratio (S/N).
- To determine whether the local contribution to environmental plutonium can be estimated using ^{244}Pu/^{239}Pu, and hence to consider the ^{240}Pu/^{239}Pu signature for this local contribution.
- To explore and understand the depth dependence of trace environmental plutonium in English Lake District soils.

1.4 Thesis Outline

This thesis describes the research undertaken to achieve the objectives described above. The content of the chapters in this thesis is summarised below:

Chapter 2: This chapter describes the background concerning radioactivity in the environment, along with a comparison of the HRGS and AMS techniques used in this research.

Chapter 3: This chapter outlines the experimental techniques that have been used including the signal-to-noise ratio method, weighted Chi-squared optimisation, and calculations of ^{241}Am and ^{241}Pu activities for the Blelham Tarn and Windermere samples, as well as measuring the plutonium isotopes using HRGS and AMS for both sites.

Chapter 4: presents the results collected to address the above-mentioned objectives.

Chapter 5: This chapter provides a discussion of the results obtained in this thesis, along with comments on possible future measurements.

Chapter 6: Presents the results of a revised method based on HF dissolution to optimise the extraction of the refractory component

Chapter 7: Concludes the work and summarises recommendations for further work.

CHAPTER 2: BACKGROUND

2.1 Environmental Radioactivity

Anthropogenic radioactivity has been emitted into the atmosphere from a wide range of sources such as material evolved by nuclear weapon tests, discharges from the nuclear fuel cycle, and that dispersed because of the use of depleted uranium munitions. Global fallout, particularly that of weapons tests conducted in the late 1950s and early 1960s, has been a global source of radioactivity in the atmosphere deposited in both terrestrial and marine environments [12]. The nuclear reprocessing facilities at the Sellafield nuclear site has been associated with radionuclides such as ^{137}Cs and ^{241}Am arising within the coastal region of North-West England in the UK [12]. Since 1952, when discharge activities peaked, this reprocessing facility discharged liquid effluents and low-level radioactive waste into the Irish Sea with more stringent constraints enacted in the 1990s [5]. The radionuclides released were diluted and dispersed via natural processes such as tidal movement. Several studies assessing the level of radionuclide activity in Cumbria, in the NW of England, have been published in the past, particularly that of Michel et al. [1], but corroboration of these measurements by AMS and extension of this work to nearby environments, such as Lake Windermere, does not appear to have been addressed until this work.

This section discusses the distinction between local and global anthropogenic radioactive material. The global fallout is defined by the corresponding global average, whether for ^{240}Pu or ^{244}Pu. The local contribution is defined as the admixture present in the area where the samples were taken for the measurements and not present elsewhere. The decision about what is global and local depends upon the interpretation of the place in which the measurements are being made. Summarises the results of previous studies of radionuclide detection procedures, including industrial sources such as Sellafield, and investigative techniques in use for such environmental assessment requirements; a summary of the history of radioactivity and radioactive elements, the atmospheric fallout from nuclear weapons tests, accidents (particularly Windscale and Chernobyl) and localised effluents are also provided in this section.

2.2 The discovery of radioactivity and radioactive materials

Radioactivity arising in the environment might be classified as naturogenic, such as uranium and thorium, or anthropogenic, such as plutonium, americium, and neptunium (trace quantities of a few of the isotopes of plutonium do occur in nature too). Uranium was discovered by Klaproth in 1789, although at that time, since radioactivity was not known, it was not understood that uranium was, itself, radioactive. Marie Curie discovered the two radioactive elements, radium, and polonium in 1898 [13], and she shared the Nobel Prize for Physics with Becquerel in 1903 for the discovery of radioactivity and latterly awarded a second Nobel Prize (for Chemistry) in 1911 for the discovery of radium and polonium.

Neptunium was discovered in 1940 by McMillan and Abelson when ^{239}Np (half-life =2.36 d) was created by the neutron capture on uranium (Equation. 1.1) in the nuclear reaction [14]. In 1942, Seaborg et al. synthesized plutonium (Pu) by bombarding uranium with deuterons to yield ^{238}Np and following beta-decay to ^{238}Pu (Equation. 1.2). With the identification of Np and Pu, as well as the comprehension of the physical processes among different nuclear elements, it became clear to the scientists of the time that several further transuranic elements were still to be identified. The fourth transuranic element after uranium, neptunium and plutonium, americium was the first produced and discovered during wartime by Seaborg (generated by intense neutron bombardment of Pu) [15].

$$^{238}\mathrm{U}\ (n,\gamma) \rightarrow {}^{239}\mathrm{U}\ (\beta^-) \rightarrow {}^{239}\mathrm{Np}\ (\beta^-) \rightarrow {}^{239}\mathrm{Pu} \qquad (1.1)$$

$$^{237}\mathrm{U}\ (\beta^-) \rightarrow {}^{237}\mathrm{Np}\ (n,\gamma) \rightarrow {}^{238}\mathrm{Np}\ (\beta^-) \rightarrow {}^{238}\mathrm{Pu} \qquad (1.2)$$

$$^{239}\mathrm{Pu}\ (n,\gamma) \rightarrow {}^{240}\mathrm{Pu}\ (n,\gamma) \rightarrow {}^{241}\mathrm{Pu}\ (\beta^-) \rightarrow {}^{241}\mathrm{Am} \qquad (1.3)$$

2.3: The abundance of U and Pu and their isotope ratios from different sources

Uranium: According to the report entitled "Geological Controls on Radon Potential in England", various areas host to greater-than-average abundances of radioactivity material, for example, with higher topsoil uranium concentrations of about 4.2 mg kg^{-1} in England, as shown in Figure 2 [16].

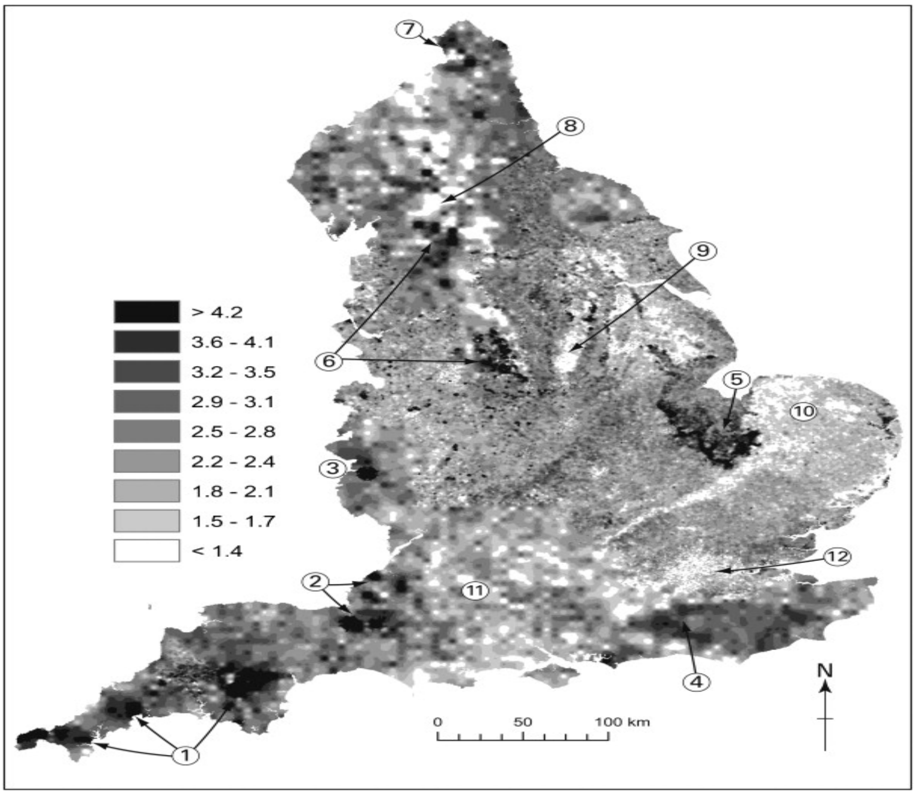

,

Figure 2: Uranium concentrations for England indicate that high typically relate ten associated with areas of significant granite abundance (mg kg^{-1}) [16].

Geological conditions can influence the inventory of these naturally radioactive regions. They typically relate to U including a variety of isotopes with about 99% of ^{238}U and below 1% of ^{235}U. The remaining uranium isotopes make up less than 0.5% of the total abundance (such as ^{234}U at approximately 0.0055 %) [16].

It is difficult to identify anthropogenic uranium contamination using concentration data alonge because of the the natural varitation of U concentrations. Determining the ^{238}U/^{235}U ratio is a more accurate mothod, which is constant in nature = 137.88 ± 0.001 as reported in [17].

Plutonium: Because of neutron capture, trace quantities of plutonium can occur in uranium ores, via the formation of ^{239}U, leading to two beta decays to become ^{239}Pu (see: Figure 3). Primarily because of nuclear weapons tests in the atmosphere, plutonium can be found in soils at temperate latitudes in the period 1950-1963 [18]. Presuming that Pu is predominantly in the surface layer to a depth of around 5 cm and an average soil density of 1000 kg/m^3 (average estimates for samples obtained at Aldermaston), the specific activity of Pu in the soil is 1.6 Bq/kg (0.5 pg g^{-1}), presuming that ^{240}Pu/^{239}Pu = 0.18, Pu isotopic ratios are shown in Table.2, for different sources and different reactors [19].

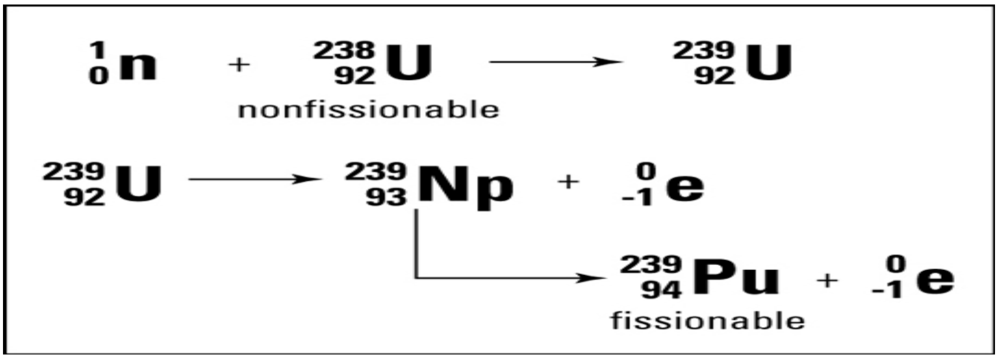

Figure 3: An illustration of the ^{238}U decay process [3].

The isotopic yield in an atmospheric nuclear weapon test can vary depending on the nature of the test [21] [22]. Due to the short half-life of ^{243}Pu (4.956 h), the yield of ^{244}Pu in nuclear fission reactors is insignificant [23], whereas an excess of ^{244}Pu can arise in the environment from weapon test fallout relative to reactor material as a result of the high neutron flux environment in a test, and this can serve as an indication of weapons test fallout, (see Table 1 for more details about half-life and decay mode of Pu) [24].

While the ^{244}Pu/^{239}Pu ratio for some individual tests, such as Ivy Mike [24], has been measured, there are few AMS-based measurements of this ratio in the terrestrial environment based on a sufficient number of counts. Amongst these, measurements pertinent to this work were reported on deep-sea sediments [22]. The average measurement of ^{244}Pu/^{239}Pu = $(14.4 \pm 1.5) \times 10^{-5}$, based on the average peak of weapons test years of 1963/64 from Lake Erie samples [22], where the uncertainty expressed is the standard deviation in the mean of the measurements corresponding to those years.

Isotope	Half Life/ years	Decay Mode
^{238}Pu	88	α
^{239}Pu	24,100	α
^{240}Pu	6537	α
^{241}Pu	14.3	α and β
^{242}Pu	375,000	α
^{244}Pu	81,000,000	α

Table 1: Plutonium half-lives and decay modes.

	$^{240}Pu/^{239}Pu$	$^{241}Pu/^{239}Pu$	$^{242}Pu/^{239}Pu$
Weapon Pre-Source, 1960 (LANL)	0.01		
Weapon Modern source,1960 (LANL)	0.055-0.065		
Chernobyl Source	0.43	0.11	0.03
Magnox Reactor	0.23	0.045	0.006
Boiling water reactor	0.40	0.177	0.055
Pressurised water reactor	0.43	0.228	0.096

Table 2: Plutonium ratios for different sources and reactors, LANL refer to Los Alamos National Laboratory [22][23][24].

2.4 Nuclear Weapons Tests as a Source of Fallout in the Environment

Fallout results from nuclear weapons tests performed by the United States, Britain, France, and the former USSR, were carried out between 1945 and 1996. The locations of the tests are shown in Figure 4 [23].

As a result of these tests, about 12,500 TBq of Pu was dispersed globally via the stratosphere [24]. Lower-mass radioactive elements in nuclear testing are generated by neutron-induced fission of ^{235}U, ^{238}U, and ^{239}Pu, as per fission yield curves comprising two peaks, one at mass 100 and another at mass 140. The type of nuclear device does not have much effect on the composition of these isotopes. The nuclei produced are radioactive and pass through a variety of different decay mechanisms after production [24].

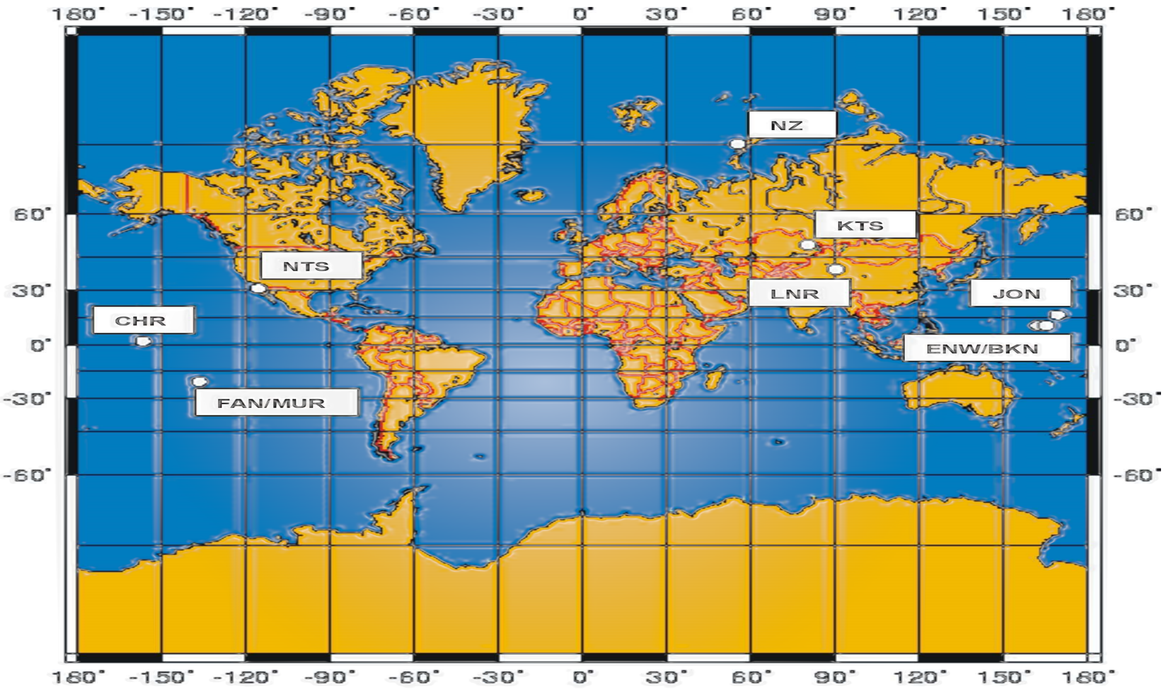

Figure 4: Atmospheric nuclear test locations, where NZ refers to Novaya Zemlya in the Union of Soviet Socialist Republics, KTS refers to the Semipalatinsk test site in Kazakhstan, and LNR refers to Lop Nor in China, and JON refers to Johnston Island in the US, ENW refers to Enwetak in US, BKN refers to Bikini in US, NTS refers to Nevada Test Site in US, CHR refers to Christmas Island in the UK, FAN and MUR refers to Muruora and Fangataufa in France [19].

Stratospheric fallout contains Pu metal oxide compounds attached to aerosols [24]. Tropospheric fallout involves elements resulting from partially vaporised ground material. There are observed variances in the chemical behaviour of Pu compounds in deposits collected from the North Atlantic Ocean [25], the Gulf of Mexico [26] and the North Pacific

[27]. All investigations indicate that the water column is rapidly cleaned of tropospheric fallout, whereas plutonium from the stratosphere stays in solution for longer than 10 to 100 years. The Nevada Test Site is the main source of the tropospheric fallout in the North Atlantic Ocean and the Gulf of Mexico, and the Pacific Proving Grounds in the North Pacific [28].

2.5 Environmental Effects from the Sellafield and Chernobyl Accident 1986

The estimation of the local proportion of trace environmental plutonium in soil samples from the Lake District in the UK, based on the ^{240}Pu/^{239}Pu ratio measured with accelerator mass spectrometry (AMS) was achieved by comparing the average ^{240}Pu/^{239}Pu ratio in soil samples from the site (which was low relative to the global average) with an estimate of the ratio for material developed in fast reactors, with the latter corresponding to the main form of production of local material in this case.

However, a more widespread requirement is to discern trace plutonium produced in thermal spectrum reactors, especially those involved in accidents or where atmospheric discharges from reprocessing facilities nearby are known to have occurred. Production in uranium-based fuels in thermal spectrum reactors is perhaps the most widespread source of local contributions to trace environmental plutonium, where accidents have occurred, but this material is unlikely to have a ^{240}Pu/^{239}Pu ratio that is sufficiently distinct from that dispersed globally as fallout from nuclear weapons tests. Conversely, although the Windscale reactors were designed to produce plutonium for weapons programmes and hence material from these might be relatively low in the higher-mass isotopes (particularly ^{240}Pu), the focus of the Sellafield site transitioned gradually to power production beyond processing of the Windscale material and the associated accident with reprocessing; firstly, of Magnox, and subsequently of Advanced Gas-cooled Reactor (AGR) spent fuel, in addition to a variety of other fuel forms. Consequently, ^{240}Pu abundance from this site may span a significant range and is unlikely to afford a reliable basis on which to discern material from this site nor other possibilities, principally Chernobyl. This complicates the ease with which the local contribution might be isolated and quantified because ^{240}Pu does not offer the same opportunity by which to discern the local proportion of ^{239}Pu as for fast breeder material. However, the range in ^{240}Pu/^{239}Pu of specific local contributions can vary considerably and potentially enable forensic identification, if the local proportion can be discerned independently of ^{240}Pu. Consider for example ^{240}Pu/^{239}Pu in global fallout [2]: 0.182 ± 0.005; Bikar Atoll [7] (Castle Bravo): 0.26 ± 0.01 and 0.30-0.34; Sellafield [5]: 0.226 ± 0.001; Magnox reactor [5]: 0.23; Ivy Mike [24]: 0.363 ± 0.004; Chernobyl [45]: 0.37 – 0.51 (± 0.01).

An established distinction [5] between local and global sources of anthropogenic plutonium is the proportion of ^{244}Pu relative to that of ^{239}Pu. The ^{244}Pu isotope is only formed in significant quantities only via high neutron flux mechanisms, i.e., nuclear weapon detonations, supernovae, and high-flux reactors, due to the relatively short half-life of the intermediary isotope, ^{243}Pu. The absence of ^{244}Pu as a by-product in almost all nuclear activities, aside from nuclear weapon detonations, suggests that its abundance relative to ^{239}Pu might enable local and global contributions to elemental plutonium in the environment to be separated from one another, if sufficient counts of this rare isotope can be achieved on practical timescales. Ketterer *et al.* highlighted this possibility with reference to their data for Loch Ness [45] on the hypothetical basis of the ^{241}Pu/^{239}Pu ratio as they were unable to measure this with sector ICPMS in the small amounts of sample that were available in that study; it has potential advantages where local-global separation based on the ^{240}Pu/^{239}Pu ratio is not possible, due to the relative scarcity of ^{244}Pu in reactor-derived material.

For the comparison described above, an estimate of $^{244}Pu/^{239}Pu$ for the global fallout contribution is necessary. Estimates from deep sea deposits ($^{244}Pu/^{239}Pu \sim 10^{-4}$) and ferro-manganese modules ($^{244}Pu/^{239}Pu \sim 10^{-3}$) from the equatorial Pacific [4], albeit with very few counts, can be too close to the Pacific Proving Grounds to be representative of the global average, as they may contain tropospheric material in greater abundance than the stratospheric material indicative of global fallout. Therefore, in this research, prior data from sediments from Lake Erie in Canada have been used for the global average [23]. These data were taken from the deepest part of the lake and yield an isotopic pattern for plutonium that resembles stratospheric fallout closely, with the peak of the distribution being that corresponding to 1963/64 analysed further [4] to yield an estimate of the global average of $^{244}Pu/^{239}Pu$.

2.5.1 Nuclear Activities and Facilities in Britain

The United Kingdom carried out a wide variety of activities in support of its nuclear programme [29]. Figure 5 shows the location of the nuclear sites in the UK.

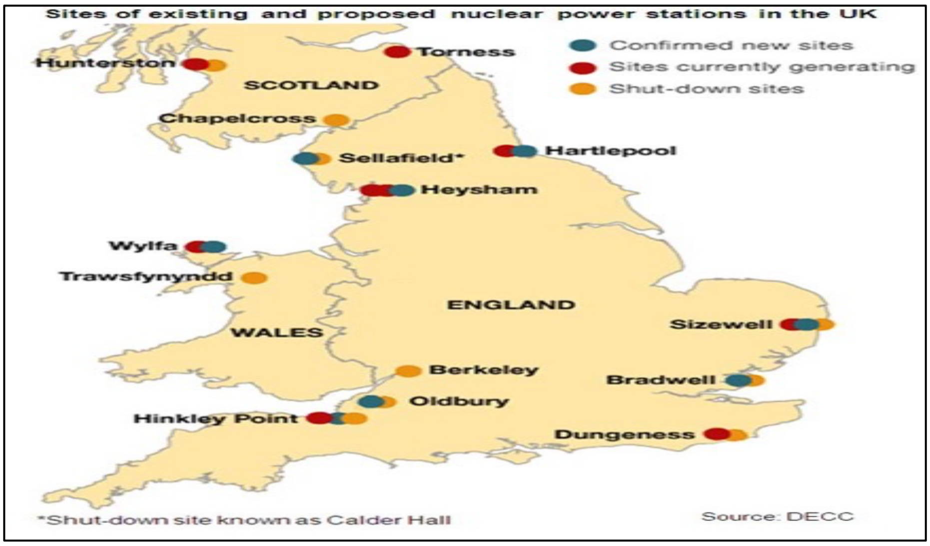

Figure 5: For nuclear facilities in the UK, the green circle indicates confirmed new sites, the red circle indicates sites currently generating and the orange circle shows the shut-down sites [30].

2.5.2 Sellafield Site, UK

The Sellafield site in west Cumbria is close to the sample sites for this thesis, and it was originally a conventional weapons factory serving the needs of World War II. The construction of two reactors at Windscale started in 1946 to produce plutonium for the United Kingdom's nuclear weapons programme. In October 1950, Pile No. 1 went into operation, and Pile No. 2 began 8 months after that. In 1952, a spent fuel recycling facility began operations. After a fire in October 1957 in Pile No. 1, the Windscale Piles were shut down and not restarted. Between October 1956 and May 1959, four Magnox reactors at Calder Hall went into service besides Windscale. These reactors, which are identical to those at Chapelcross, produced electricity as well as plutonium and closed finally in 2003 [31].

Sellafield is one of the main sources of plutonium that is released to the environment, and concentrations of sediments near the plant contain up to 15,800 Bq/kg $^{239+240}$Pu [31]. In the Esk estuary sediment, the ranges of ^{240}Pu/^{239}Pu were found from 0.16-0.26 [29]. Soil samples taken between 1976 and 1986 within 10 km of the plant have ^{240}Pu/^{239}Pu ratios that vary depending on the location of sampling. The range of this ratio in the soil samples is from 0.057 to 0.126 [32]. Activity concentrations in $^{239+240}$Pu range from 0.64 to 30 Bq/kg [32]. The relatively low ^{240}Pu/^{239}Pu suggests this plutonium is due mostly to aerial releases in the initial years of operation [33].

2.5.3 The Chernobyl accident 1986

The Chernobyl RBMK reactor accident, on April 26, 1986, is another source of environmental radioactive contamination, some of which reached the UK including a variety of actinides and fission products [34]. The movement of the radioactive plume over Europe and the European region of the Soviet Union was tracked as shown in Figure 6. Initially, the wind was responsible primarily for the deposit that occurred in Scandinavia, the Netherlands, Belgium, and the UK, blowing the radioactivity in a north-westerly direction. Residues from the plume have been observed in the Northern Hemisphere from places as far away as the United States and Japan [34], whereas the Southern Hemisphere did not show any signs of deposition. Since actinide residues were present mostly in larger, heavier particles, they were deposited nearer to the site of the incident. The most significant quantities of radioactive isotopes identified outside of the Soviet Union were associated with ^{131}I, ^{132}Te and ^{137}Cs.

Although the actinides had relatively little radioactive effect outside of the former Soviet Union, a $^{238}Pu/^{239+240}Pu$ ratio of 0.46 was observed in Berlin (Germany), which was around 10 times greater than the average value of this ratio in 1985 [35]. In Austria, aerosol samples from different locations indicate the activity as being between 0.33-0.76 of $^{238}Pu/^{239+240}Pu$ and the ratio of $^{241}Pu/^{239,240}Pu$ ratio in the range of 5.7-74.6. These results were recorded shortly after the disaster [36]. In areas with high rainfall (waterlogged areas), the deposition density of ^{137}Cs reaches values of 2,300 Bq/m^2, and in predominantly dry areas the densities are between 4 Bq/m^2 and 25 Bq/m^2 [37].

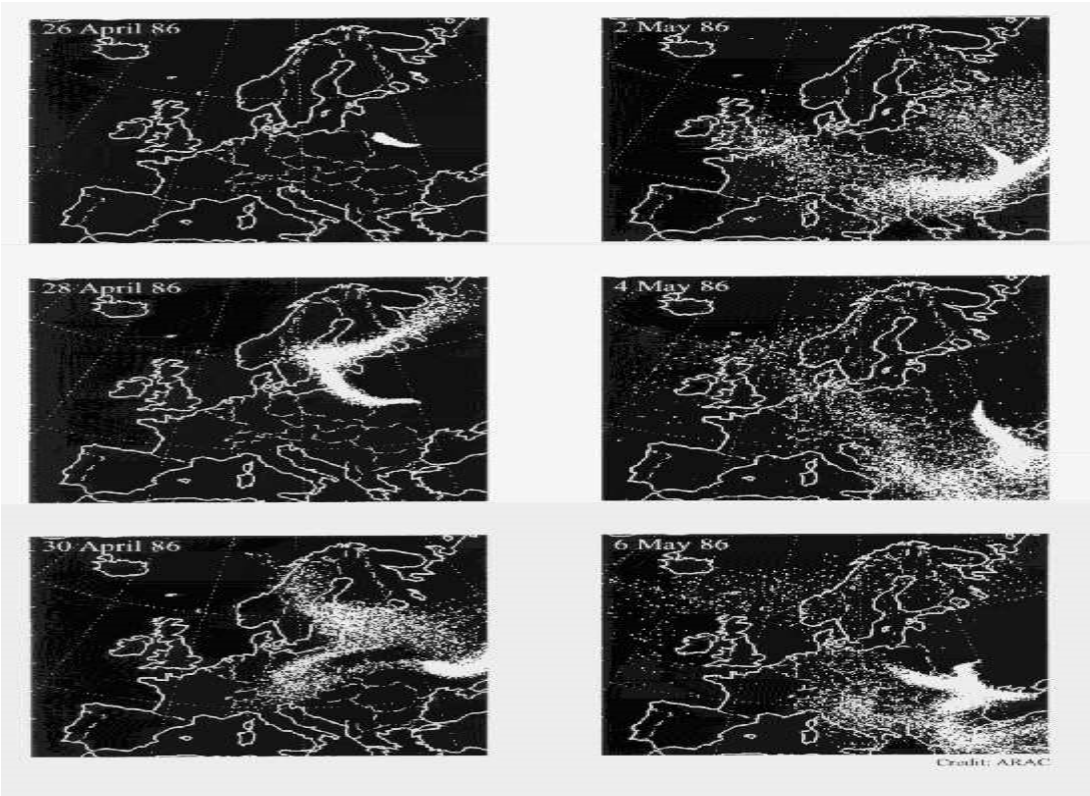

Figure 6: The movement of the radioactive cloud from the Chernobyl Nuclear Reactor Accident [38].

2.6 Lake District History

The Lake District is in the North-West of England. Sediment radioactivity is contributed to by both the direct atmospheric influence and the indirect atmospheric influence through the catchment. The catchment activity is carried to the sediment by the rivers and the direct streaming. The objective of this section is to describe the main characteristics of both sites that are referred to in this project (Blelham Tarn and Windermere) and give more details of soil composition. These two sites were chosen because Blelham Tarn and Windermere locations in the Lake District are relatively undisturbed, non-industrial sites in a UNESCO World Heritage site, and hence serve as relevant comparisons for land remediation assessments further west, nearer to Sellafield. Plus, Blelham had been considered before, Fell foot or the first time, and both are relevant to the Windermere catchment and relatively near to Sellafield.

2.6.1 Blelham Tarn

Blelham Tarn is located off the North-western shore of Windermere in Lake District (see Figure. 7). The tarn is moderately fertilised, obtaining contributions from a few of the naturally richer soils in the area on the western coast of Windermere. The mean depth, maximum size, and volume of the tarn are 6.8 m, 15 m and 0.69×10^6 m^3, respectively [1]. In 2010, it also had the greatest mean annual alkalinity, and concentration of potassium, magnesium, and calcium with a pH of about 7.1 [39]. In addition, Scanning Electron Microscopy with dispersed X-ray evaluation of energy (SEM-EDX) has been used to discover the single phases in the sample and consider the full sample composition in a unique manner. Since the 1930s, scientists have been interested in Blelham Tarn and have conducted numerous investigations there [40].

(A) (B)

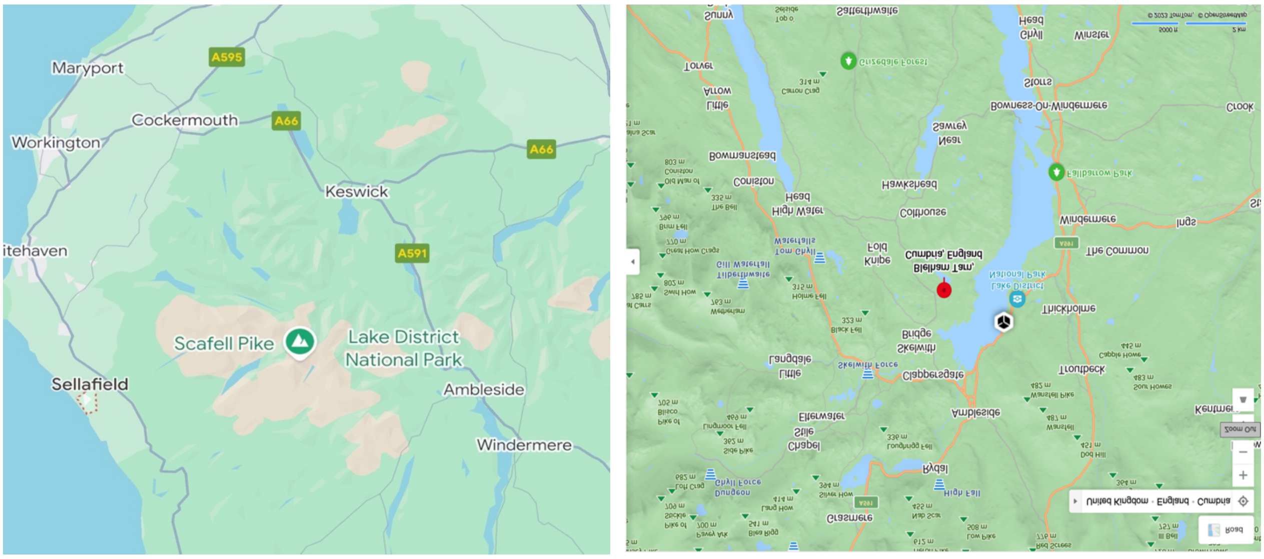

Figure 7: (A) Sellafield side, (B) Blelham Tarn location in the Lake District of England created by Digi map.

2.6.2 Windermere (Fell Foot)

Windermere is the largest natural lake in the Lake District (see Figure 8), with a length exceeding 18 km. The south basin of Windermere has around 80% of the area and half the volume of the north basin [41]. Additionally, water is received from the northern side of the lake; through Cunsey Beck, Esthwaite's water goes to the South Lake. The South Basin have a significant level of nutrient concentrations such as phosphorus, and is rich in metalloids, including aluminium and silicon. In addition, the alkalinity has increased dramatically and the pH of 7.4 [42].

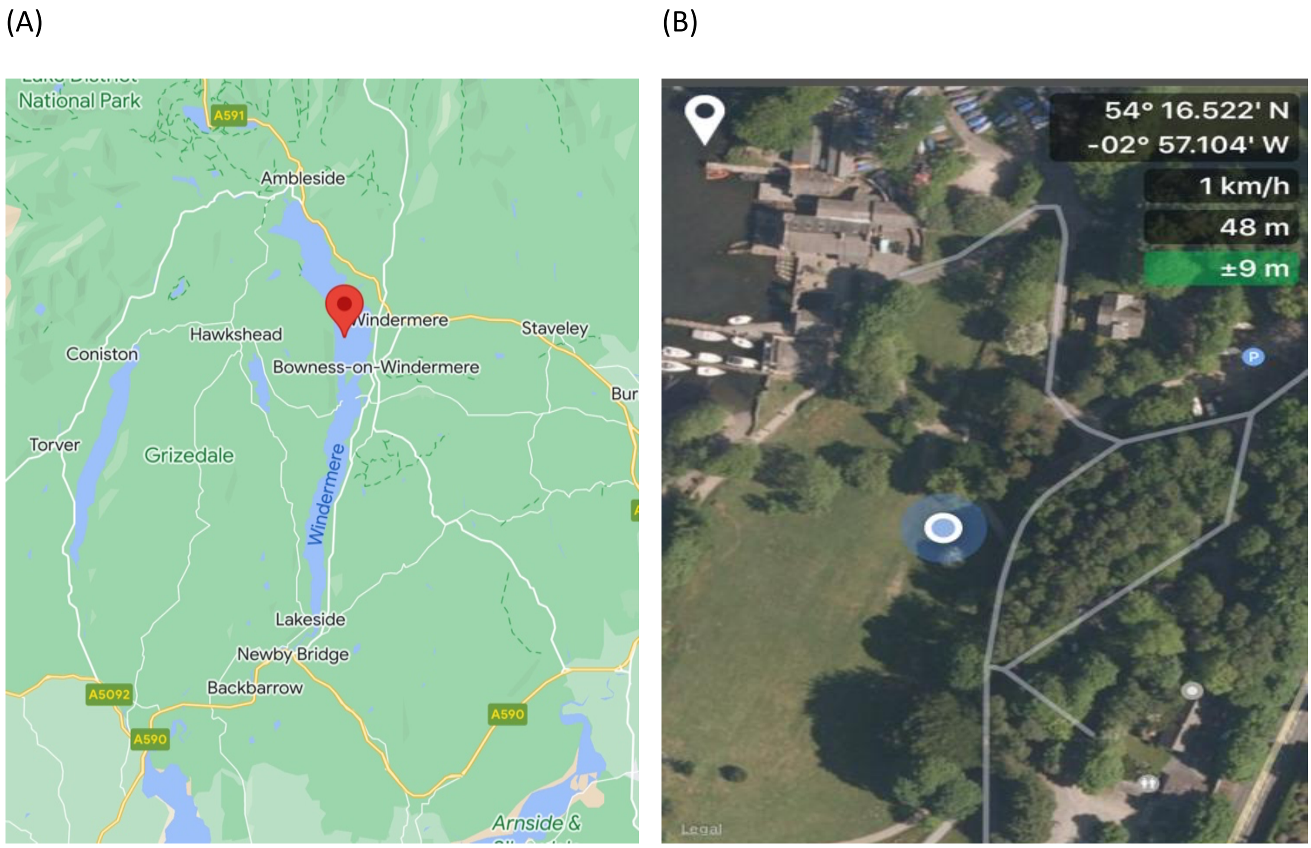

Figure 8: (A) Windermere location in the Lake District, (B) Fell Foot Park is the site from which the collection of samples takes place, (Cumbria UK).

2.7 High-Resolution, γ-Ray Spectroscopy (HRGS)

HRGS is a technique for measuring the concentration of radioactivity in soil samples. Gamma-ray spectra are analysed to identify an abundant gamma emitter in soil samples. In soils, these spectra are predicted to include a significant amount of uranium decay series daughters as well as peaks from several common radionuclides such as ^{40}K and ^{137}Cs. Additionally, from these spectra, it is possible to identify the ^{241}Am peaks (59.5 keV), which could provide, for example, an estimation of ^{241}Pu for project samples.

This section aims to present the findings of a study of ^{241}Am, ^{241}Pu and ^{241}Am/$^{239+240}$Pu inventory levels in Blelham Tarn and Fell Foot in Cumbria (UK). Additionally, some of these radionuclides may have been deposited in 1986 due to fallout from the Chernobyl reactor disaster, along with other radioactive material from nuclear weapons tests. Further, the fallout inventory was produced by assessing soil cores (depth 8-25 cm depth), and the results are compared with the prior data [1], published 20 years ago.

2.8 Accelerator Mass Spectrometry (AMS)

AMS can be used to find long-lived radionuclides, which are often present in the environment but in such dilute form that radioactivity measurements are not sufficiently sensitive to measure their concentration directly. Actinides in sediments have been detected successfully by AMS at ETH Zürich [43].

AMS was used to measure the levels of actinide in the soil samples. AMS is known for its high sensitivity, which means it can detect the abundance of different types of isotopic in a small mass of sample around 5 g. This research uses AMS to identify ^{239}Pu, ^{240}Pu, ^{242}Pu and ^{244}Pu atom concentrations at femtogram levels in soil samples and the ^{240}Pu/^{239}Pu, ^{244}Pu/^{239}Pu and ^{244}Pu/^{242}Pu (at/at) isotopic ratios. These measurements highlight potential advantages for the evaluation of Pu, particularly in comparisons that may be made with HRGS.

The measurements of the prior studies, such as those reported by Harley (1980) gave the average of ^{239}Pu abundance inside the range of global fallout of (7 – 1600) fg g^{-1}, [44].

The average of ^{240}Pu/^{239}Pu reported by Steier et al. on the soil samples from Sellafield (UK): is 0.226 ± 0.001 [5]. The global distribution of ^{240}Pu/ ^{239}Pu of the samples collected from Wick (Scotland) of 0.182 ± 0.005 [2], which is consistent with Ketterer et al. [45]

Furthermore, the literature reporting mass spectrometry-determined ^{244}Pu/^{239}Pu ratio for the soil samples taken from the Sellafield, at 11 cm depth is <3.5 x10^{-6} [5]. Additionally, the average of ^{244}Pu/^{239}Pu results from Lake Erie, corresponding to 1963/64 years, has been reported as (14.4 ± 1.5)×10^{-5} [22]. The Abundance of prior art and the ratio data are shown in Table 3 (A, B).

A)

^{241}Am (fg/g)	1.98 ± 0.23 Blelham Tarn Michel et al. [2002] [1]	3.24 ± 0.23 (T8: 7.3-8.2 cm) Srncik et al. [2008] [46]	182-15819 Belarus Boulyga et al. [2003][47]	20– 18941 Irish Sea Zhang et al. [2022][48]
^{241}Pu (fg/g)	2.33 ± 1.23 Blelham Tarn Michel et al. [2000][1]	2.1 ± 1 (0-4 cm) Switzerland Corcho et al. [2011][49]	183.6 Sellafield D. Ray et al. [2020][50]	20191 Irish Sea Zhang et al. [2022][51]
^{239}Pu (fg/g)	1290 Wick regain Kelley et al. [2]	6700 Semipalatinsk Nuclear Yamamoto et al. [52]	7-1600 Global fallout Harley [44]	2-6200 Cigar Lake Curtis et al [99]
^{240}Pu (fg/g)	61 On the Dounreay site Tighe et al [83]	(0.246 -6.74) Semipalatinsk Nuclear Test Yamamoto et al. [1996] [52]	10-100 In Ontario Lake By Green et al [3]	
^{244}Pu (fg/g)	(3.9) × 10^{-3} On the Dounreay site Tighe et al [83]	(0.31 - 44) In Savannah River C.R.Armstong [105]		

B)

^{240}Pu/^{239}Pu	0.182 ± 0.005 Global fallout Kelley et al. [1999] [2]	0.367 Semipalatinsk Nuclear Test Yamamoto et al. [1996] [52]	0.32 ± 0.01 Bikini Atoll Lachner et al. [2010] [53]	0.20 ± 0.08 Irish sea Steier et al. [2013] [5]
^{241}Pu/^{239}Pu	$(1.14 \pm 0.85) \times 10^{-3}$ Global fallout Kelley et al. [1999] [2]	$(2.27 \pm 0.029) \times 10^{-3}$ Semipalatinsk Nuclear Test Yamamoto et al. [1996] [52]	$(0.7 - 5.5) \times 10^{-3}$ Bikini Atoll Lachner et al. [2010] [53]	$(6.18 \pm 0.09) \times 10^{-3}$ Irish See Steier et al. [2013] [5]
^{242}Pu/^{239}Pu	$(3.71 \pm 0.3) \times 10^{-3}$ Global fallout Kelley et al. [1999] [2]	0.019 ± 0.003 Semipalatinsk Nuclear Test Yamamoto et al. [1996] [52]	$(2.5 - 5.7) \times 10^{-4}$ Bikini Atoll Lachner et al. [2010] [53]	$(6.85 \pm 0.11) \times 10^{-3}$ Irish Sea Steier et al. [2013] [5]
^{244}Pu/^{239}Pu	$(14.4 \pm 1.50) \times 10^{-5}$ Global fallout (Lake Erie) Winkler [2007] [20]	$(11.8 \pm 0.7) \times 10^{-5}$ Semipalatinsk Nuclear Test Yamamoto et al. [1996] [56]	$(41.8 \pm 12) \times 10^{-5}$ Bikini Atoll Lachner et al. [2010] [53]	$<3.5 \times 10^{-6}$ Irish Sea Steier et al. [2013] 5]

Table 3: Abundance prior art and the ratio data in a summary, with all the corresponding references.

CHAPTER 3: EXPERIMENTAL METHODS

Introduction

The objective of this chapter is to describe the experimental methods that have been used in this research. This is essential to assess the concentrations of radioactivity in a total of nine soil samples that have been collected from Blelham Tarn and approximately fifteen of the soil samples from Fell Foot Park in the Lake District area. This was made by using HRGS and AMS techniques. In addition, it incorporates a description of the statistical methods used in the analysis of the data such as signal-to-noise minimisation and describes soil sample preparation, the HRGS system, the AMS method, and the chi-square distribution technique.

3.1 Sampling and preparation of soil cores

Soil sample and preparation have comprised two stages as described in this section and Section 3.2:

Soil samples were gathered from the environments described in Chapter 2: for Blelham Tarn (54.3966° N, 2.9766° S), which has been studied previously (a site of special scientific interest (SSSI)) [54], nine soil samples were sourced from the northern shore (see: Figure 11) in 2019, from places chosen to correlate with the prior art [1]. Four samples from this location were characterized as wet (waterlogged) and another as having moisture (i.e., slightly damp).

Fifteen samples were collected from Fell Foot (54.2130° N, 25610° S) in 2020 (see: Figure 12), for which there are no known past studies related to the measurement of radioactivity and radionuclide ratios in soils at this time. All the cores from this location were wet (slightly wet). Several samples were collected from distinct sample points with a measured depth of approximately 15 cm, having a 51 mm diameter cylindrical aluminum corer (see: Figures 9 and 10). The sampled locations, which were recorded with GPS, are provided in the appendix A. After collection, these samples were transferred to Lancaster University.

Figure 9: Picture showing the collection and preservation of samples from Blelham Tarn for processing at Lancaster University.

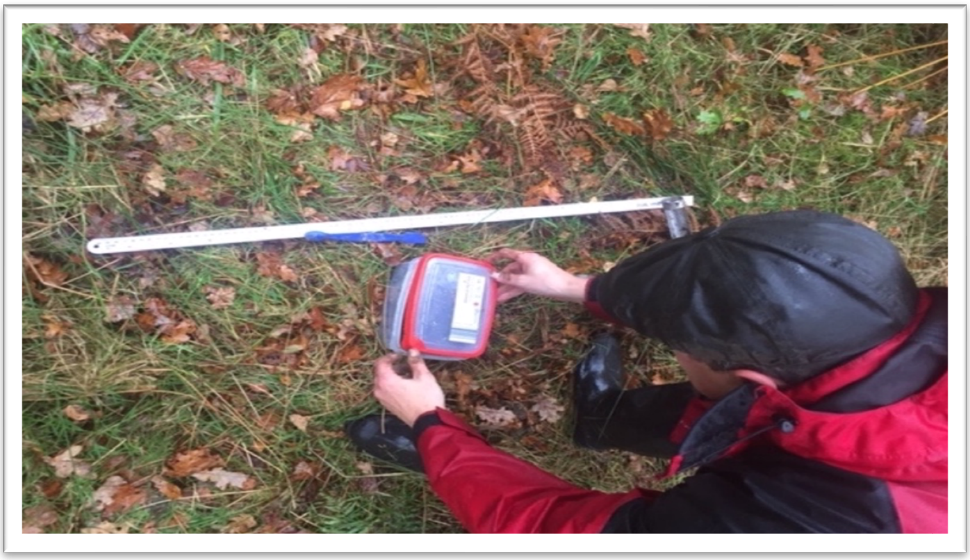

Figure 10: Picture showing the collection and preservation of samples from Fell Foot for processing at Lancaster University.

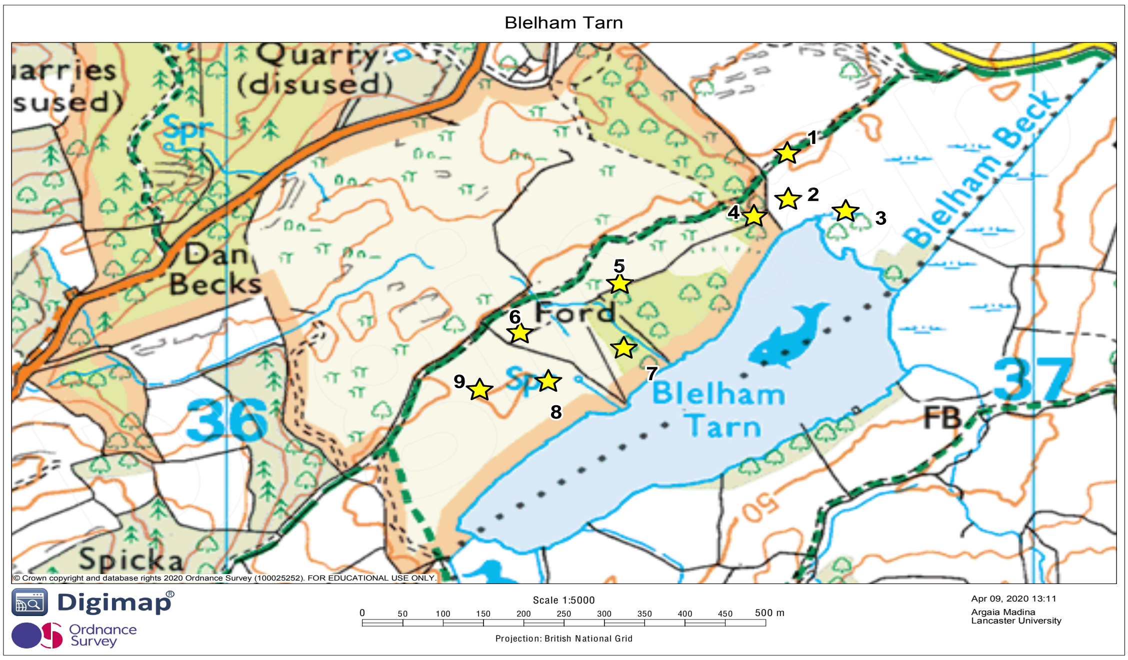

Figure 11: A map indicating the location (stars and numbers) of soil cores from the Blelham Tarn. Lake District (Cumbria, UK) collected in September 2019.

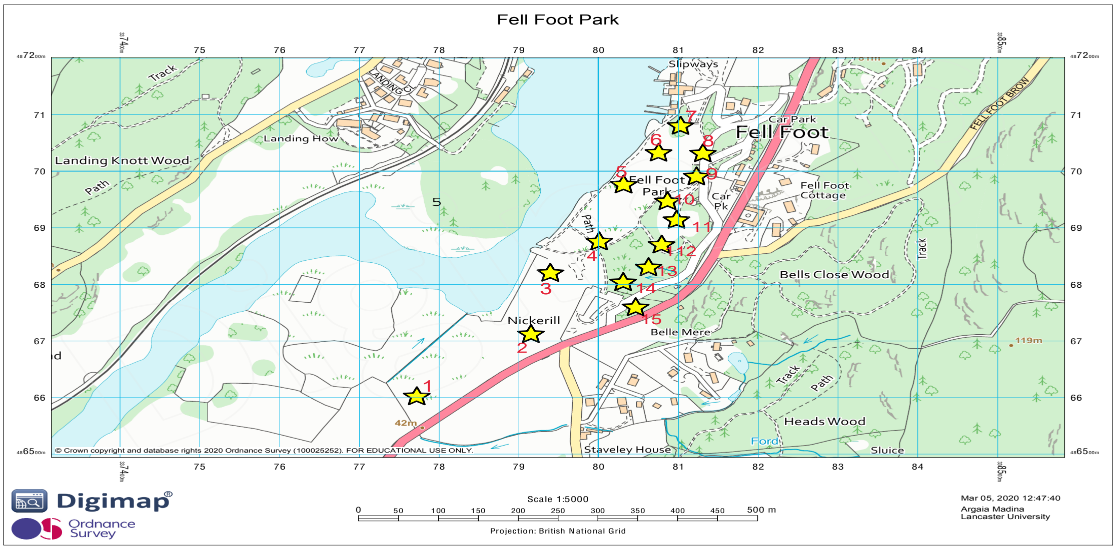

Figure 12: A diagram showing the location (stars and numbers) of soil cores from Lake Windermere (Fell Foot) in the Lake District area, (Cumbria UK) collected in March 2020.

3.2 Soil sample preparation

Each soil core was transferred to a baking plate and placed in an electric oven set at 100°C for at least twenty-four hours to guarantee all the moisture from samples was removed [55]. Subsequently, grinding was carried out using SWECO Vibro- -Energy Grinding Mills to produce a powder form for subsequent analysis. All the samples were sieved to a size of 5 mm to remove small pebbles and roots. Each sample was put into a 250 ml Marinelli Beaker, labelled, and sent to the CTL laboratory at the University of Liverpool (see Figure 13). The same samples were packed into Petri dishes and delivered to the Culham Centre for Fusion Energy (CCFE) near Abingdon and evaluated in a broad-energy HRGS system to determine the ^{241}Am abundance in each sample. The data were then used to determine ^{241}Pu activity based on several lifetime scenarios, ahead of the AMS technique as shown in section 3.8 and 3.9.

Figure 13: A schematic diagram depicting the process for sampling, drying, milling, and sieving the samples.

3.3 Soil sample composition

The composition of soil varies across geographical sectors and depths. Moreover, all samples of soil have particular types influenced by the actions of persons and other living creatures over significant periods of time. Multiple transmission and analytical procedures have been implemented for considering and differentiating soil types, involving macroscopic and X-ray fluorescence (XRF), X-ray diffraction (XRD) and SEM-EDX [56][57].

3.4 SEM-EDS Investigation

Among all these technologies mentioned above, the last analysis of SEM-EDS is beneficial for both discriminating and finding single elements for considering the full sample composition in a unique manner. In this section, the analysis of SEM-EDS, with the utilisation of the forensic soil evaluation experimental-based methodology is being utilised to identify the differences in soil samples' composition gathered from multiple sectors inside the Windermere and Blelham Tarn. The SEM evaluation of the compressed samples of soils has been undertaken utilising a Scanning Electron Microscope (SEM) of JEOL 6010-LV (JEOL (UK) Ltd., Herts, UK) at Lancaster University as shown in Figure 14 [58].

A)

B)

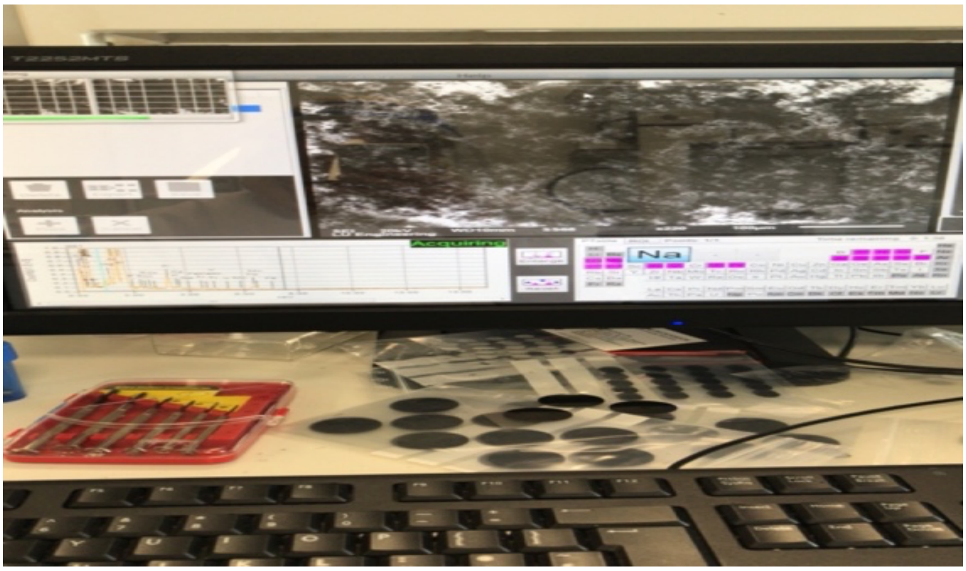

Figure 14: Scanning Electron Microscope (SEM) at Lancaster University: (A) machine image, (B) Pc connected with the machine to analyse the pressed pellet.

3.5 XRD evaluation

X-ray diffraction analysis (XRD) is a method that involves irradiating a material with X-rays and measuring the intensities and scattering angles of the X-rays that exit the substance (see Figure 15). The materials science technique of XRD is used to determine a material's crystallographic structure. The main use of traditional X-ray powder diffraction is to identify major and minor or several phases in an unknown material. A phase is a crystalline material whose atoms are arranged in a regular 3-dimensional pattern. The positions and intensities of the recorded diffraction peaks serve as a kind of crystalline phase fingerprint. A search-match technique is used to compare the measured pattern with both entries in reference databases to identify the object [59].

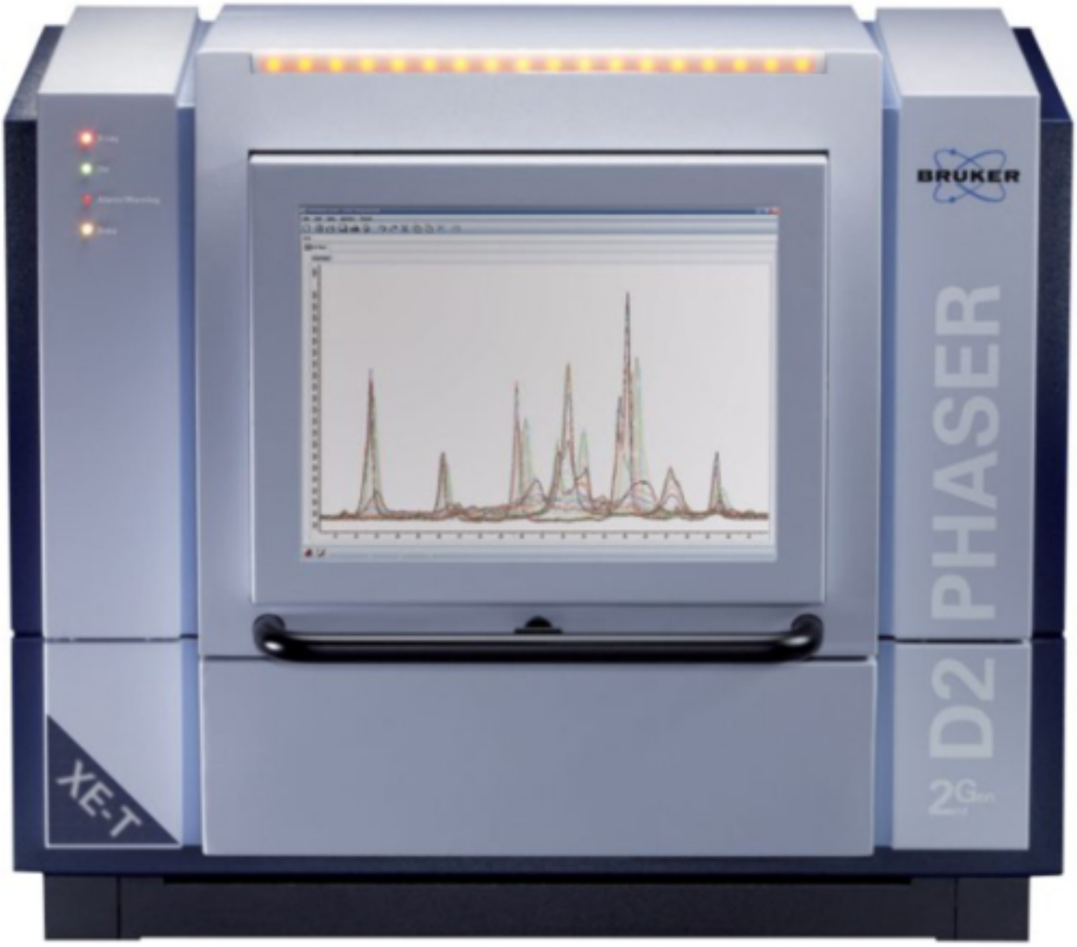

Figure 15: X-Ray Diffraction phases were identified using a Bruker D2 XRD machine [59].

3.6 Preparation for SEM-EDS and XRD

The identified differences in soil sample composition were collected from the Blelham Tarn and Lake of Windermere using SEM-EDS to find a single element. In addition, XRD is the second technique to identify the phases (chemical components) inside the soil samples.

Following the sample preparation described in section (3.2), one gram of each sample was sieved again by using a 0.5 mm stainless steel sieve. The sifted portion of every soil sample, ranging from 100 to 150 mg, was then pelleted into a 12 mm die assembly, in which at least 9 tonnes per cm^2 of pressure is applied by utilising an Atlas manual for hydraulic press for approximately two minutes [57]. The resulting tablets were separated from the die and fitted onto adhesive carbon decals for SEM-EDS evaluation. A camera picture of a sample is shown in Figure 16.

A)

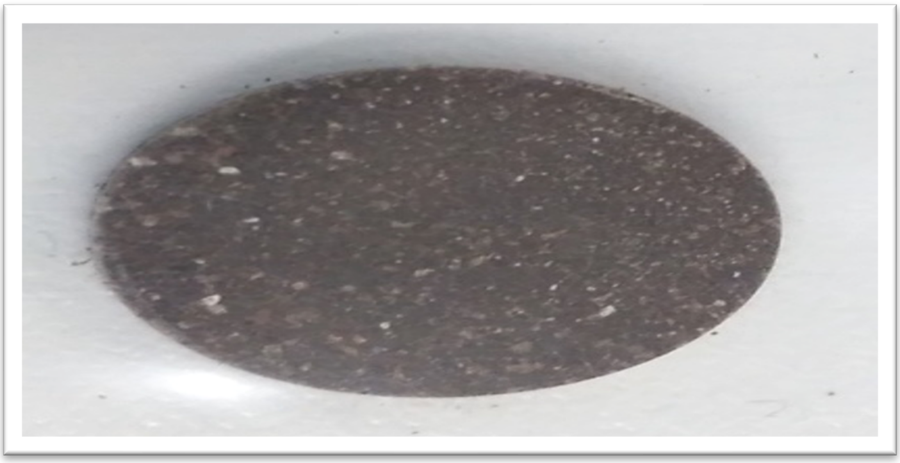

B)

Figure 16: (A) The pressed pellet generated from Sample 1 Blelham Tarn. (B) The homogenised pellets were mounted onto adhesive carbon stickers for SEM-EDS analysis.

3.6.1 SEM-EDS Analysis

The SEM evaluation of compressed soil samples has been undertaken using a Scanning Electron Microscope (SEM) of JEOL 6010-LV (JEOL (UK) Ltd., Herts, UK) [57]. The investigations of scanning electron microscopy were done at 21 keV with the help of compositional backscatter imaging (BEC) and instrument resolution ranging from 5 nm.

A BEC that is magnified to 50x was obtained from the middle of the pellet, which is followed by an EDS spectrum at a similar resolution of magnification. This type of spectrum was used to identify the materials qualitatively present in the samples of soil and a relevant range of 5 EDS spectra, with a magnification of 200x covering a distinct sector of the pellet every time a measurement was undertaken. The spectra of EDS were then evaluated quantitatively to consider the percentage of the relative mass of each material.

3.6.1.1 50× magnified BEC image

The imagej.net software is an open-source software that is being used to process and analyse specimens. ImageJ software can be used to display, edit, interpret, calculate, evaluate, and print image information. The BEC images are 50x magnified for each sample from Blelham Tarn and Fell Foot are shown in Figure 17.

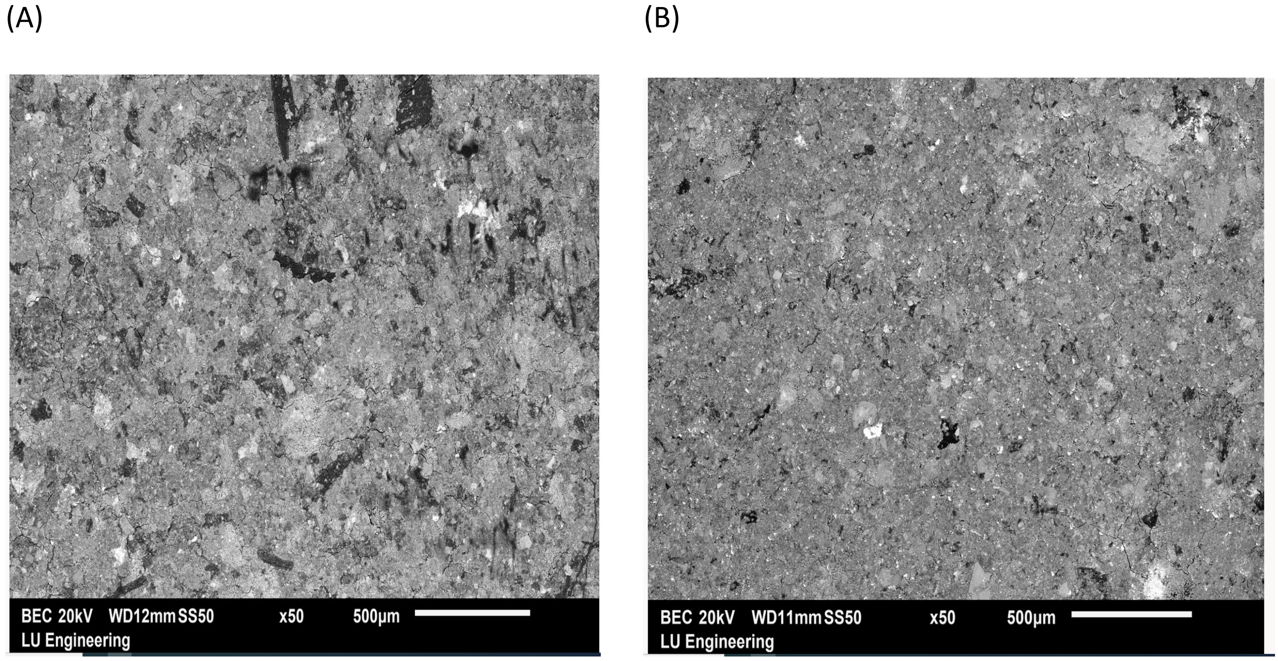

Figure 17: 50× magnified BEC micrographs of (A) Sample 1 of Blelham Tarn site, (B) Sample 1 of Fell Foot Park, Cumbria (UK).

3.6.2 XRD analysis

For XRD, the samples were ground and sieved in order to remove any organic matter and then packed into a powder tray and spun to avoid preferential orientation effects. They were measured with a Bruker D2. XRD data was collected from various locations on the sintered pellets to confirm the homogeneity in structure. The lattice parameters of the solid samples were determined over ranges from 0 - 80° for 60 mins, and full range zoom. figures are provided in the results chapter to show all the patterns observed during the analysis with 0.02 step size. In addition, the X-ray wavelength (LW) was 1.5060 Å (CuK_{α}), generated by the electron bombardment of Cu. Phases were identified using Bruker D Analytical X-Ray Systems with Fit software and the Crystallographic Open Database (COD) library [59].

3.7 Gamma Spectroscopic Measurements

In this section, a brief description of the experimental procedures used to calculate the natural and fallout radioactivity from the soil samples is provided. The methods that were used here behave as the foundation for predicting the levels of radioactivity of different samples of the environment, in the counting geometry of the Marinelli beaker with the application of gamma spectrometers. To calculate the activity concentration in each soil sample, the system of the BEGe detector is characterised first by energy calibration and detection efficiency [60]. This will be elaborated on in detail in the further section of this chapter.

3.7.1 Energy Calibration

The BEGe system's energy calibration was undertaken by using the Marinelli calibration resource NPRL 664 at the radiation laboratory of the University of Liverpool. The resource of calibration relied on a resin matrix in a Marinelli flask of 250 ml to get a similar counting geometry as the samples of soils that were analysed. This source included around 14 isotopes (^{241}Am, ^{109}Cd, ^{57}Co ^{139}Ce, ^{51}Cr, ^{113}Sn, ^{85}Sr, ^{137}Cs, ^{54}Mn, ^{88}Y, ^{65}Zn, ^{60}Co, ^{60}Co, ^{88}Y, the energy range of the Marinelli calibration source NPRL 664 between 59.5 keV (^{241}Am) and 1835.9 keV (^{88}Y). In addition, 14 peaks were identified and detected at the time of the measurement and used for the calibration and were investigated in the same circumstances as for the soil cores (see: Figure 18). The resource was situated on the endcap of the detector and the counting for 24 hours to give a spectrum of energy calibration. Peaks are highlighted using ProSpect® software [61], which automatically adds a Gaussian fit to subtracts the background. When highlighting peaks, it is important to include 3 or 4 channels of background on either side of the peak for this background subtraction to be accurate. Each peak is identified and added manually to the calibration.

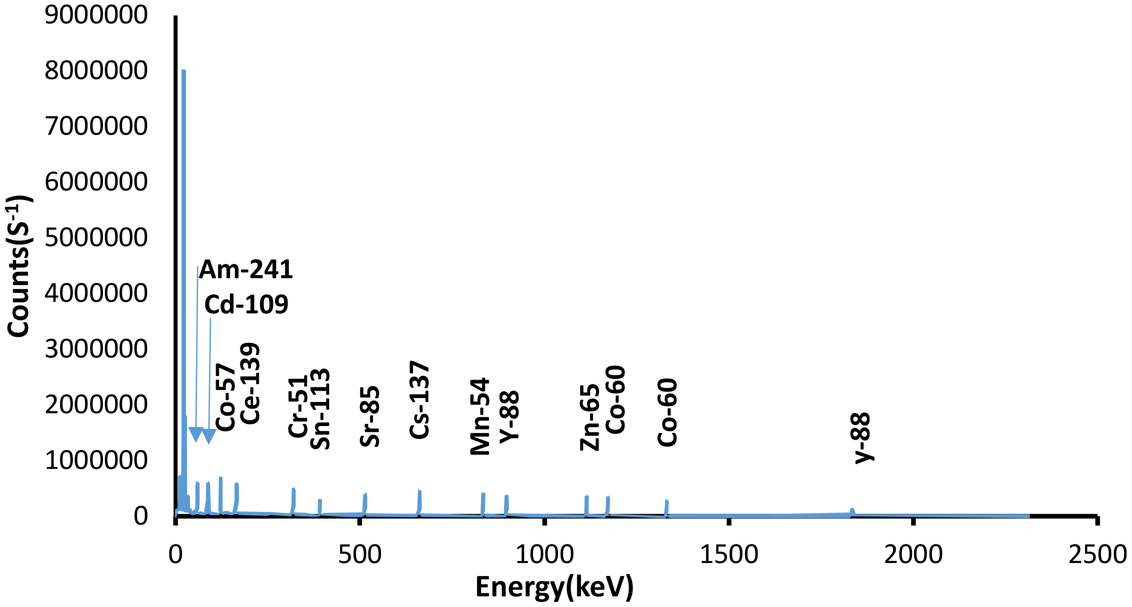

Figure 18: The calibrated energy spectrum for the NPRL 664 Marinelli calibration source.

3.7.2 Peak Area Determination

The method used to calculate the total peak area is described in this section. Using the ProSpect® software, this technique subtracts the background to determine the net area peak between the lower and higher background regions (as described in Figure 20). The two main sources of the background are the photoelectronic emission from the detector crystal or photon Compton scattering, both of which contribute to a somewhat greater background on the lowest setting of the photopeak.

For the ^{241}Am peak at 59.5keV, the automatic fitting of ProSpect was not effective, probably because the peaks are small and below the working limits of the automatic fitting function of the software. For this peak, the background was subtracted manually as follows:

the background radiation was averaged for a number of channels directly above and below the photopeak; The background radiation was consistent above and below the photopeak, so, the upper and lower background areas are aggregated over a number of channels to approximate the peak background which will be subtracted from the peak gross area to achieve the net count; The total number of counts in the peak was then determined by adding the counts in each channel of the peak and subtracting the average background per channel. The number of channels used was kept consistent for every sample [61].

3.7.3 Efficiency Calibration

The efficiency calibration of the BEGe system was carried out using the Marinelli calibration source NPRL 664, subsequent to the energy calibration section. The efficiency curve was calculated using various energies of elements from the calibration source (see Figure 19). In order to obtain accurate results, samples should be counted under the same measurement conditions as when the system was calibrated [62]. The absolute efficiency calibration was derived using Equation (3.1).

$$\varepsilon_{\mathrm{abs}} = \mathrm{N} / (\mathrm{L_t} \times P_\gamma \times \mathrm{A}) \tag{3.1}$$

where N is the count rate (net area peak) can be measured by highlighting the region of interest using the ROI function in Prospect® software, $\mathrm{L_t}$ is the live time, which is the time duration of the calibration source (NPRL 664) over 24 hours, P_γ is the probability of gamma emission at the energy used and A is the source activity (Activity today was estimated at the time of the measurement in December 2020).To calculate the source activity A, first use equation (3.2) ,which is:

$$\mathrm{A} = \mathrm{A_0} \mathrm{e}^{-(\lambda \mathrm{T})} \tag{3.2}$$

Where A_0 is the source activity of the radionuclide in the calibration source sheet (in Appendix C) λ is the decay constant, given by the following equation:

$$\lambda = \frac{In\,2}{T_{1/2}} \qquad (3.4)$$

$T_{1/2}$ is the half-life of the radionuclide and T is the time in seconds between the date radionuclide activity was measured until the time of the measurements.

Radionuclide	**Calibrated Energy (keV)**	**Source Activity (Bq)**	**Activity Today (Bq)**	**Efficiency (Eff)**	**Uncertainty**	**Eff (%)**
^{241}Am	59.5	887	318	0.045	0.002	4.5
^{109}Cd	88.0	8350	297	0.052	0.003	5.2
^{57}Co	122.1	433	346	0.054	0.002	5.4
^{139}Ce	165.9	543	380	0.047	0.002	4.7
^{51}Cr	320.1	9280	468	0.037	0.001	3.7
^{113}Sn	391.7	856	473	0.023	0.001	2.3
^{85}Sr	514.1	1378	991	0.019	0.001	1.9
^{137}Cs	661.7	2131	1810	0.012	0.0005	1.2
^{54}Mn	835.0	2200	2072	0.011	0.0004	1.1
^{88}Y	898.1	2570	2021	0.090	0.0004	0.9
^{65}Zn	1115.5	6190	2867	0.008	0.0004	0.8
^{60}Co	1173.2	3340	3304	0.007	0.0003	0.7
^{60}Co	1332.5	3340	3308	0.006	0.0003	0.6
^{88}Y	1835.9	2570	2139	0.005	0.0002	0.5

Table 4: The calibrated energy (keV) against absolute efficiency (Eff %).

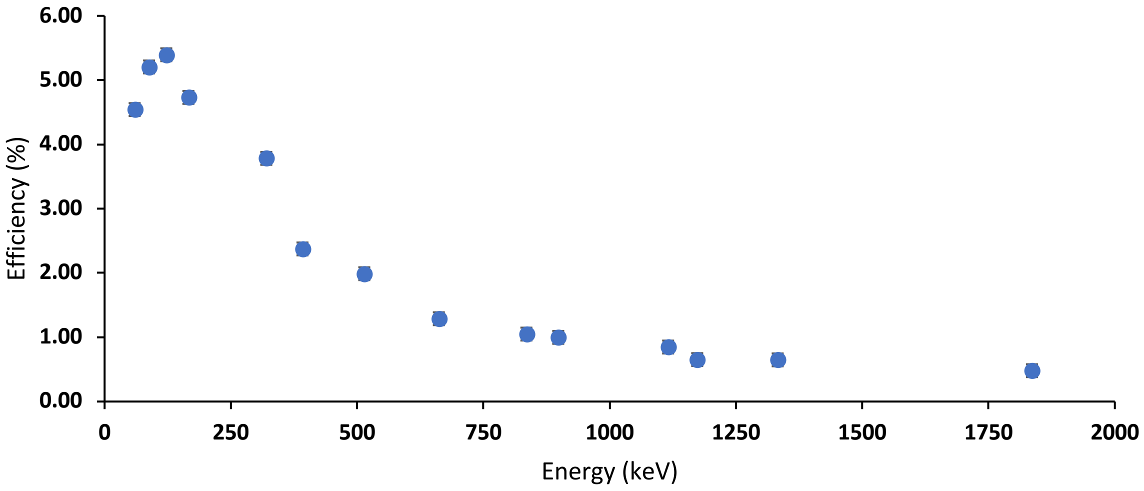

Figure 19: The calculated absolute efficiency of the BEGe detector versus radionuclide energy (keV) in NPRL 664 calibration source (all radionuclides shown in the certificate were measured).

3.7.4 Subtraction of Background

An actual peak in any recorded gamma-ray spectrum from the natural sources of radioactivity derived in the environment surrounding the detector and from other sources consisting of background peak, and should be subtracted, such as, the ^{40}K (1460 keV) gamma ray is present in all soil samples; this actual peak is indicated as the background and should be corrected after the assessments. The background spectra were measured for 24 hours to ensure that proper background subtraction was performed for each soil sample [63].

3.7.4.1 Optimizing Background Subtraction Method

Background removal is one of the most important pre-processing procedures for getting accurate detection results. The statistical investigation using program such as Excel together with hand calculations and the ProSpect® software, have been done to assess the ^{241}Am peak in Blelham Tarn and Fell Foot samples. In addition, an acquisition live time of Marinelli source counting, soil sample measured, and background spectrum was 24 hours. Furthermore, all samples within the analysis confirmed that the ^{241}Am peak is identifiable, which may be verified through Signal-to-Noise techniques and optimised for several subtraction strategies. Figure 20 has more details on how the Signal-to-Noise method works:

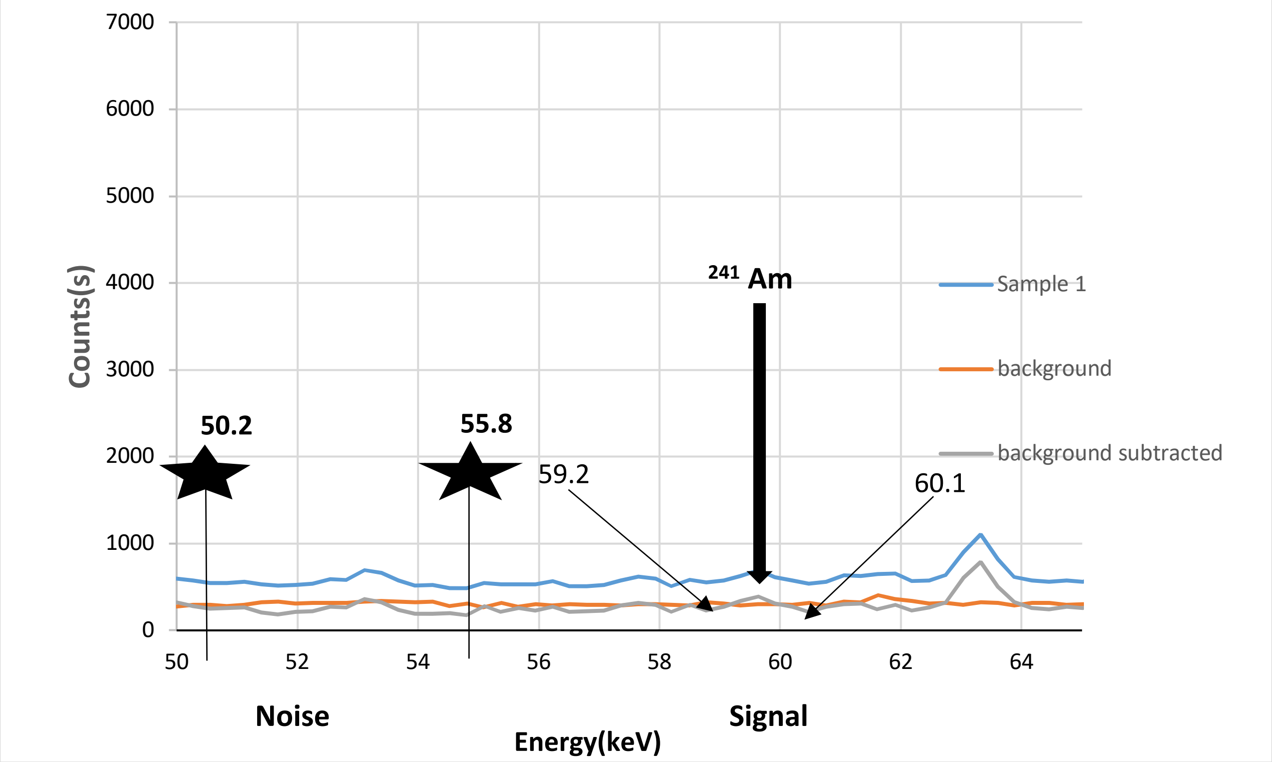

Figure 20: The sample 1 spectrum shown ^{241}Am has a little raised peak in the sample spectrum and nothing appeared in the background spectrum around this region.

It was difficult to determine ^{241}Am peak because of signal-to-noise. Is it just a positive variation randomly in the right place or is it a real peak? So, the background spectrum (orange line) shows there is no rising there as can be seen in Figure 19, which is reassuring this is the real peak. But various things can be done analytically to support such as this type of calculation: signal-to-noise.

The noise (N) would be the average level of counts in the background spectrum and the signal (S) is how many accounts there are in the peak. In addition, this way can be done the same for the subtracted spectrum (grey line). Subsequently, signal (S) is divided by noise (N), if the signal-to-noise in the subtracted spectrum increases (S/N in subtracted is higher than the background). Furthermore, this indicates that something quantitative would be inclined to say whether this is a real peak. This calculation has been done for the Blelham Tarn sample as shown in Table. 3.

NO. samples	Signal-to-Noise ratio in background	Signal-to-noise ratio in subtraction
B1	3.0 ± 0.2	4.0 ± 0.3
B2	4.0 ± 0.2	5.0 ± 0.3
B3	2.0 ± 0.1	4.0 ± 0.2
B4	5.0 ± 0.4	7.0 ± 0.4
B5	3.0 ± 0.2	4.0 ± 0.3
B6	4.0 ± 0.3	6.0 ± 0.3
B7	3.0 ± 0.3	6.0 ± 0.4
B8	4.0 ± 0.3	6.0 ± 0.4
B9	2.0 ± 0.2	3.0 ± 0.2

Table 5: Signal-to-noise data for both background and subtraction spectrum for Blelham Tarn samples.

3.7.4.2 The optimum background for several subtractions

There are two perspectives in the subtraction of background, signal-to-noise to confirm the ^{241}Am peak certainly in the soil sample, (as illustrated in the signal-to-noise section) or could use a more efficient method such as optimised background subtraction. Following the sample 1 spectra (see: Figure 20), if the user starts to deduct the fraction from the background, for example, 10%, and continues subtracting, then the signal-to-noise ratio will increase after that decreasing due to over-subtraction. Identifying the optimum level of background subtraction is crucial, especially when trying to isolate the low-energy γ-ray line from the α decay of ^{241}Am, as shown in Figure 21.

$$^{241}\text{Am} \rightarrow {}^{237}\text{Np} + \alpha + \gamma \text{ (59.5 keV)}$$

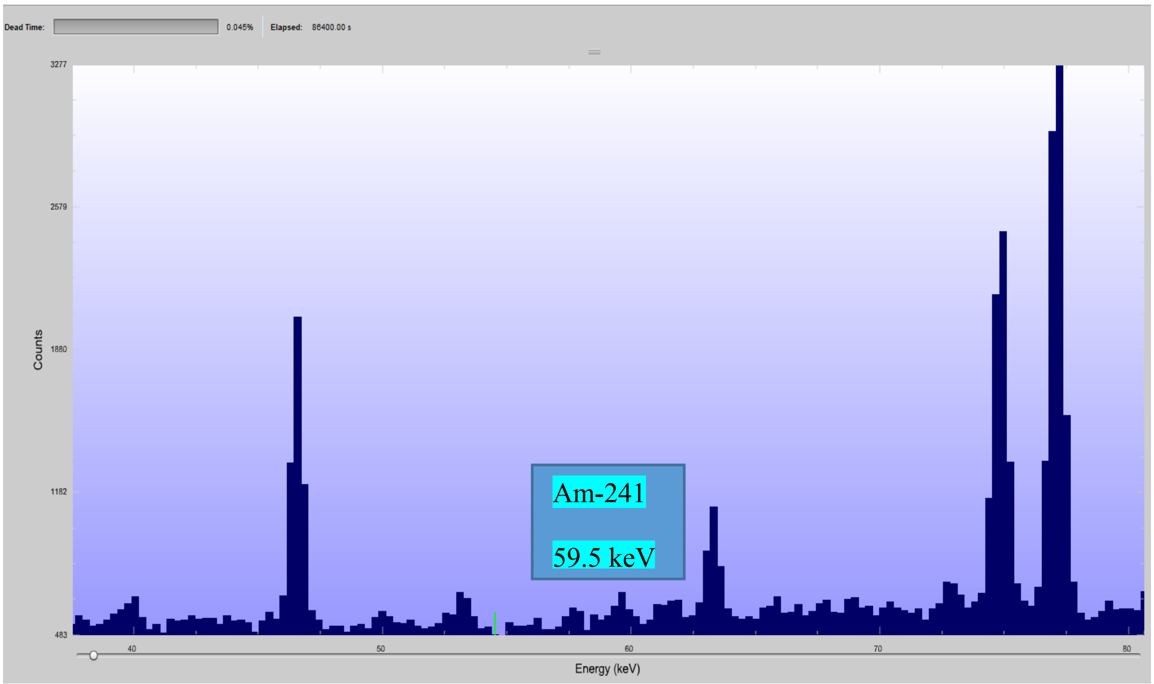

Figure 21: Spectrum of soil sample 2 to show the ^{241} Am peak.

An example HRGS spectrum is given in Figure 20 for a sample studied in this research, with the ^{241}Am peak highlighted and seen adjacent to the more intense lines from ^{228}Ac and uranium. There are few reports of such optimization methods [64], beyond what is provided in commercial analysis packages. The background contribution in this lower-energy scatter region can be sample-dependent: without a sample, ^{241}Am is not expected (trace contaminants in the materials of the detector are guarded against in manufacture); with a sample, γ rays from isotopes in the sample that do not deposit all their energy in the detector contribute to the background (assuming no suppression detector). We have estimated peak-to-background (signal-to-noise, S/N) as a function of the proportion of background subtracted, to determine the optimum proportion to subtract for the best S/N. S/N ratio against % background spectrum subtracted for an average of BEGe measurements of samples #1 and #2 is given in Tables. 4, 5, and Figure 22.

Background (%)	Signal to noise ratio (S/N)
10 %	3.7 ± 0.3 ⇧
20 %	3.8 ± 0.2 ⇧
30 %	3.9 ± 0.2 ⇧
40 %	4.1 ± 0.2 ⬆
50 %	3.9 ± 0.2 ⬇
60 %	3.7 ± 0.2 ⬇
70 %	3.6 ± 0.2 ⬇

Table 6: Signal-to-noise for various subtractions of sample1 from Blelham Tarn samples.

Background (%)	Signal to noise ratio (S/N)
10 %	4.6 ± 0.3 ⬆
20 %	4.7 ± 0.3 ⬆
30 %	4.8 ± 0.3 ⬆
40 %	5.0± 0.3 ⬆
50 %	4.8 ± 0.3 ⬇
60 %	4.7 ± 0.3 ⬇
70 %	4.5 ± 0.3 ⬇

Table 7: Signal-to-noise for various subtractions of sample 2 from Blelham Tarn samples.

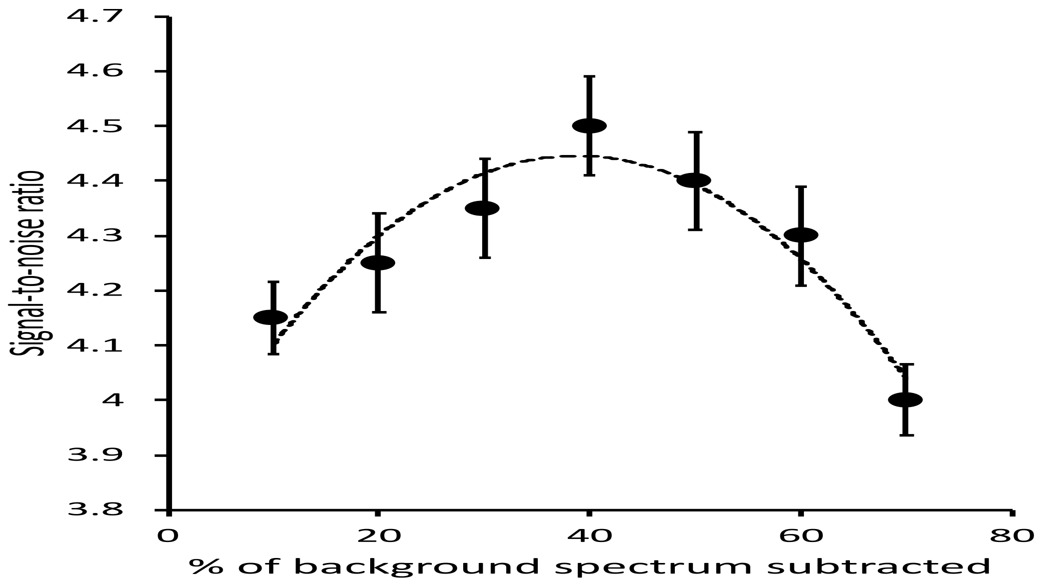

Figure 22: Signal-to-noise ratio for several subtractions on samples 1 and 2 against % background subtracted from measurements.

3.8 Gamma-ray measurements

This section explains the measurements of ^{241}Am and ^{241}Pu activities (Bq/g) via HRGS using a BEGe detector for Blelham Tarn and Fell Foot. These were carried out at the University of Liverpool and Culham Centre for Fusion Energy (CCFE). The purpose of these measurements is not just to compare them with the prior art plutonium and americium records from sediment cores in Blelham Tarn [1]. However, it is interesting to see if what is known about Blelham Tarn and whether it is the same for other lakes or not, that is why Lake Windermere was selected as an example in this research as well. this considers the radioactivity in the soil samples collected from Blelham Tarn and Fell Foot Park.

Broad energy germanium detector (BEGe) from Canberra [63] is a technology frequently used to locate and estimate gamma radiation in situations where there may be widely dispersed and distinct energy deposits. The model of this detector was BE2825; it contains a p-type high-purity germanium detector (HPGe) crystal. The germanium crystal is held in place with copper support encapsulated inside an aluminium cryostat having a cross-sectional of 28 cm^2 and a 25 mm thickness (see: Figure 23). More data specified by the manufacturer on the detector proportions are in Appendix B. The energy range of the BEGe detector is 3 keV to 3 MeV [63]. The detector is coupled with a Canberra 2002C charge-sensitive preamplifier and the output signal from the pre-amplifier is supplied as an input to the Canberra Lynx Digital Signal Analyser as shown in Figure 24. The digitised signals (pulse-height spectrum) can be viewed from a monitor (PC) with the proprietary ProSpect® software [61].

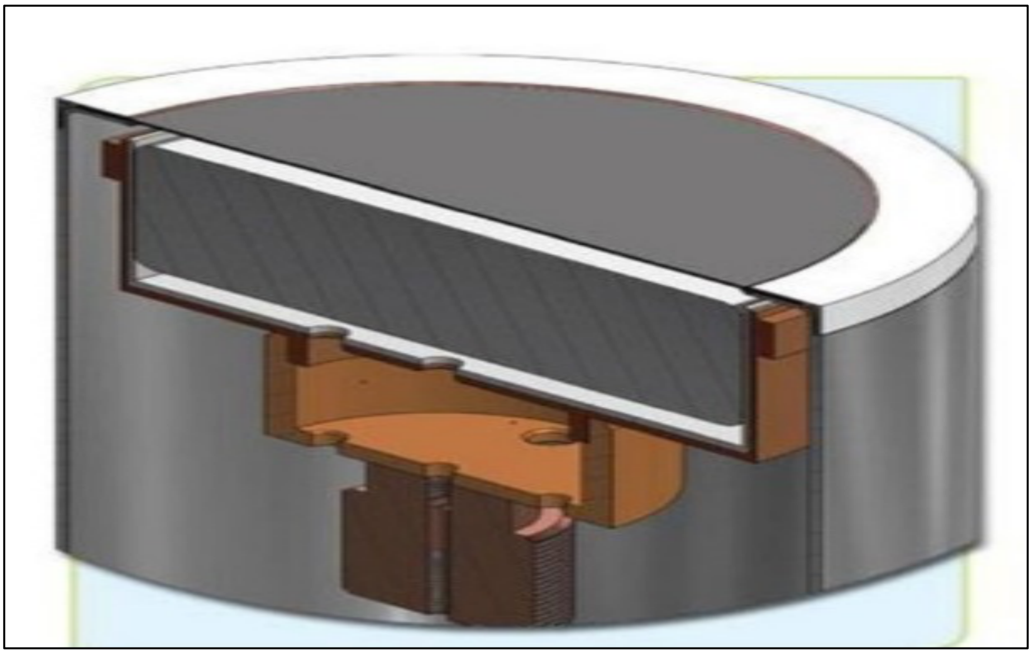

Figure 23: The area for a cross-sectional of the BEGe Detector from 20 to 28 cm^2 and the thickness from 20 to 25 mm t [63].

Figure 24: An illustration of the detector, the detector is coupled with a Canberra 2002C charge-sensitive preamplifier and the output signal from the pre-amplifier is supplied as an input to the Canberra Lynx Digital Signal Analyser The digitised signals (can be viewed from a monitor (PC) with the proprietary ProSpect® software.

The BEGe detectors are calibrated at the University of Liverpool and at CCFE with a mixed point source (as shown in energy calibration section 3.7.1). Details of this source are found in the appendix. Each sample within this research was transferred into Marinelli beaker containers for the Liverpool detector and Petrie dishes for CCFE detector. Throughout observation were positioned effectively on the germanium crystal.

The time for each sample in the BEGe detector was 24 hours, and the spectrum from each measurement was recorded. The ISOCS/LabSOCS model of the BEGe detector was used to generate the efficiency calibration data and used for efficiency correction as part of the analysis for calculating specific activity of ^{241}Am, both efficiency files from Liverpool and CCFE can be found in the Appendix D and Appendix E [65].

The Geometric efficiency was determined using the Genie software, considering efficiency range energies from 45 to 2000 keV. For indication, the closest point to ^{241}Am (59.5ke V) in the efficiency file is at 60.00 keV with an efficiency of (13.02 ± 1.30) %, although the best fit may be able to get closer to 59.5 keV line. The efficiency estimated in Liverpool was (0.034 ± 1.0) %, the efficiency curve data from LabSOCS for soil sample can be found in appendix D.

All the files of spectra that were received from Liverpool and CCFE were analysed in Lancaster using ProSpect® software from Canberra [61].

In addition, checking each step in the process by which these specific activities have been obtained from Liverpool and CCFE included:

1. Peaks fitted in the gamma-ray spectra from the BEGe to record the net peak count rate per second for estimating the ^{241}Am abundance. Important factors to consider here include background subtraction, efficiency correction, and quality of the fit for the 59.5 keV line at ^{241}Am. So, background subtraction for the Liverpool data Culham

data was done using gross area, identifying ^{241}Am peak and subtracting the equivalent region of a background spectrum.

2. For each sample, the number of counts in the 59–60 keV energy range, which is close to the 59.5 keV peak, was totalled. The total number of ^{241}Am atoms that decayed over the 24 hours was determined using values from the ^{241}Am decay scheme [66]. Finally, the total value of ^{241}Am atoms per sample that decayed for 24 hours was measured and then converted to decays per second (Bq) to Bq per g (divided by the sample mass).
3. The efficiency in this energy region is very dynamic; therefore, a detailed consideration of this is necessary, especially in terms of its influence on uncertainty. It has already been calculated the Liverpool data from a calibration Marinelli source (see section 3.7.3) and using LabSOCS as well. Equal consideration has been made with the CCFE data, to verify the efficiency.
4. The ^{241}Am (59 keV) transition will have a known, quantitative intensity associated with it, which means that only a proportion of the 59 keV decays correlate to disintegrations of ^{241}Am needs to be factored in at approximately 36% [67].
   The γ branching ratio for Am-241 = 0.359, which is the probability that a 59.5keV gamma is emitted.
5. Because ^{241}Am and ^{241}Pu activities are highly correlated, with about 99.7% of the intensity of decay ^{241}Pu to ^{241}Am, as there are two modes of decay and it has nothing to do with half-life (see Figure 25), it was possible to calculate the quantity of ^{241}Pu present from each spectrum using the assessed quantities of ^{241}Am via the 59.5 keV ^{241}Am peak. This can be done using the Bateman equation [68] [69] [70], which characterises the abundance and activity of radioactive elements in a decay chain as

a function of time, depending on the decay rates (of the daughter) and original abundances of the isotopes (parent) in the supplied material. It can be clarified the number of unstable nuclei of the parent and daughter isotopes at time t are N_P (t) and N_D (t), respectively [71].

$$A_D(t) = \frac{\lambda_D A_P(0)}{(\lambda_D - \lambda_P)}\left(e^{-\lambda_P t} - e^{-\lambda_D t}\right) + A_D(0)e^{-\lambda_D t} \qquad (3.1)$$

Where A_P and A_D are parent and daughter activities, respectively:

$$A_{Am}\,(t) = \frac{\lambda_{Am} A_{Pu}(0)}{(\lambda_{Am} - \lambda_{Pu})}\left(e^{-\lambda_{Pu} t} - e^{-\lambda_{Am} t}\right) + A_{Am}(0)e^{-\lambda_{Am} t} \qquad (3.2)$$

A_{Am} (0) =0 “standard boundary conditions”

$$A_{Am}(t) = \frac{\lambda_{Am} A_{Pu}(0)}{(\lambda_{Am} - \lambda_{Pu})}\left(e^{-\lambda_{Pu} t} - e^{-\lambda_{Am} t}\right) \qquad (3.3)$$

$$A_{Pu}(0) = \frac{A_{Am}(t)(\lambda_{Am} - \lambda_{Pu})}{(e^{-\lambda_{Pu} t} - e^{-\lambda_{Am} t})\lambda_{Am}} \qquad (3.4)$$

λ_{Am}= Americium-241 decay constant

λ_{Pu}= Plutonium-241 decay constant

t~30 years

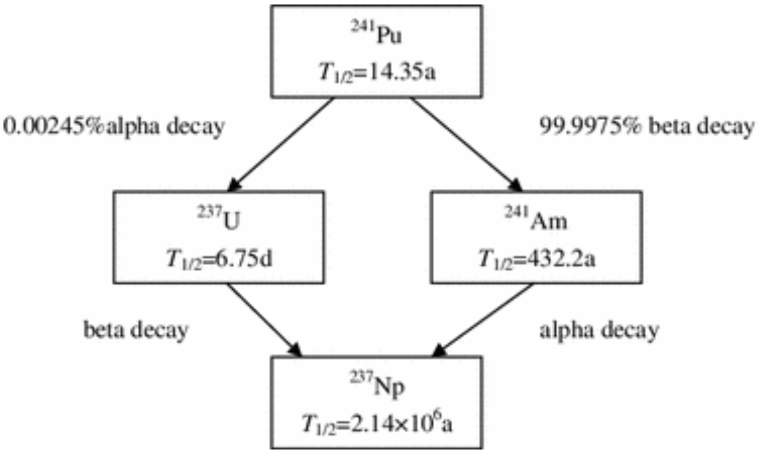

Figure 25: The decay probability of ^{241} Pu to 99.997 of ^{241}Am and 0.002 of ^{237}U [72].

3.9 Accelerator Mass Spectrometry (AMS)

AMS is generally used for the rapid and accurate measurement of several specific isotopes (particularly radiocarbon). AMS identifies the atoms of a particular element by their atomic mass. Radiocarbon dating using accelerator mass spectrometry is a two-part process. In the first stage, the ions are rapidly accelerated to very high kinetic energies and then analysed using a mass spectrometer. [74].

3.9.1. AMS set up for Pu abundances and Pu isotope ratios

- A terminal voltage to determine long-lived radioisotopes in AMS is about 260 KV, which is constrained by the bending capability of HE magnets. Considering the sum of ion source (Cs) and sample potential of 46 KV.
- Actinide ions have a stripping energy of about 285KeV. Additionally, choosing the three-pulse charge state the final actinide energy is approximately over 1 MeV.
- The signal from the first anode of the GIC is used for the detection of rare actinide isotopes. A 3 × 3 mm² or a 4 × mm² silicon nitride (Si N) detector.
- The rare actinide isotopic ratios are determined by sequential injection of each isotope into the gas ionization chamber (GIC).
- All three magnets (p/q) filters) should keep at the constant field (as shown in brown-coloured equipment in Figure 26, in order to allow for repeatable sequential switching to various rare isotope compounds, with different isotopes (masses) investigated at different energies.

- The injection of the negative actinide oxide beam of relevance is achieved by applying a constant voltage to the chamber of the low-energy magnet.
- The electrostatic quadrupole triplet lens is modified to account for the varied concentration of the chosen mass from the molecular breakup of the actinide oxide injection (blue /yellow coloured equipment in Figure 26) [73].

3.9.2 Sample Preparation and Chemical Processing

Prior to performing some calculations using AMS data, (soil sample preparation as the first stage as described in section 3.1), this section explains the chemical processes that the samples were subjected to in order to prepare them for AMS.

A weight of 5 g of each sample was subjected to acid leaching techniques, iron co-precipitation and removal chromatography before AMS analysis. Particular chemical processes have been described by Chamizo et al. [74][75]. For Pu radiochemistry, the weighed soil sample was damped by putting it in a Teflon^{TM} beaker and then spiked with almost 3 pg. of ^{242}Pu.

Following the procedures of Sakaguchi et al. [76], the extraction of Pu isotopes from the soil was achieved by mixing it with concentrated Suprapur® nitric acid and hydrogen peroxide in a hotplate. The centrifugal and filtration of the acid solution was performed three times, then the solution was evaporated until dry then was diluted with 8M suprapur® nitric acid. 3M sodium nitrite was used to amend the valences of plutonium before co-precipitation with clean $Fe(OH)_3$ to achieve full separation of plutonium isotopes. The iron precipitates were re-dissolved in 8M suprapur® nitric acid and then subjected to TEVA and UTEVA columns (Triskem International, France) consecutively, in order to remove the Pu.

The eluate of the Pu component was co-precipitated using 1.25 mg of purified Fe^{3+} solution and then it was evaporated to dryness. All Pu isotopes were heated to 650°C and combined with 1.3 mg of niobium, in order to be refashioned to an oxide state, and then they were compressed into AMS cathodes. Procedural blanks (n = 24) batched with deionized water were processed similarly to the samples and were included in every analytical batch to consider any influence on Pu isotopes. All the samples were assessed by AMS at the ETH- TANDY AMS facility, in Zürich, Switzerland and Lancaster, described later.

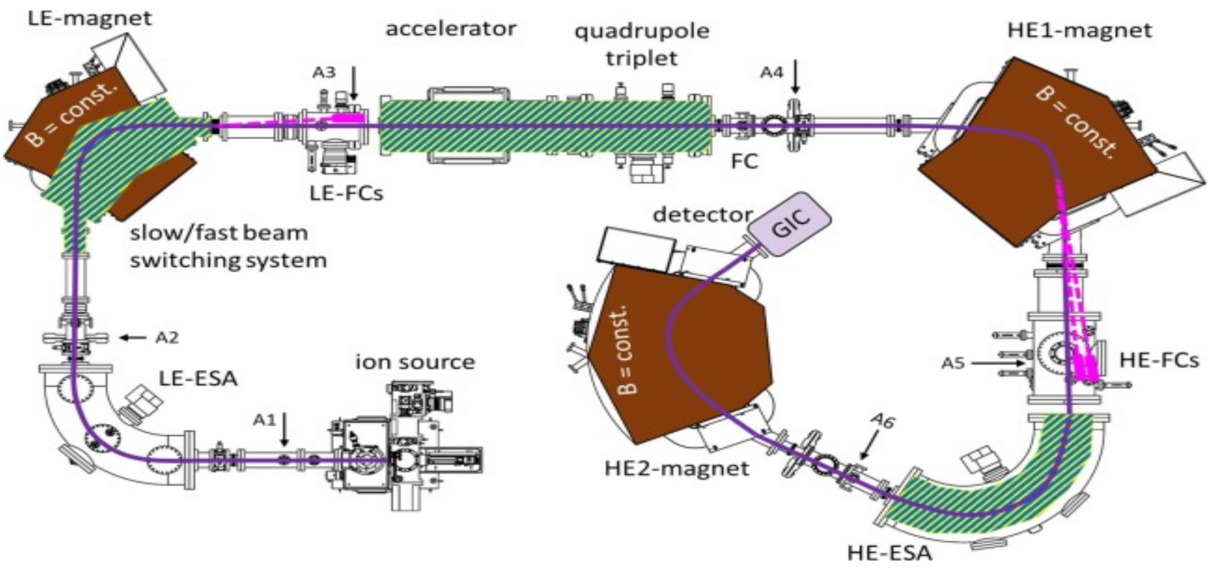

Figure 26: A diagram of the TANDY AMS at ETH Zϋrich [83].

3.10 Chi-Square Distribution Technique

The chi-square test is often used for hypothesis testing. The Chi-square statistic is a test to determine how well a model fits the actual data. The Chi-square test is used to determine whether the observed outcome is consistent with the expected outcome [78]. Chi-square tests are used when analysing data from a random sample and the variables are categorical variables. Therefore, chi-square analysis is often the most effective way to test this type of data [79] [80].

Left and right Chi-Square curve and critical values using the GeoGebra website, the Chi-Square curve can be automatically generated with a value for the degree of freedom and Chi-square critical value in the box shown on Figure 27 [81].

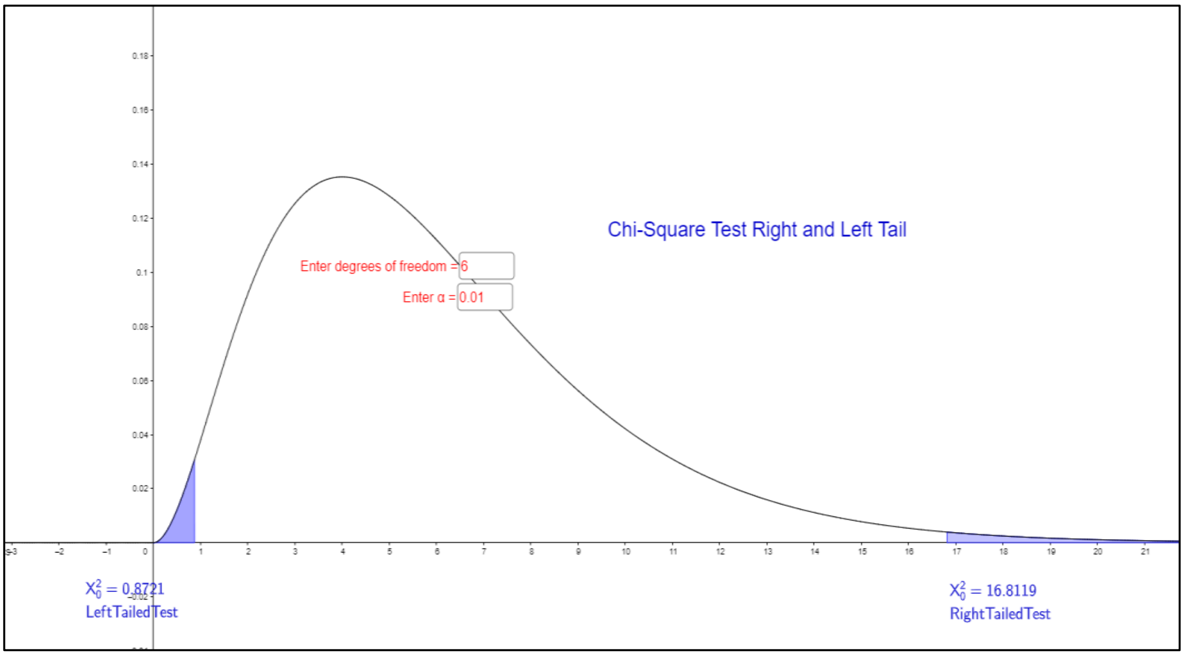

Enter degrees of freedom = 6

Enter α = 0.01

Figure 27: Left and right Chi-Square curve and critical values using the GeoGebra website [86]

3.10.1 Example for determining the weighted average of $^{240}Pu/^{239}Pu$ per mass of dry soil (AMS data)

This technique has been applied to the datasets in order to determine which samples are consistent with the weighted average and the prior art, and which are not (based on χ_{υ}^{2}), the results in Table 6 and Figure 28, which can be seen that the plot of the data from this work and the χ_{υ}^{2} analysis gives a χ_{υ}^{2} of 0.76 with the degree of freedom was 8 for Blelham Tarn. In addition, χ_{υ}^{2} for Fell Foot samples was 1.59 with the degree of freedom 14. The equation used to obtain the bounds of the Chi-square distribution, and the bounds of this calculation were from 0.21 to 2.51 and 0.33 to 2.55, in 98% critical limit for Blelham and Fell Foot, respectively. Furthermore, it can be often specified as the 'reduced' Chi-square, which is the weighted sum of squares divided by the number of degrees of freedom [74].

A)

Sample Number	^{240}Pu/^{239}Pu	Error	Ratio (at/at)	
	ratio(at/at)		Average	
B1	0.172	0.008	0.181	
B2	0.179	0.004		
B3	0.187	0.004		
B4	0.184	0.015		
B5	0.193	0.010		
B6	0.181	0.009		
B7	0.179	0.007		
B8	0.184	0.005		red. CHI^2=
B9	0.174	0.009		0.76
		DF	Chi- min(98%CL)	Chi-max (98% CL)
		8	0.21	2.51

B)

Sample Number	^{240}Pu/^{239} Pu	Uncert	Ratio(at/at)	
	Ratio(at/at)		Average	
F1	0.189	0.004	0.181	
F2	0.189	0.005		
F3	0.188	0.009		
F4	0.158	0.008		
F5	0.183	0.006		
F6	0.188	0.005		
F7	0.177	0.006		
F8	0.167	0.004		red. CHI^2=
F9	0.181	0.005		1.59
F10	0.173	0.006		
F11	0.181	0.006		
F12	0.187	0.005		
F13	0.173	0.006		
F14	0.180	0.004		
F15	0.188	0.008		
		DF	Chi- min(98%CL)	Chi-max (98% CL)
		14	0.33	2.55

Table 8: The Chi-square distribution for Blelham Tarn (A) and Fell Foot (B) samples.

A)

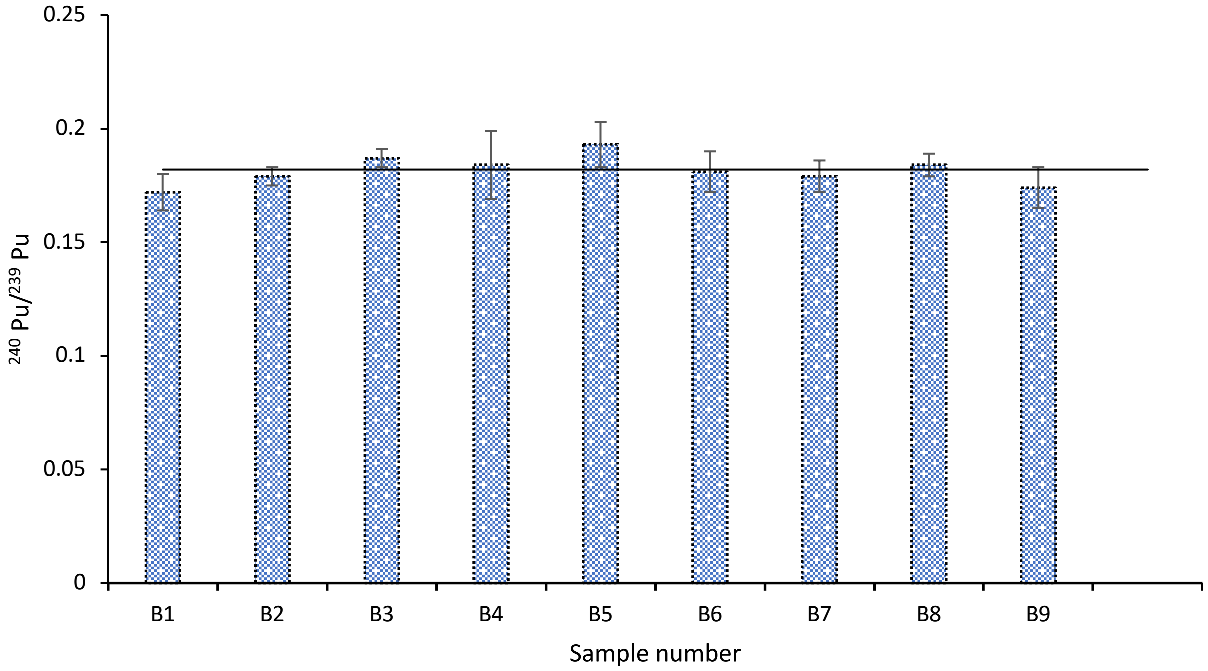

B)

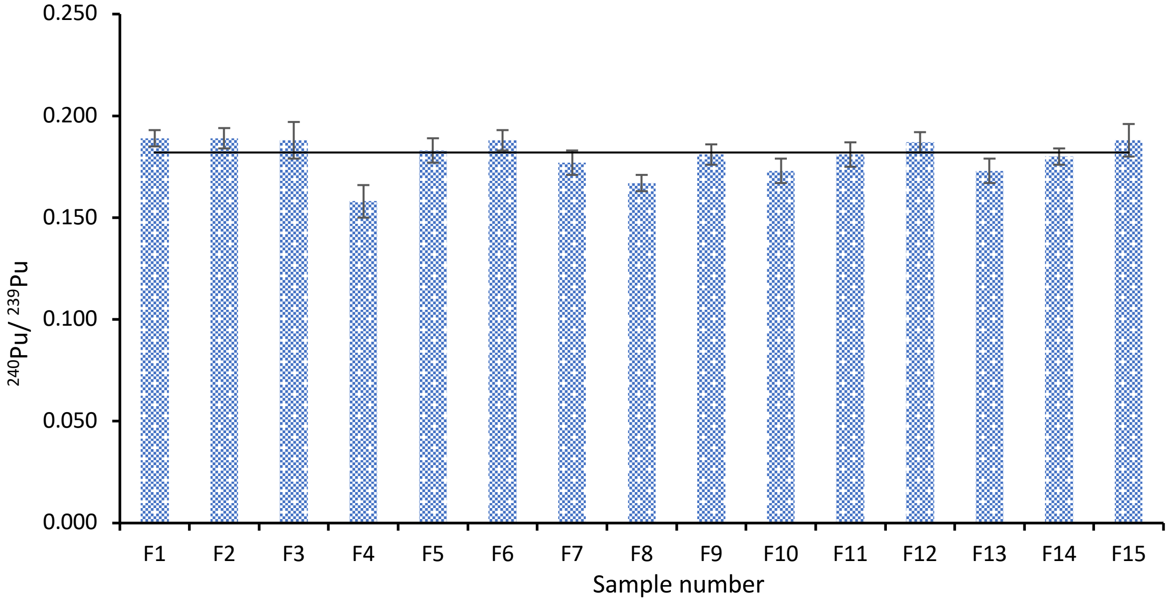

Figure 28: Example of ^{240}Pu/^{239}Pu isotopic ratio as measured with the AMS system at ETH Zürich From Blelham Tarn (A) and Fell Foot (B).

CHAPTER 4: RESULTS

4.1 Compositional Analysis of Soil Sample Results

4.1.1 SEM-EDS spectrum

EDS analysis of each specimen revealed similar elemental compositions across all samples; each sample contains the fundamental elements such as C, N, O, Na, Mg, K, Ca, P, S, Al, Si, Ti, V, Mn and Cl. An example SEM-EDS spectrum of sample 1 for Blelham Tarn is shown in Figure 29 and sample 1 for Fell Foot is illustrated in Figure 30.

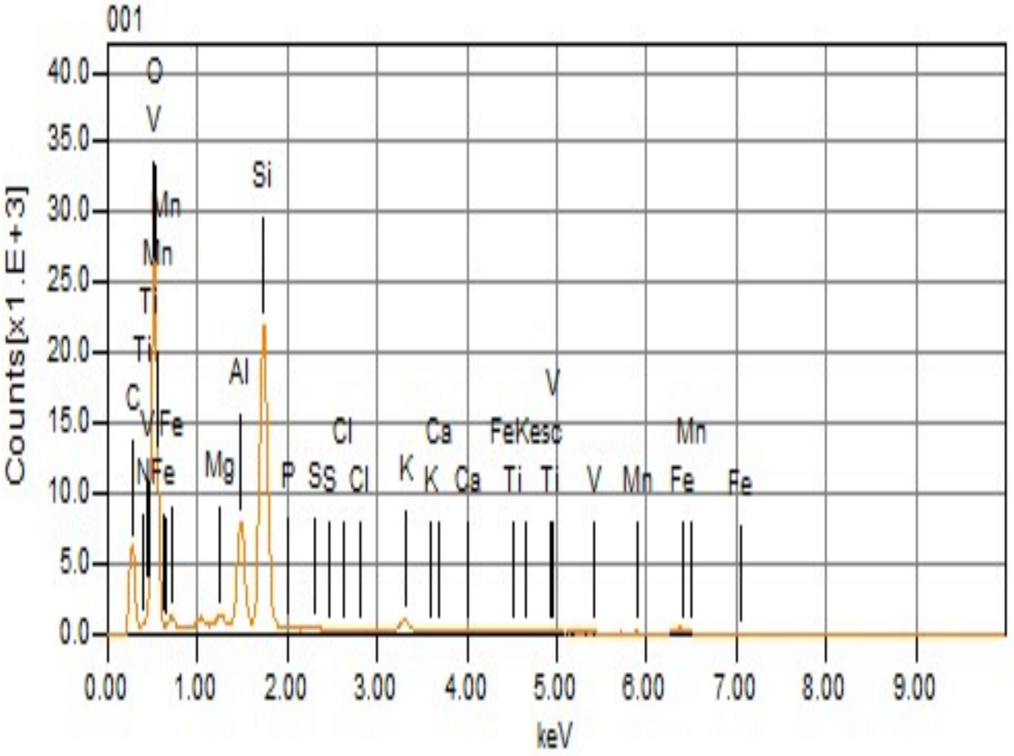

Figure 29: SEM-EDS spectrum of soil Sample 1 Blelham Tarn to determine the relative mass % of each element, with the standard deviation as a function of the five areas analysed.

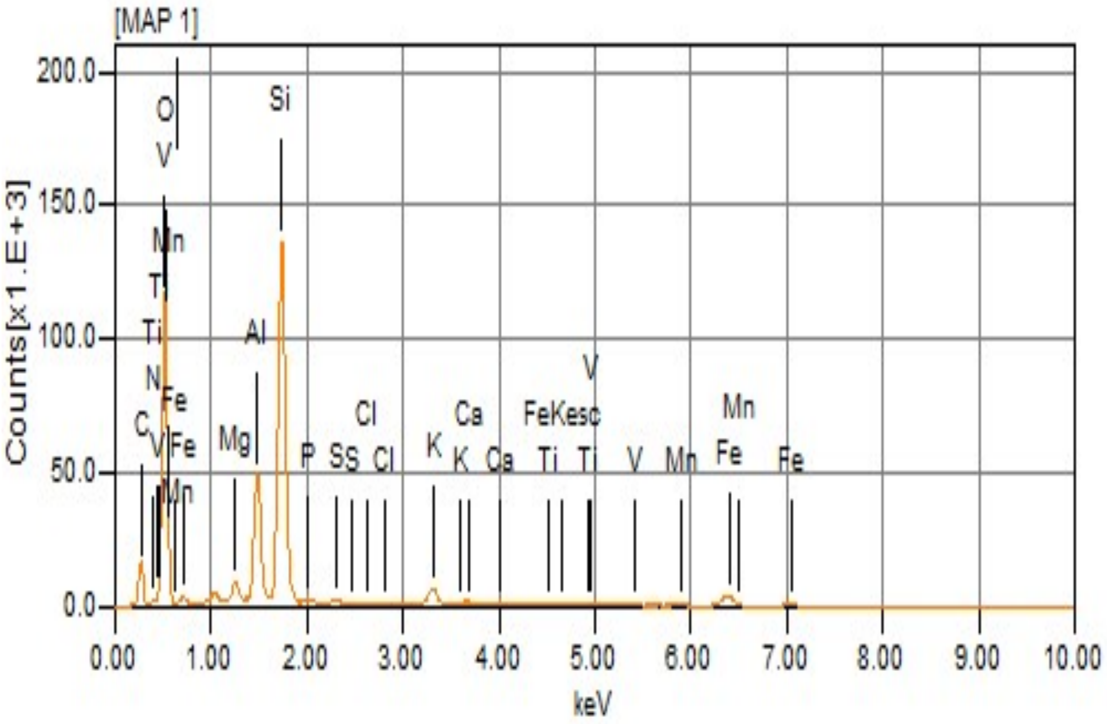

Figure 30: SEM-EDS spectrum of soil Sample 1 for Fell Foot to determine the relative mass % of each element, with the standard deviation a function of the five areas analysed.

The spectrum of soil Sample 1 for Blelham Tarn and Fell Foot as shown in Figures 29 and 30 obtained from EEM-EDS analyses was used to qualitatively identify the elements present in the sample. A subsequent series of five EDS spectra at 200× magnification covering a different pellet area each time was taken. EDS spectra were then quantitatively analysed to determine the relative mass % of each element, with the standard deviation a function of the five areas analysed [56].

This process was carried out on four samples from each site. For Blelham Tarn, samples were selected according to their location on the map (see Figure 11). For example, sample 7 was selected because it is very close to the lake and to compare the soil elements in this sample with the rest of the selected samples: sample 1, sample 2 and sample 3. Such elements can be considered as originating from the following sources (see Figure 31):

1. Biomass includes C, N and O. This covers any biological material, i.e., sticks, leaves, and insect matter that has passed through sieving.
2. Nutrients such as Na, Mg, K, Ca, P, S, Cl, N. for Na, Mg, Ca and K come from either salts or small mineral phases within the soil. P, S, N and Cl are associated with phosphates, sulfates, nitrates, and chlorides within the soil.
3. Al and Si – Metalloids. Aluminosilicates are associated with common mineral phases such as feldspar or clay.
4. Ti, V, Mn, and Fe – Metals. Again, such material indicates the degree of mineral phases in the soil. Fe originates from iron/iron oxide minerals within the soil, e.g., magnetite, hematite, etc. Ti originates from titanium oxides, e.g., rutile, ilmenite and sphene. V is low in concentration but is usually found in carnotite, roscoelite, vanadinite, and patronite as well as some phosphate-containing rocks. Finally, Mn originates from minerals such as pyrolusite, romanechite and rhodonite. Many of these elements also have beneficial plant growth effects and may also be classified as nutrients, although for EDS analysis they are here classified as metals.

A) Blelham Tarn

produce a great comparison of the soil elements in Blelham Tern and Fell Foot samples as show in Figure.32.

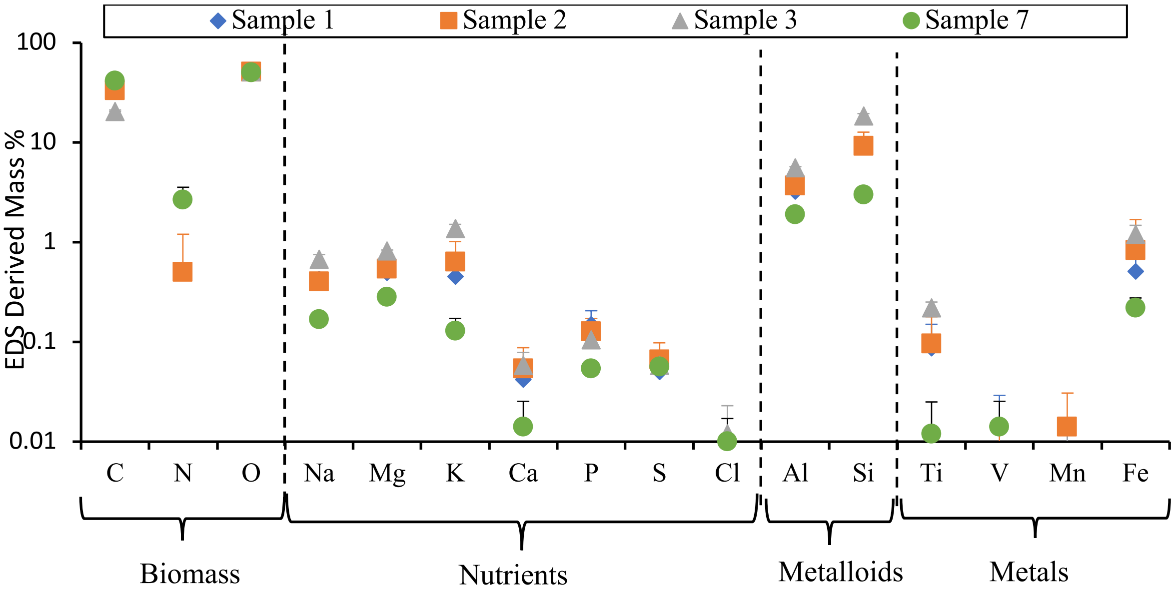

B) Fell Foot

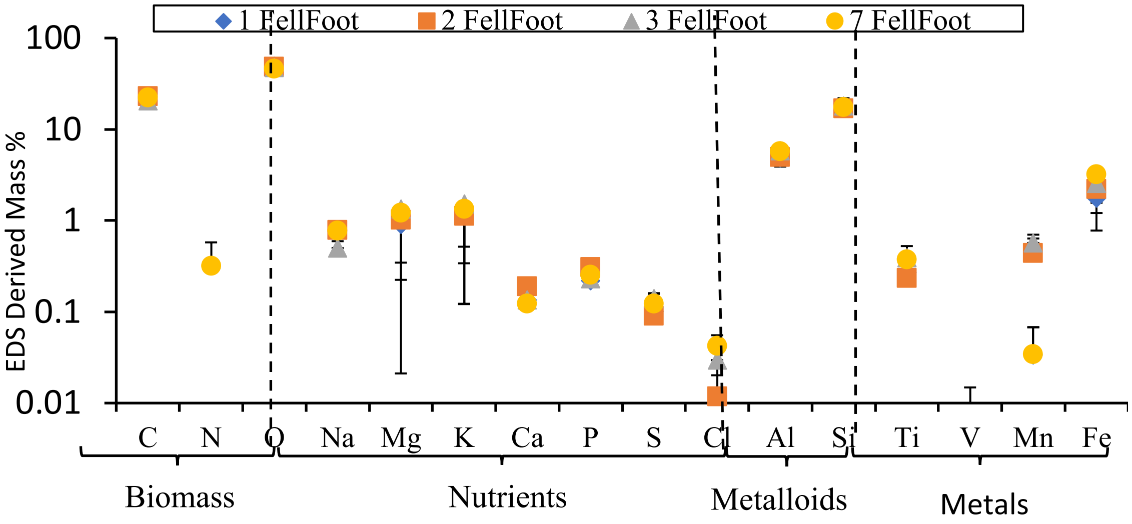

Figure 31: The relative mass % of elemental composition for different samples from Blelham Tarn (A) and Fell Foot (B)

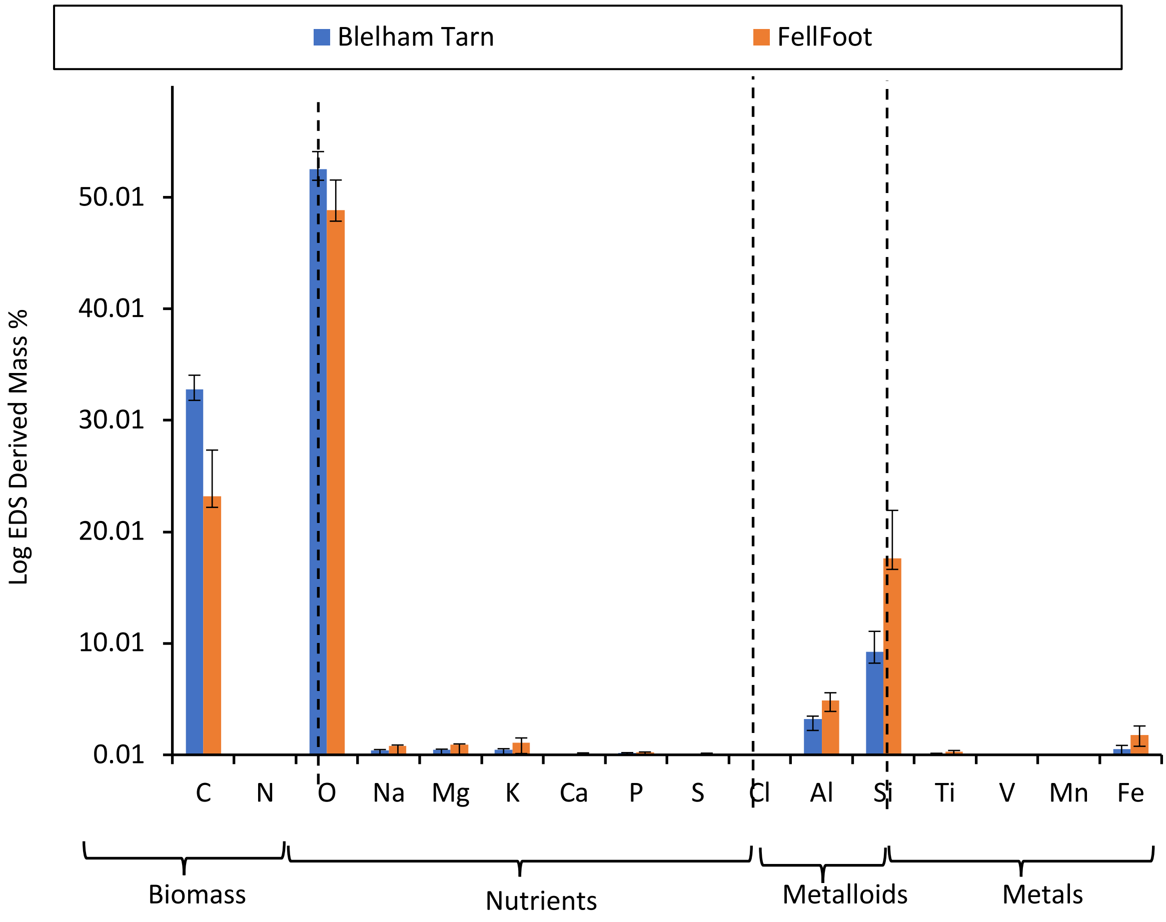

Figure 32: SEM-EDS elemental comparison for Blelham Tarn and Fell Foot samples.

4.1.2 XRD analysis

Examples of COD Match and fit (all that means is that is using a database to match the peaks and then fit known phases to available reflections) what phases might be present in soil samples are shown in Figures 33 and 34, respectively. The main point here is that while the XRD is telling us qualitatively what phases are there, it is not telling us how much of each phase is there (quantitative), so matched phases from a database (used Match, it is an XRD software and COD) could use to do a quantitative Rietveld Refinement to determine the weight % of each phase.

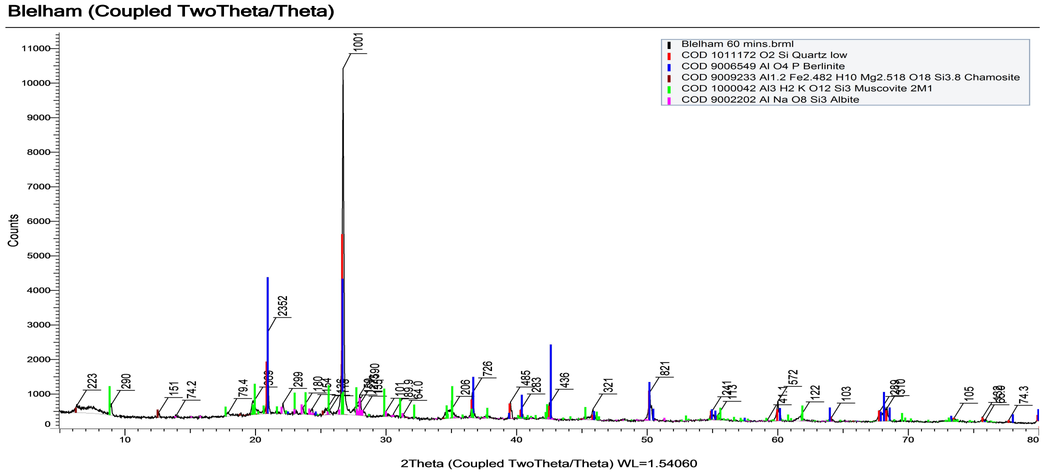

Figure 33: Matching and fitting of Blelham Tarn sample 1 using COD.

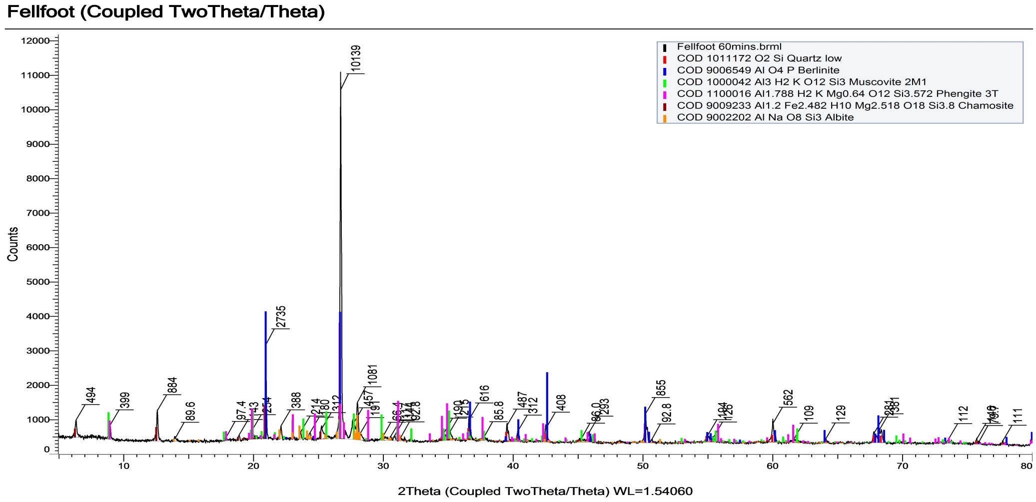

Figure 34: Matching and fitting of Fell Foot sample 1 using COD.

So, Pictures 33 and 34 used Match software and the COD (crystallographic open database) to match the peaks with the peaks of materials, high-quality patterns for each phase can be found in ICSD (Inorganic Crystal Structure Database) and then fitting them using the Rietveld Refinement in MAUD; (MAUD is a software package designed for the analysis of X-ray diffraction data). An example of pattern refinement is shown in Figure 35.

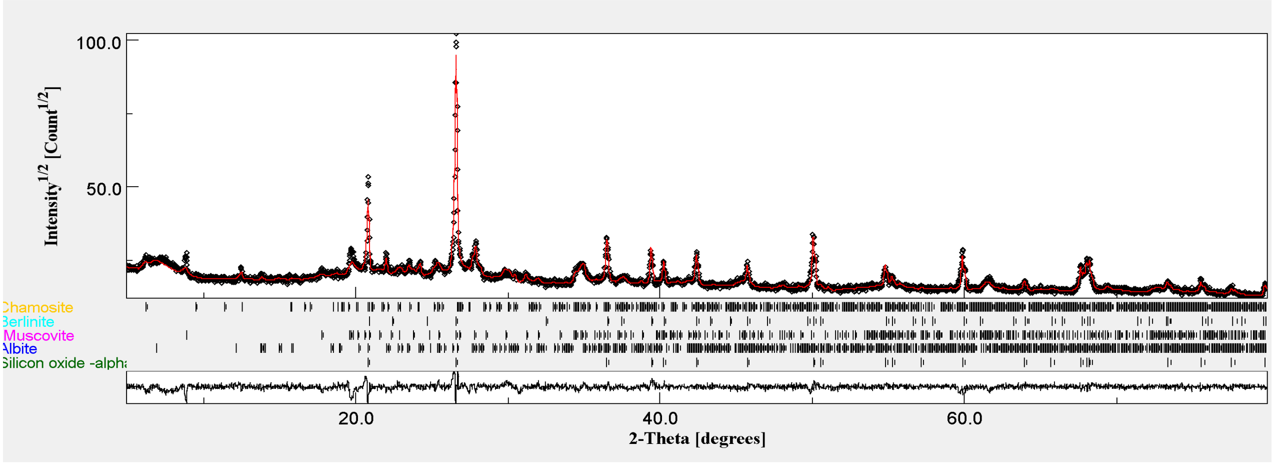

Figure 35: Example Rietveld Refinement using MAUD for Blelham Tarn sample 1.

Rietveld fits were performed on both soil samples, indicating good fits were achieved, and the limitations in terms of quantitative analysis were usually about 1 atom %, other things to be aware of with Rietveld: 1) Accurate crystal structures are required for all phases, 2) Amorphous components cannot be considered, 3) Relative weights are normalised to 100%, thus if there is an unidentified phase in there other phases may be an overestimate. A summary of the quantitative amounts of each phase derived from these fits is shown in Table 7:

Minerals	**Blelham Tarn (mass %)**	**Fell Foot (mass%)**
Silicon Oxide	49 ± 0.1	48 ± 0.1
Albite	12 ± 0.5	14 ± 0.3
Muscovite	36 ± 1.1	31 ± 0.8
Berlinite	0.17 ± 0.5	0.43 ± 0.4
Chamosite	3 ± 0.3	7 ± 0.2

Table 9: Rietveld refined quantitative analysis of the main phases found in Blelham Tarn and Fell Foot soils.

4.1.3. Summary of SEM-EDS and XRD Approaches

Several observations can be made as to the nature of the soils based on the results of the SEM-EDS analysis of pelleted samples. Samples from Blelham Tarn area show a biomass-rich environment. Nutrient analysis reveals lower mineral salts, Na, Mg, Ca, and K levels. The soil is low in mineral phases, particularly aluminosilicates and Mn, Ti and Fe oxides, compared to the collected soil sample from Fell Foot Park.

XRD in this context mainly provides phase ID, so mineral types are contained in soil samples (see Table 6). also, try a quantitative analysis (e.g., Rietveld refinement) to ascertain the differences in mounts of phases between samples. As can be seen in the Fell Foot sample (Figure 34), the quantity of phengite 3T is quite high (mass: 3.13 ± 4) %, as it is not even present in the Blelham Tarn sample (Figure 33). Whereas Blelham Tarn sample is Chamosite dominant, and Fell Foot is Berlinite dominant. Further, the major peaks and their intensities match with the reference.

4.2 Gamma-ray Measurement Results

Measurements were carried out to investigate the possibility of the assessment of trace actinides in Blelham Tarn and Fell Foot soil samples. This section describes the results achieved from a broad-energy, high-resolution γ-ray spectroscopy (HRGS) at the University of Liverpool and CCFE, where the peaks of interest are displayed and analysed to obtain estimates of activity values of actinides to compare with the samples from earlier studies. Furthermore, a combination of experimental results will be used to make additional assessments, such as ^{241}Am and ^{241}Pu abundances within the samples.

4.2.1 ^{241}Am abundance

The gamma spectra show clear evidence of a ^{241}Am peak in all samples, as shown in Figure 36. The results following spectral analysis are also displayed, including the transformation of the counts to absolute mass concentrations, the background subtraction, efficiency correction and using the Bateman equation to estimate the mass per gram of ^{241}Pu using estimates of the mass of ^{241}Am derived from these data. In addition to americium, there is a line at 63.3 keV ^{234} Th peak, a decay product of ^{238}U, where the abundance of ^{238}U accepts neutrons and covert to ^{239}Pu. ^{241}Am concentrations (Bq g^{-1}) were determined for all the samples collected from Blelham Tarn and Fell Foot. Example for ^{241}Am peaks (in line 59.5 keV) as highlighted from sample 1, for Blelham Tarn (A) and Fell Foot (B) of a 24-hour count as illustrated in Figure 36.

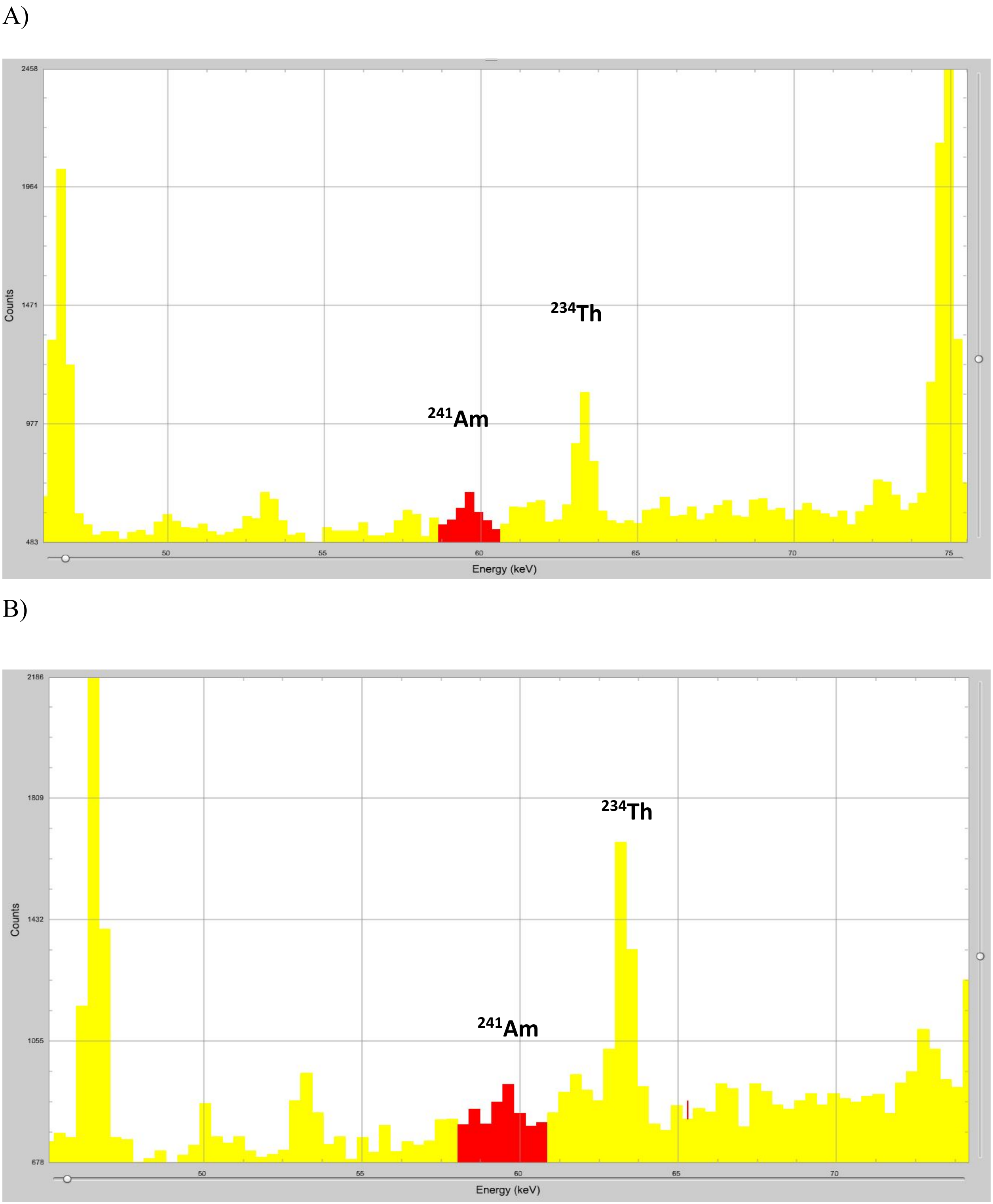

Figure 36: ^{241}Am peaks (in line 59.5 keV) as highlighted from sample 1, for Blelham Tarn (A) and Fell Foot (B) of a 24-hour count, the Energy (keV) and count per second as shown in X and Y scales, respectively.

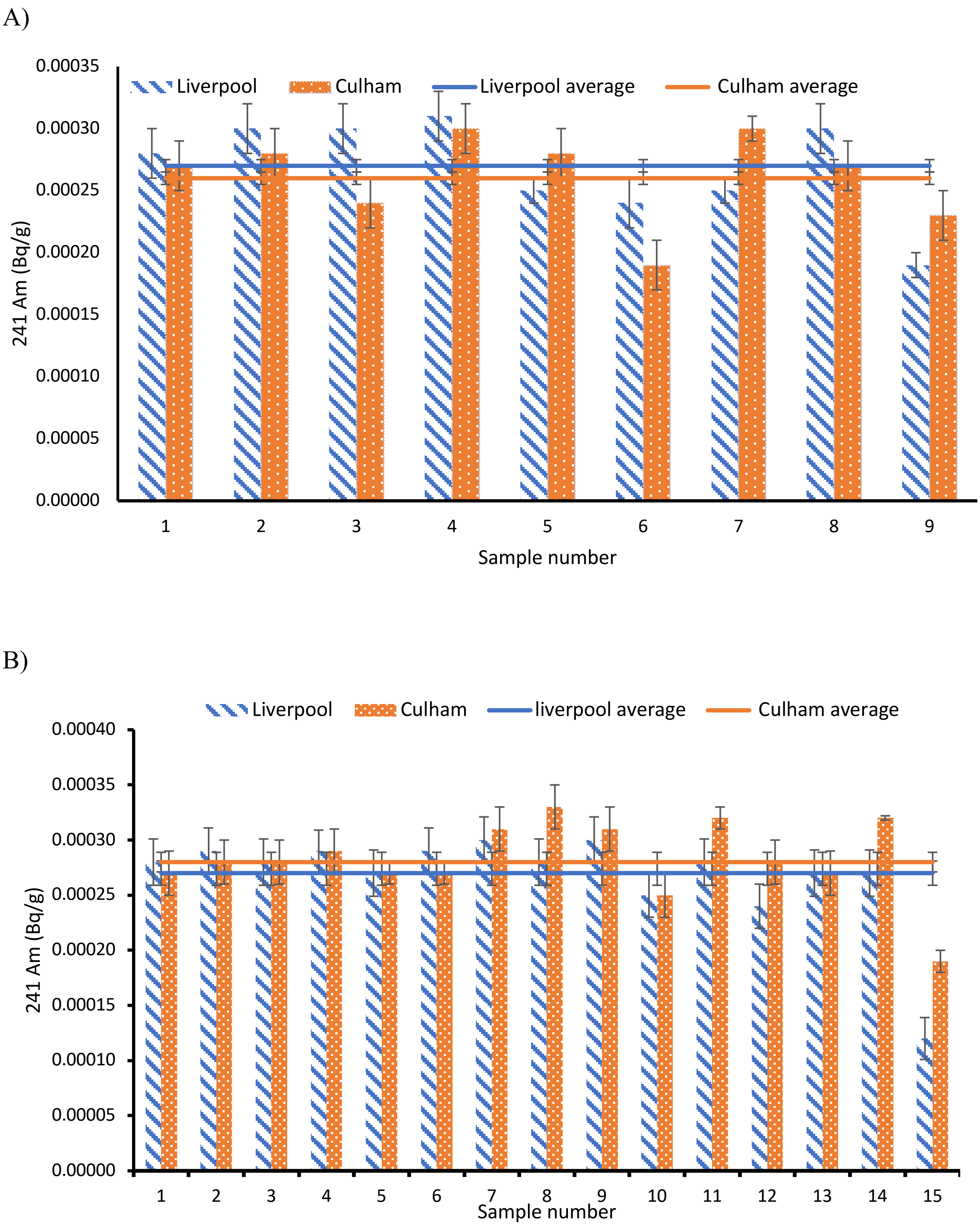

Figure 37: ^{241}Am abundance (Bq g^{-1}) calculated from the counts measured in the ^{241}Am 59.5 keV peak in the gamma-ray spectra measured using the BEGe detector at Liverpool University and CCFE From (A) Blelham Tarn and (B) Fell Foot Location

In summary, ^{241}Am abundance has been identified in most Blelham Tarn and Fell Foot samples utilising HRGS. As seen in Figure 36, the highlighted peak of interest was taken from B1 and F1 spectra for a 24-hour count to show the ^{241}Am peak in the region of 59.5keV. It is a small peak but significant enough to identify using experimental procedures that are described in Chapter 3 (Signal-to-Noise technique and the optimum background for several subtractions).

Furthermore, the average level of ^{241}Am of Blelham Tarn samples was $(27 \pm 1) \times 10^{-5}$ (Bq g^{-1}) and $(27 \pm 1) \times 10^{-5}$ (Bq g^{-1}), these measurements took place at the University of Liverpool and CCFE, respectively, to estimate the mass concentration of ^{241}Am across the samples. Similarly, the abundance of ^{241}Am was $(26\pm 1) \times 10^{-5}$ (Bq g^{-1}) and $(28 \pm 1) \times 10^{-5}$ for Fell Foot samples determined at Liverpool and CCFE. ^{241}Am averages can be clarified in Table 10:

Measurements at	**Blelham Tarn**	**Fell Foot**
^{241}Am (Bq kg^{-1}) Liverpool average	0.27 ± 0.01	0.27 ± 0.01
^{241}Am (fg g^{-1}) Liverpool average	2.13 ± 0.10	2.11 ± 0.09
^{241}Am (Bq kg^{-1}) CCFE average	0.26 ± 0.01	0.28 ± 0.01
^{241}Am (fg g^{-1}) CCFE average	2.07 ± 0.09	2.24 ± 0.07

Table 10: ^{241}Am averages of Blelham Tarn and Fell Foot samples that were estimated at Liverpool and CCFE.

4.2.2 ^{241}Pu abundance

The assessment of the mass concentration of ^{241}Pu using estimates of ^{241}Am and techniques for this calculation were described in the experimental chapter (using the Bateman equation), Figure 38 presented the ^{241}Pu (Bq kg ^{1}) for Blelham Tarn and Fell Foot samples

A)

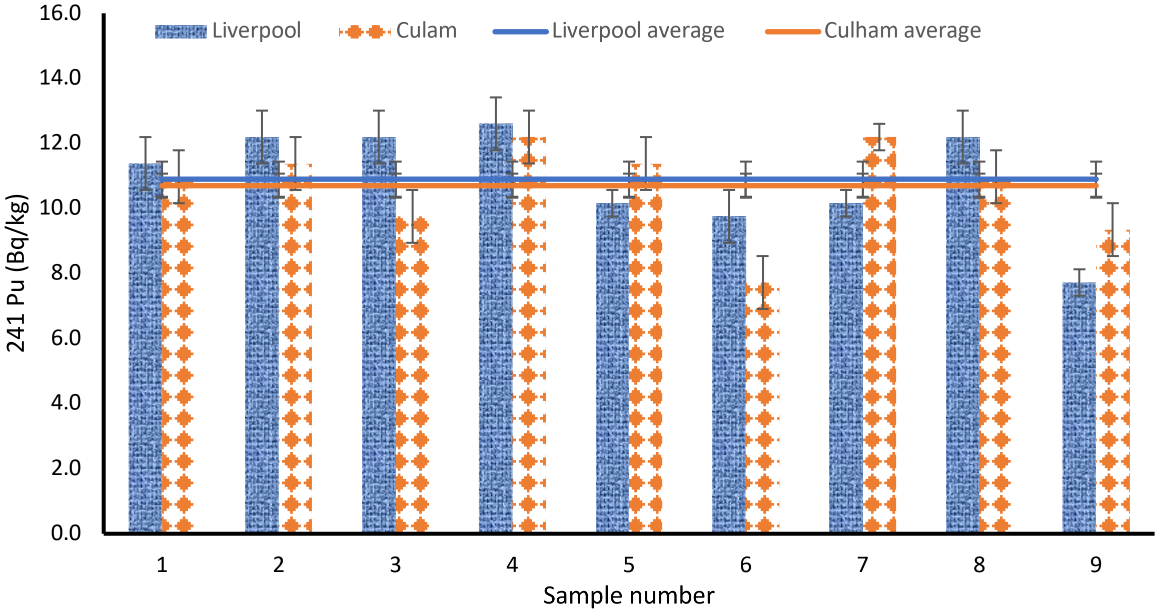

B)

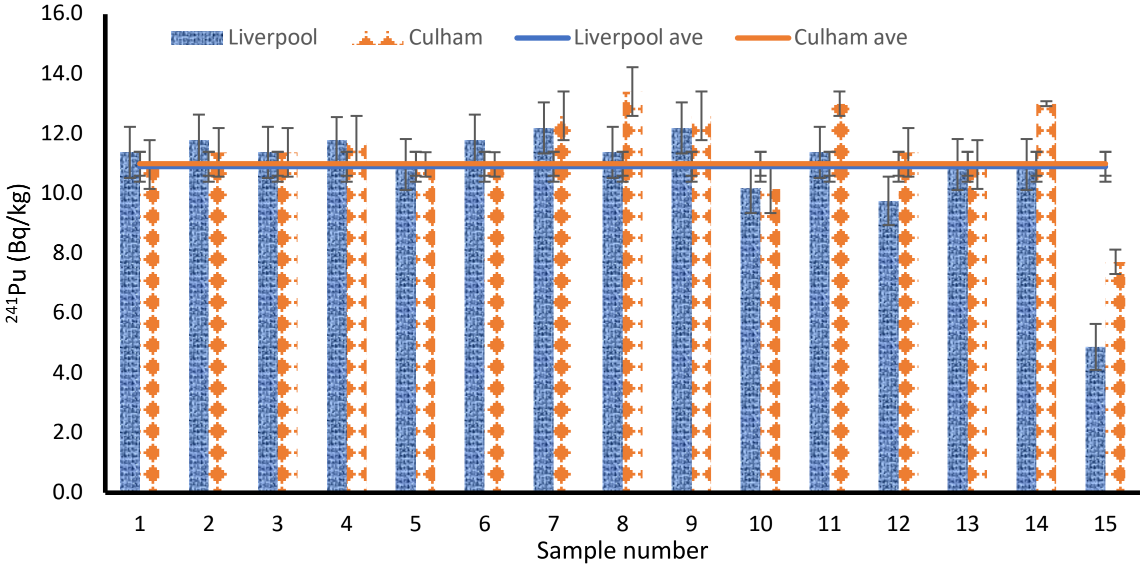

Figure 38: ^{241}Pu abundance (Bq kg ^{1}) calculated from abundances of ^{241}Am. As a result, the abundances are directly proportional to those of ^{241}Am from the Blelham Tarn (A) and Fell Foot (B)

In summary, because ^{241}Am and ^{241}Pu are highly correlated, with about 99.7% of the intensity of decay ^{241}Pu to ^{241}Am, as there are two modes of decay and it has nothing to do with half-life, it was able to calculate the quantity of ^{241}Pu present in each spectra using the assessed quantities of ^{241}Am through the 59.5 keV ^{241}Am peak. This can be done using the Bateman equation and assuming the time for 30 years [70], which characterizes the abundances and activity of radioactive elements in a decay chain as a time function, depending on the decay rates (daughter) and original abundances of the isotopes (parent) in the supplied material.

$$A_{Am}(t) = \frac{\lambda_{Am}\, A_{Pu}(0)}{(\lambda_{Am} - \lambda_{Pu})}\left(e^{-\lambda_{Pu}t} - e^{-\lambda_{Am}t}\right) \qquad (4.1)$$

$$A_{Pu}(0) = \frac{A_{Am}(t)\,(\lambda_{Am} - \lambda_{Pu})}{\left(e^{-\lambda_{Pu}t} - e^{-\lambda_{Am}t}\right)\lambda_{Am}} \qquad (4.2)$$

The data of ^{241}Pu for Blelham Tarn and Fell Foot samples can be shown in Table 11, these measurements took place at the University of Liverpool and CCFE.

Measurements at	**Blelham Tarn**	**Fell foot**
^{241}Pu (Bq kg ^{1}) Liverpool average	11 ± 0.5	11 ± 0.5
^{241}Pu (fg g ^{1}) Liverpool average	2.9 ± 0.1	2.8 ± 0.1
^{241}Pu (Bq kg ^{1}) CCFE average	10 ± 0.5	11 ± 0.4
^{241}Pu (fg g ^{1}) CCFE average	2.8 ± 0.1	3.0 ± 0.1

Table 11: ^{241}Pu averages of Blelham Tarn and Fell Foot samples that were estimated at Liverpool and CCFE.

4.3 Accelerator Mass Spectrometry Measurements

Following the HRGS detection, the need for a complementary assessment of the other plutonium isotopes in the soil was identified. The AMS measurements were carried out at ETH Zürich. The results of the AMS measurements are presented in the figures below as mass concentrations per gram of sample of ^{239}Pu, ^{240}Pu and ^{244}Pu. As the ratio of plutonium ^{240}Pu/^{239}Pu and ^{244}Pu/^{239}Pu. it is presented and compared to the radiation measurement results, including the average value calculated for the project samples for comparison with the previous studies.

^{239}Pu, ^{240}Pu and ^{244}Pu abundances data across the Blelham Tarn and Fell Foot samples are indicated in Figures 39, 40, 41, 42 and 43, respectively. ^{240}Pu/^{239}Pu and ^{244}Pu/^{239}Pu isotopic ratios data across the Blelham Tarn and Fell Foot samples are shown in Figures 44 and 45, respectively.

4.3.1 ^{239}Pu abundances for Blelham Tarn and Fell Foot Park

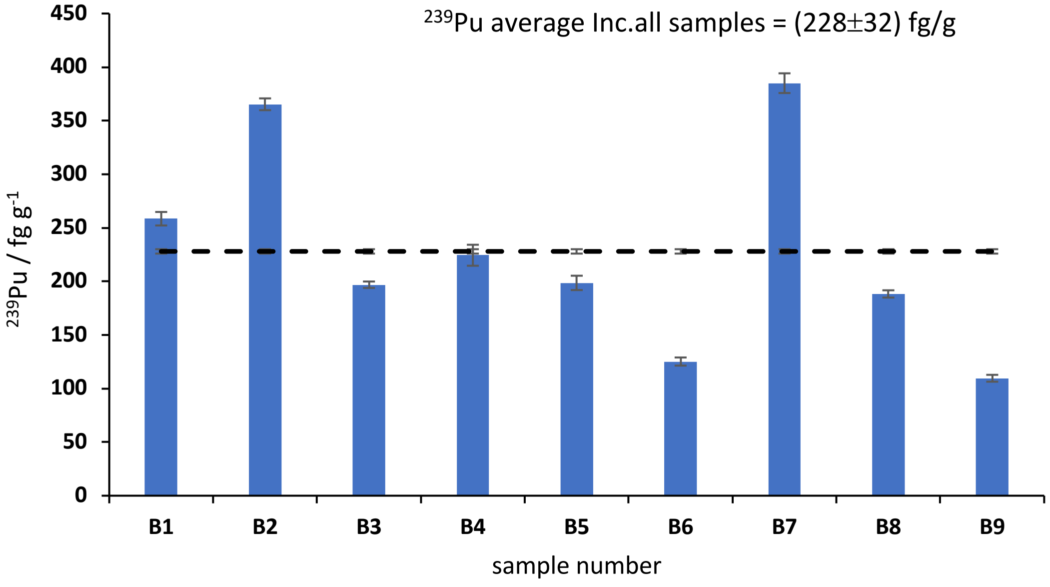

B)

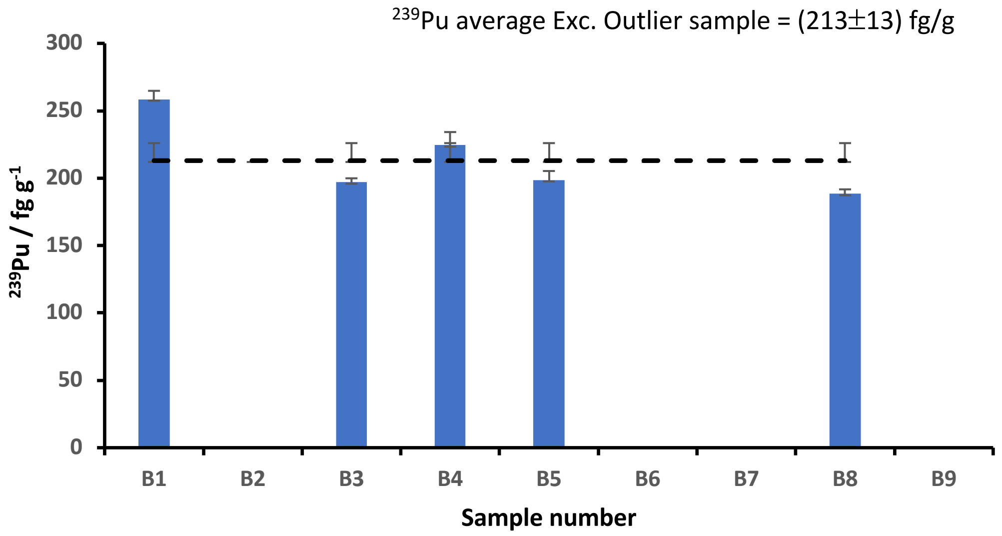

Figure 39: Abundances of ^{239}Pu as measured with the AMS system at ETH Zürich for Blelham Tarn samples, (A) the dashed line indicates the average of ^{239}Pu includes all the samples, (B) shows the average of ^{239}Pu excludes outlier sample.

A)

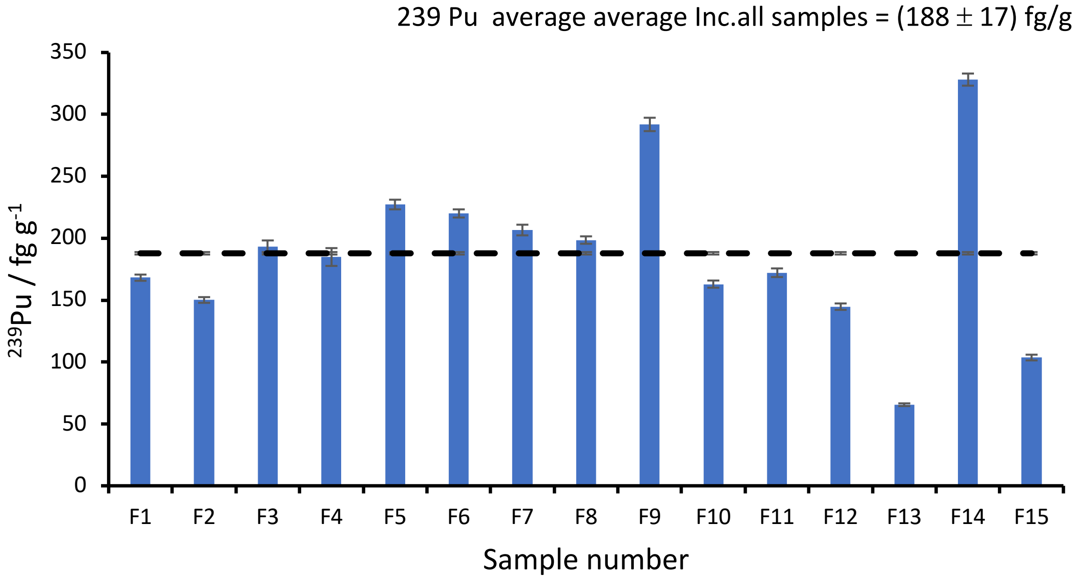

B)

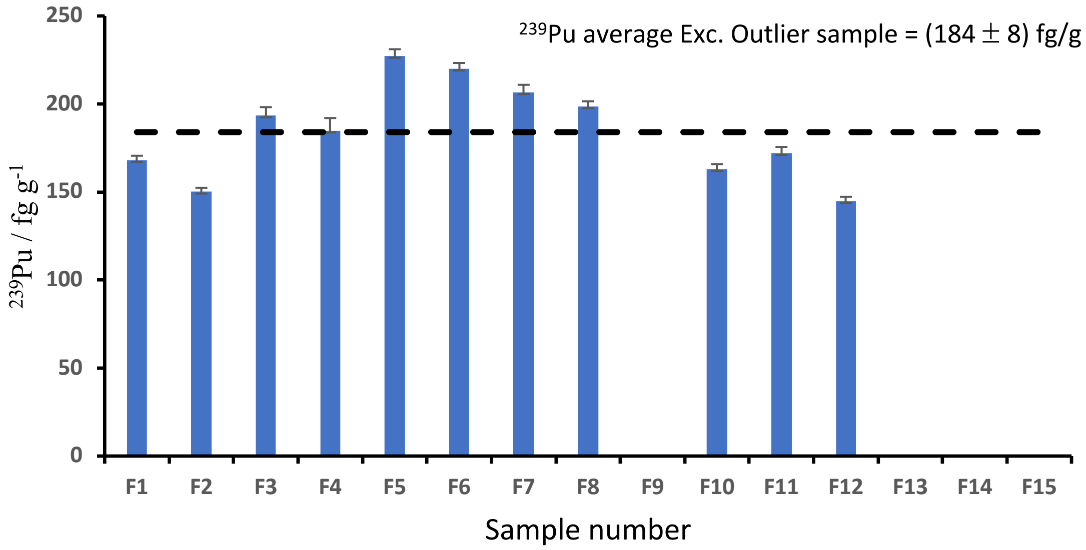

Figure 40: Abundances of ^{239}Pu as measured with the AMS system at ETH Zürich for Fell Foot samples, (A) the dashed line indicates the average of ^{239}Pu includes all the samples, (B) shows the average of ^{239}Pu excludes outlier sample.

4.3.2 ^{240}Pu abundances for Blelham Tarn and Fell Foot Park

A)

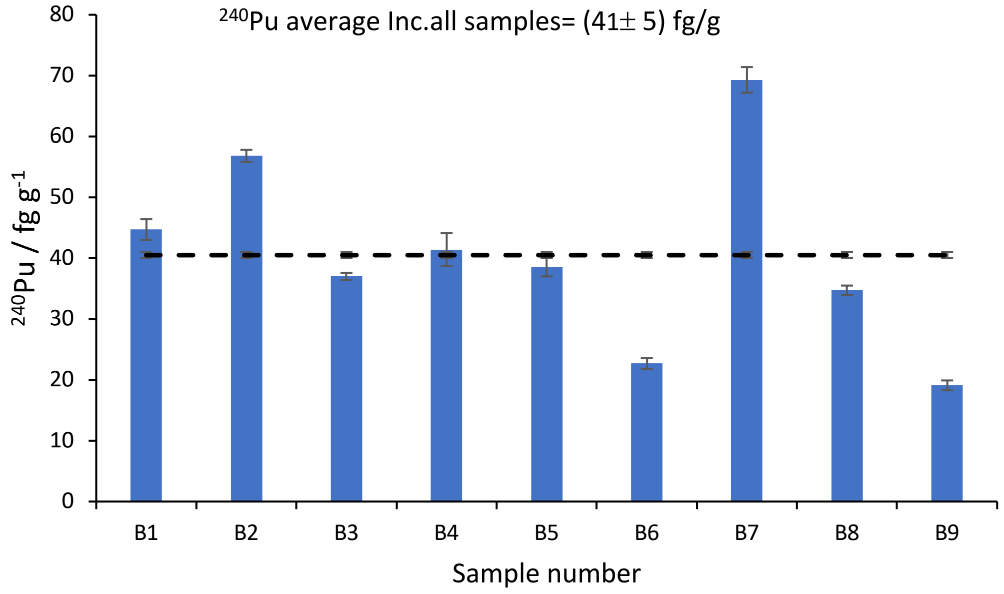

B)

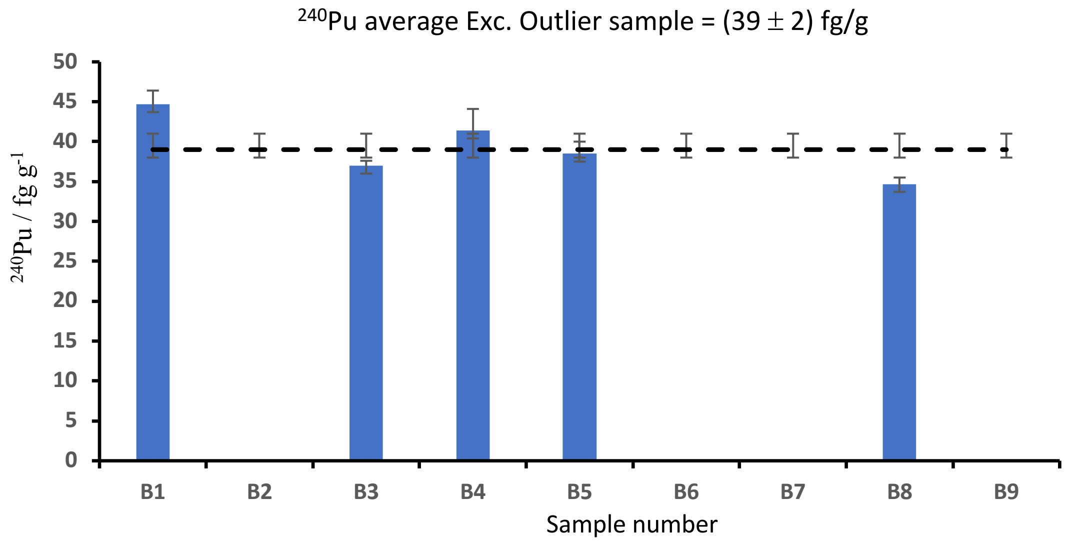

Figure 41: Abundances of ^{240}Pu as measured with the AMS system at ETH Zürich for Blelham Tarn samples, (A) the dashed line indicates the average of ^{240}Pu includes all the samples, (B) shows the average of ^{240}Pu excludes outlier sample.

A)

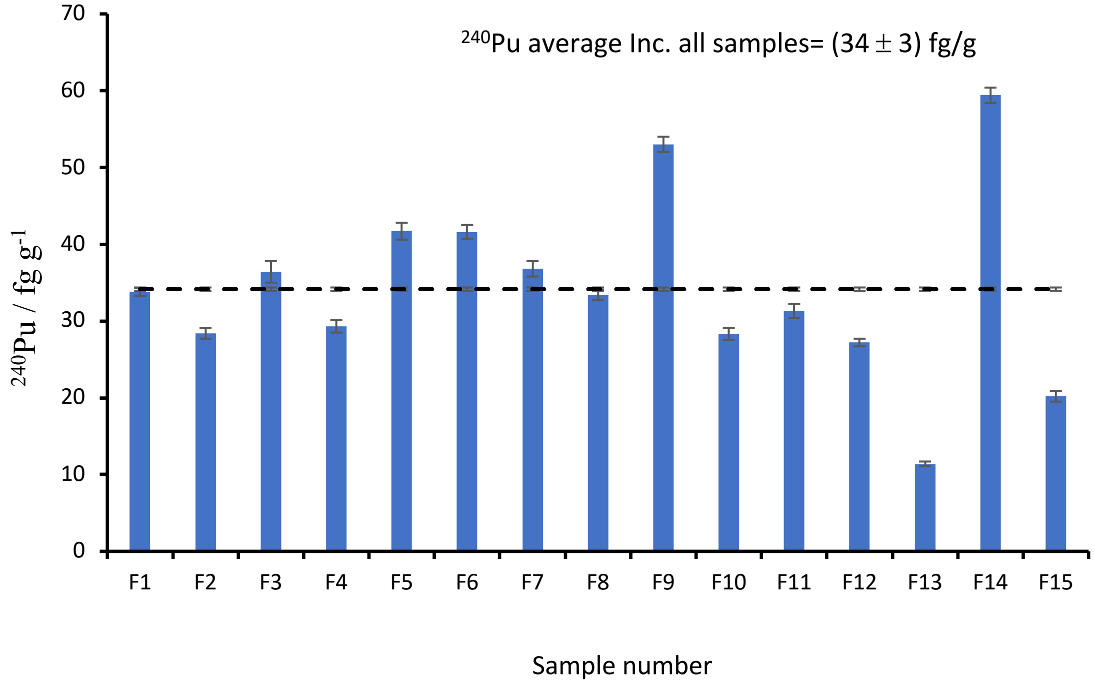

B)

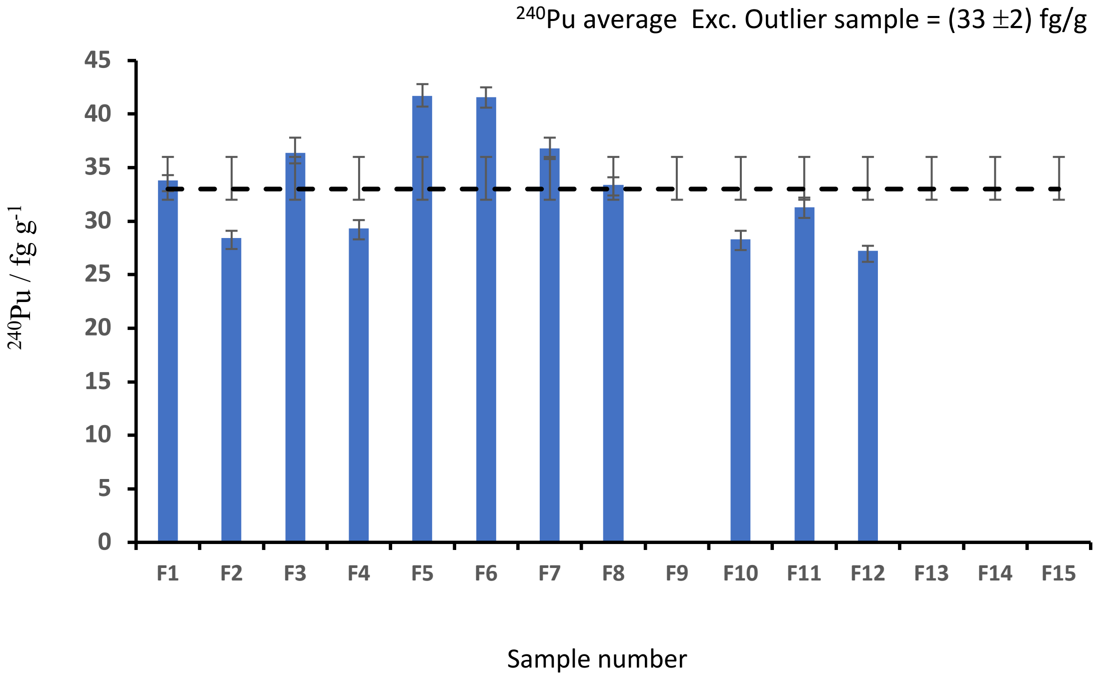

Figure 42: Abundances of ^{240}Pu as measured with the AMS system at ETH Zürich for Fell Foot samples, (A) the dashed line indicates the average of ^{240}Pu includes all the samples, (B) shows the average of ^{240}Pu excludes outlier sample.

4.3.3 ^{244}Pu abundances for Blelham Tarn and Fell Foot Park

It can be noted that results for samples B4 - B9, F3 and F15 are not shown (see Figure 43), because AMS did not get a signal count for ^{244}Pu, so we could instead show an upper limit for ^{244}Pu in those samples using the estimate by Feldman and Cousins [82].

In brief, they calculated that for a given level of confidence the number of counts you might expect (based on Poisson Statistics) considering the number of counts it measured and the number of counts of the blank sample. Further, we could measure zero counts (n (0) = 0) and the average counts of the 1.7cts, in the table suggested that the underlying interval for the Poisson signal ranges from 0 to 3.26 counts. So, it has taken 3.26 counts to calculate an upper limit for each sample with 0 ^{244}Pu counts "based on 99% CL), by using the one count equivalent for ^{244}Pu, multiplying that by 3.26 and dividing it by 5 g (sample weight) and 1000 (atto-gram → femtogram) to get the upper limit for the ^{244}Pu concentration for each sample that had zero counts on ^{244}Pu. The following tables illustrate the measurements of ^{244}Pu from Zürich (the combined data =2.6×10^{-2} fg g^{-1}, n=16) and the upper limit of ^{244} Pu for Blelham (see Table. 12) and Fell Foot (see Table 13) using the estimate by Feldman.

Sample number	**^{244}Pu data from Zürich for Blelham Tarn (fg g^{1})**	**^{244}Pu upper limit for Blelham using the estimate by Feldman (fg g^{1})**
B1	0.029 ± 0.011	0.029 ± 0.011
B2	0.059 ± 0.015	0.059 ± 0.015
B3	0.035 ± 0.015	0.035 ± 0.015
B4	n.a.	$0.264 \pm 3.24\times10^{-5}$
B5	n.a.	$0.119 \pm 4.83\times10^{-5}$
B6	n.a.	$0.092 \pm 5.48\times10^{-5}$
B7	n.a.	$0.123 \pm 4.75\times10^{-5}$
B8	n.a.	$0.048 \pm 7.61\times10^{-5}$
B9	n.a.	$0.042 \pm 8.13\times10^{-5}$

Table 12: The actual data of ^{244}Pu (fg/g) received from Zürich as shown in the first column and the upper limit for the ^{244}Pu concentration for Blelham Tarn samples (B4, B5, B6, B7, B8, B9) as shown in the second column. Overall, the upper limits in samples B4 to B9 are higher than the other samples' results because they generally had low output.

Sample number	**^{244}Pu data from Zürich for Fell Foot (fg g^{1})**	**^{244}Pu upper limit for Fell Foot using the estimate by Feldman**
F1	0.014 ± 0.009	0.014 ± 0.009
F2	0.016 ±0.026	0.016 ± 0.026
F3	n.a.	$0.030 \pm 9.65\times10^{-5}$
F4	0.028 ± 0.029	0.028 ± 0.029
F5	0.037 ± 0.029	0.037 ± 0.029
F6	0.040 ± 0.010	0.040 ± 0.010
F7	0.016 ± 0.009	0.016 ± 0.009
F8	0.018 ± 0.007	0.018 ± 0.007
F9	0.027 ± 0.028	0.027 ± 0.028
F10	0.025 ± 0.026	0.025 ± 0.026
F11	0.014 ± 0.011	0.014 ± 0.011
F12	0.007 ± 0.011	0.007 ± 0.011
F13	0.008 ± 0.007	0.008 ± 0.007
F14	0.041 ± 0.020	0.041 ± 0.020
F15	n. a.	$0.062 \pm 6.71\times10^{-5}$

Table 13: The actual data of ^{244}Pu (fg/g) received from Zürich as shown in the first column and the upper limit for the ^{244}Pu concentration for Fell Foot samples (F3 and F15) as shown in the second column. Overall, the upper limits in samples F3 and F4 are higher than the other samples' results because they generally had low output.

A)

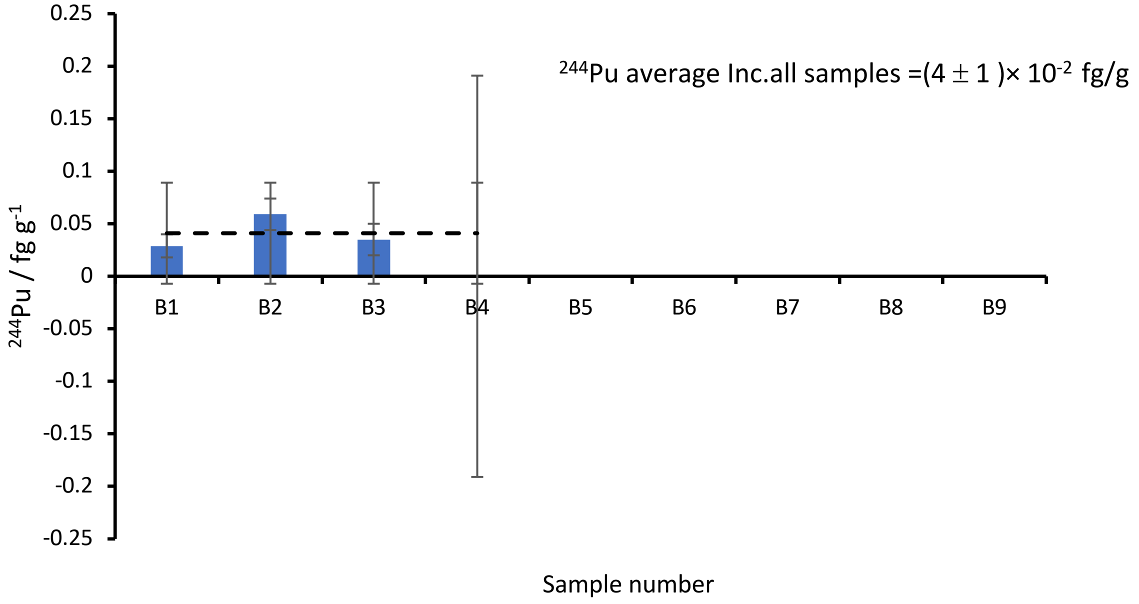

B)

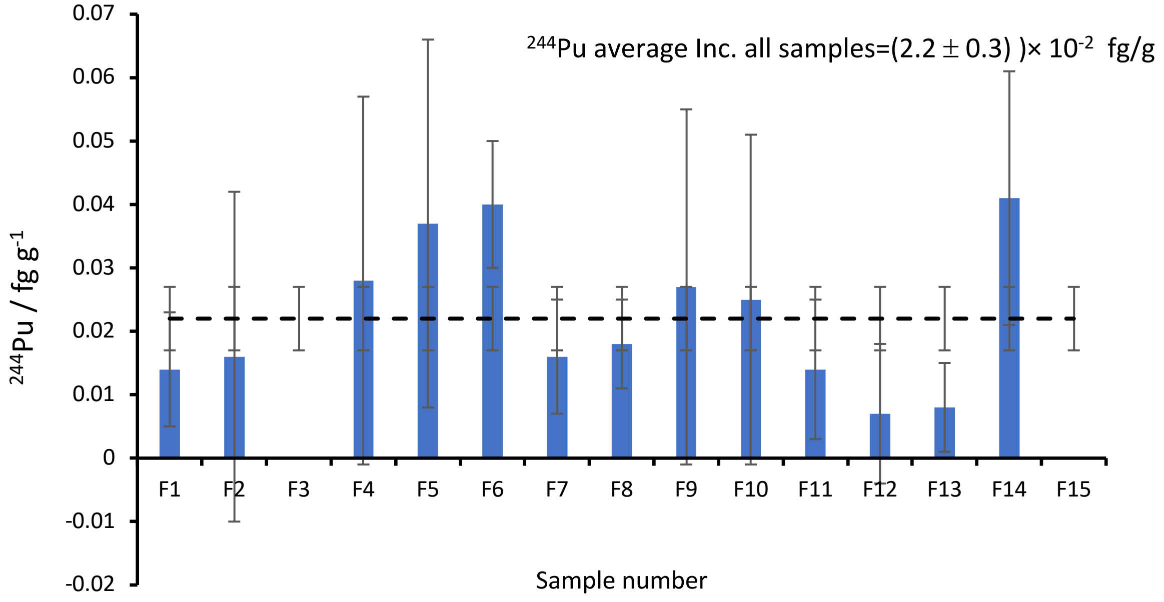

Figure 43: Abundances of ^{244}Pu as measured with the AMS system at ETH Zürich From Blelham Tarn(A) and Fell Foot (B).

The results of Pu concentrations, particularly in Figures.39, 40 41, 42 and 43 (see sections 4.3.1, 4.3.2 and 4.3.3) show that ^{239}Pu levels in B2 and B7 are significantly higher due to the quality and depth of the samples (more details can be explained in the discussion chapter). The ^{239}Pu averages in B2 of (365 ± 5.5) fg g^{-1} and in sample B7 of (385 ± 9.2) fg g^{-1} are double the dataset averages. However, B6 and B9 show a lower level of ^{239}Pu than the rest of the samples of (125 ± 4) fg g^{-1} and (107 ± 3.2) fg g^{-1}, respectively, in terms of the Chi-square distribution χ_v^2. In addition, ^{239}Pu abundances in Fell Foot samples demonstrate considerably lower levels than in Blelham Tarn samples. As seen in Figure 40, in the 4.3.1 section, the greatest level of ^{239}Pu is shown in F9 and F14 at (292 ± 5.4) fg g^{-1} and (328 ± 5) fg g^{-1}, respectively, this amount is approximately triple the level at samples F13 and F15.

Moving to ^{240}Pu abundance, the highest level is deserved in samples B7 and B2 of (56 ± 1) fg g^{-1} and (69.3 ± 2.1) fg g^{-1} respectively. The average level of ^{239}Pu,^{240}Pu, and ^{244}Pu with the combined data for Blelham Tarn and Fell Foot and the corresponding χ_v^2 are validated in Table 14:

Site	**Blelham / fg g^{-1}**				**Fell Foot / fg g^{-1}**				**Combined / fg g^{-1}**
Isotope	Complete	χ_v^2	Exc. outliers	χ_v^2	Complete	χ_v^2	Exc. Outliers	χ_v^2	
^{239}Pu	228 ± 32	315	213 ± 13	3.2	188 ± 17	653	184 ± 8	2.8	203 ± 16
^{240}Pu	41 ± 5	230	39 ± 2	2.3	34 ± 3	385	33 ± 2	1.9	37 ± 3
^{244}Pu / $\times 10^{-2}$	4 ± 1		4 ± 1		2.2 ± 0.3		2.2 ± 0.3		2.6 ± 0.4

Table 14: ^{239}Pu, ^{240}Pu, ^{244}Pu averages of Blelham Tarn and Fell Foot samples estimated at University Liverpool and CCFE.

Overall, the data of ^{239}Pu, ^{240}Pu and ^{244}Pu abundances for Blelham Tarn, including all the samples were (228 ± 32) fg g^{-1}, (41 ± 5) fg g^{-1}, and (4 ± 1) fg g^{-1}, respectively. Moreover, the data of ^{239}Pu, ^{240}Pu and ^{244}Pu abundances for Blelham Tarn, excluding the outlier the samples were (213 ± 13) fg g^{-1}, (39± 2) fg g^{-1}, and (4 ± 1) fg g^{-1}, respectively. In addition, the data of ^{239}Pu, ^{240}Pu and ^{244}Pu abundances for Fell Foot, including all the samples were (188 ± 17) fg g^{-1}, (34 ± 3) fg g^{-1}, and (2.2 ± 0.3) fg g^{-1}, respectively. Moreover, the data of ^{239}Pu, ^{240}Pu and ^{244}Pu abundances for Fell Foot, excluding the outlier the samples were (184 ± 8) fg g^{-1}, (33± 2) fg g^{-1}, and (2.2 ± 0.3) fg g^{-1}, respectively. It should be highlighted in more detail how was the uncertainty calculated for the average mass of each value; the calculation of the mean values and then the propagation of the analytical errors of each data point, which got quite small uncertainties for the mean value. When calculating the standard error of the mean (standard deviation divided by square root (n), the value is significantly larger. This indicates that there is some additional scatter ("geological scatter) in the samples that is not reflected by the analytical uncertainties (AMS errors). This means, they indeed reflect different levels of contamination. In summary, the suggestion is that the standard error of the mean is used instead of the propagated analytical uncertainties.

4.3.4 ^{240}Pu/^{239}Pu Ratio

A)

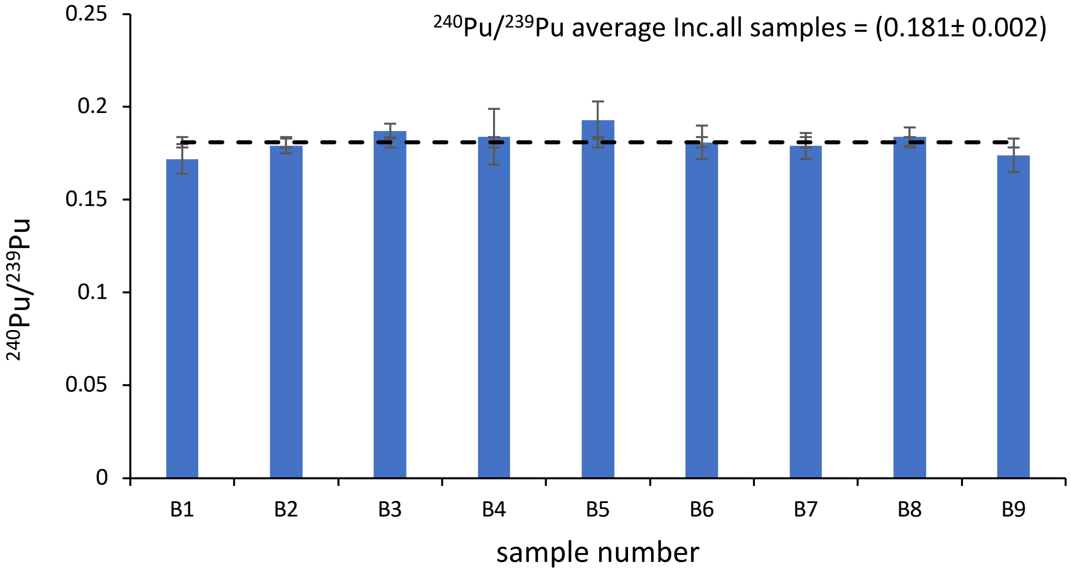

B)

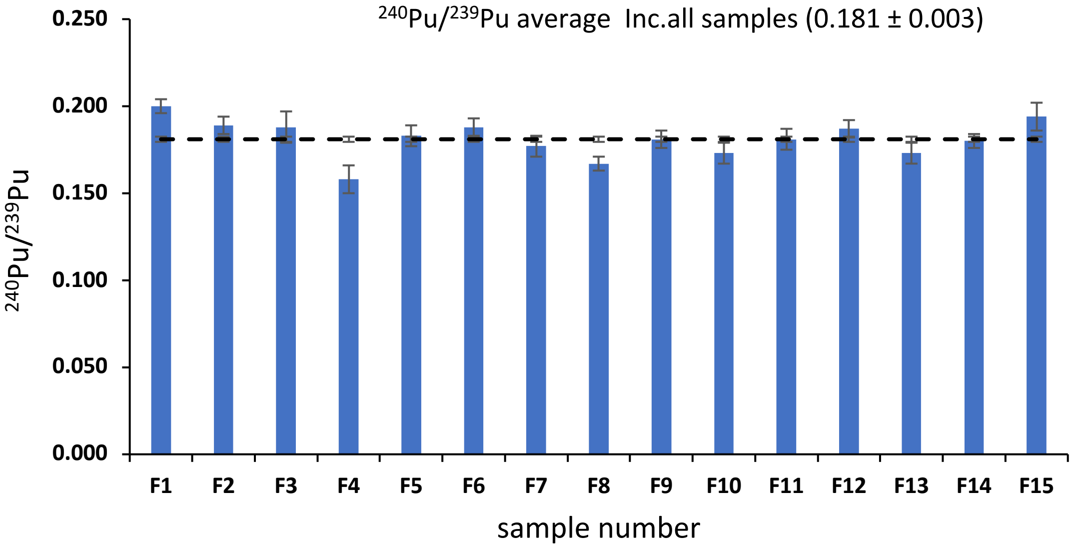

Figure 44: ^{240}Pu/^{239}Pu isotopic ratio as measured with the AMS system at ETH Zürich From Blelham Tarn (A) and Fell Foot (B). The broken line indicates the average of ^{240}Pu/^{239}Pu.

4.3.5 ^{244}Pu/ ^{239}Pu Ratio

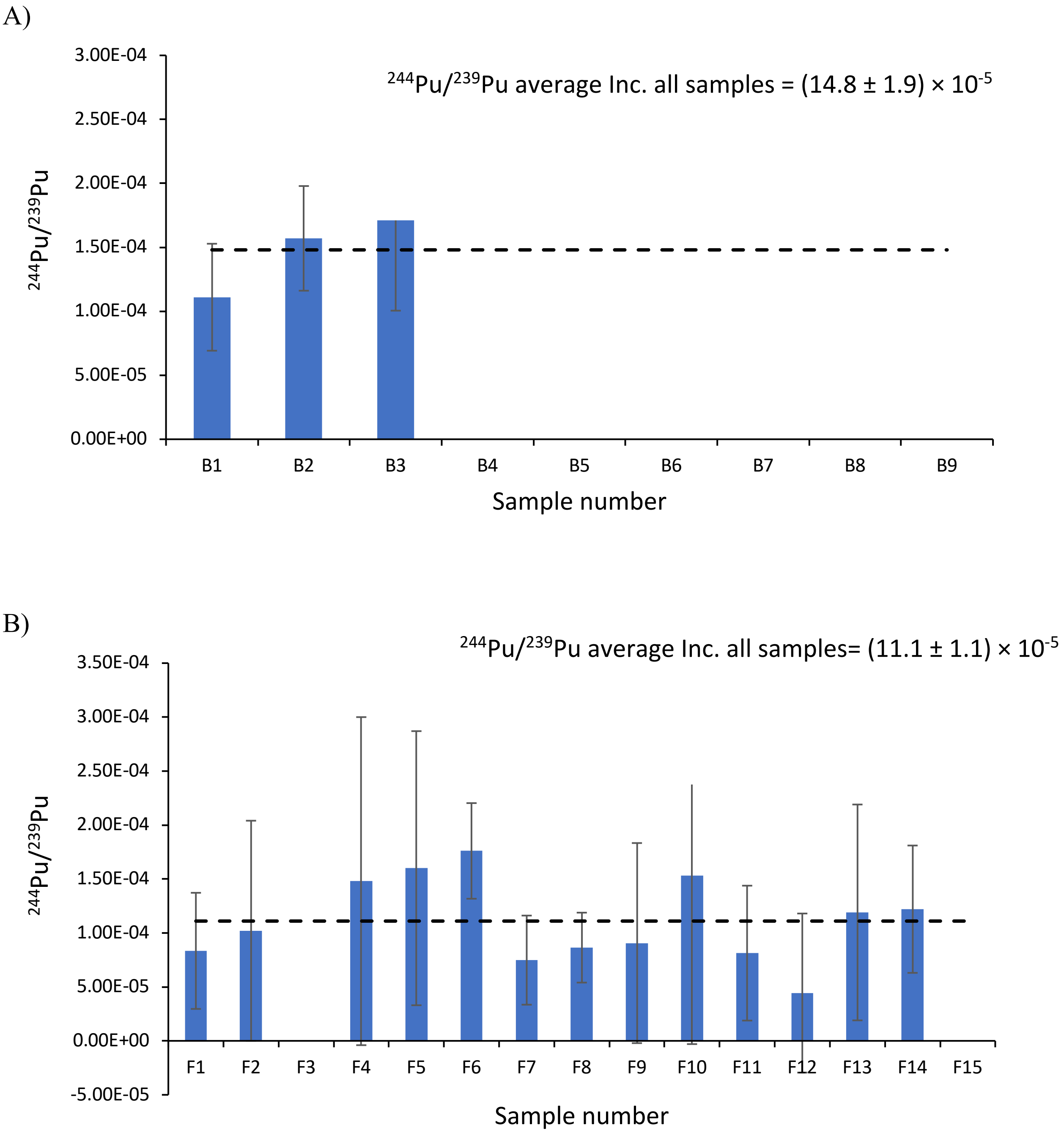

Figure 45: The ^{244}Pu/^{239}Pu isotopic ratio as measured with the AMS system at ETH Zürich From Blelham Tarn (A) and Fell Foot (B). The break line indicates the average of ^{244}Pu/^{239}Pu.

Because AMS did not get a single count for ^{244}Pu/^{239}Pu, so we could instead show an upper limit for ^{244}Pu/^{239}Pu in those samples using the estimate by Feldman and Cousins [82]. The average isotopic ratio of ^{244}Pu/^{239}Pu measured in Blelham Tarn using the Feldman mothed is (44 ± 12) × 10^{-5} for (n=9), and the average isotopic ratio of ^{244}Pu/^{239}Pu for Fell Foot samples is (15± 3) × 10^{-5} for (n=15) as shown in table 15.

A)

Sample number	**^{244}Pu/^{239}Pu without upper limit (× 10^{-5})**	**$^{2\ 44}$Pu/^{239}Pu with upper limit (× 10^{-5})**
B1	11.4 ± 4.27	11.4 ± 4.27
B2	16.1 ± 4.17	16.1 ± 4.17
B3	17.9 ± 7.17	17.9 ± 7.71
B4	n. a	11.8 ± 5.14
B5	n. a	59.7 ± 2.01
B6	n. a	73.8 ± 2.27
B7	n. a	31.9 ± 0.76
B8	n. a	25.4 ± 0.46
B9	n. a	38.3 ± 1.14

B)

Sample number	**^{244}Pu/^{239}Pu without upper limit (× 10^{-5})**	**^{244}Pu/^{239}Pu with upper limit (× 10^{-5})**
F1	8.51 ± 1.62	8.51 ± 1.62
F2	10.4 ± 1.68	10.4 ± 1.68
F3	n. a	15.4 ± 0.39
F4	15.1 ± 1.55	15.1 ± 15.5
F5	16.3 ± 1.29	16.3 ± 12.9
F6	18.0 ± 4.52	18.0 ± 4.52
F7	7.64 ± 4.22	7.64 ± 4.22
F8	8.82 ± 3.31	8.82 ± 3.31
F9	9.25 ± 9.47	9.25 ± 9.47
F10	15.6 ± 1.60	15.6 ± 16.0
F11	8.30 ± 6.38	8.30 ± 6.38
F12	4.52 ± 7.52	4.52 ± 7.52
F13	12.1 ± 1.02	12.1 ± 10.2
F14	12.4 ± 6.02	12.4 ± 6.02
F15	n. a	59.4 ± 1.31

Table 15: isotopic ratio for ^{244}Pu/^{239}Pu as measured with the AMS system at ETH Zürich with upper limit and without upper limit for Blelham Tarn (A) and Fell Foot (B).

The average ratios of $^{240}Pu/^{239}Pu$ across the samples are consistent with a global fallout average ratio [2]. Additionally, the combined level of $^{244}Pu/^{239}Pu$ at (11.8 ± 1) × 10^{-5} as shown in Table 16 used for local contribution to the environment in the next section.

Ratio (at/at)	**Blelham Tarn**	**Fell Foot**	**Combined**
$^{240}Pu/^{239}$ Pu	0.181 ± 0.002	0.181 ± 0.003	0.181 ± 0.001
$^{244}Pu/^{239}Pu$**/× 10^{-5}**	14.8 ± 1.9	11.1 ± 1.1	11.8 ± 1.0

Table 16: $^{240}Pu/^{239}Pu$ and $^{244}Pu/^{239}Pu$ isotopic ratios for Blelham Tarn and Fell Foot with combination data.

4.4 Depth Dependence

The average mass concentration of ^{239}Pu measured in the soil samples obtained at regions of Blelham Tarn is (228 ± 32) fg g^{-1} (n=9). Sample B2 (365.3 ± 6) fg g^{-1} and sample B7 (385 ± 9) fg $g^{-1}$are significantly higher in mass concentrations of ^{239}Pu compared to the other sample, although, samples B6 (125 ± 4) fg g^{-1} and B9 (109 ± 3.2) fg g^{-1} have a lower abundance of ^{239}Pu than the set of samples.

Fell foot is significantly lower for ^{239}Pu than Blelham Tarn at abundances of (188 ± 17) fg g^{-1} (n=15) in the sample set. Sample F9 (292 ± 5) fg g^{-1} and sample F14 (328 ±5) fg g^{-1} are greater for ^{239}Pu concentration than the average of the sample set, while samples F13 and F15 are significantly lower for ^{239}Pu than the most Fell Foot samples at the level of (65±1.1) fg g^{-1} and (103 ± 2.3) fg g^{-1}, respectively.

The depth data for Blelham and Fell Foot suggests that the association for ^{239}Pu mass distribution with depth is related to equations (4.4.1) and (4.4.2). The abundance of ^{239}Pu in samples B6, B9, F13 and F15 is lower, hypothetically because they are deeper, given the depth range of these samples was from 12 to 25 cm (sample depth in Table. 15). In addition, the mass concentrations of ^{239}Pu in samples B2, B7 F9 and F14 were higher due to the depth of these samples being shallower approximately 7 - 8 cm. Showing the overall pattern: shallow sample have a higher level of mass concentration for ^{239}Pu, and deeper sample has a lower level of mass concentration for ^{239}Pu.

Depth of samples for Blelham Tarn and Fell Foot, fitted using equations (4.4. 1) and (4.4.2) is shown in the Tables B15 and C15, respectively, and samples collected from both sites in different sample depths d1, d2, d3……. etc are presented in Table. A 15. The data have been analysed in terms of mass concentration (m) versus depth (d), where d is defined as the mid-point of the length of each sample. The uncertainty Δd in d has been determined assuming a Gaussian distribution of depth across a sample, as $\Delta d = d/6$ since the whole of each sample was used in the experimental preparation. In order to produce coefficients for the power function associating ^{239}Pu mass concentration (m) and depth (d), the data are displayed in Figure 43 as Log_e (m) against $\log_e$ (d) from equation (4.4.1), as per:

$$m(d) = \frac{m_0}{d^n} \qquad (4.4.1)$$

Further in Figure 44, for the exponential dependence in terms of $\log_e$ (m) against d, according to a current statement from Zhang et al [48], as per:

$$m(d) = m_0 e^{-\lambda\, d} \tag{4.4.2}$$

The coefficients m_0 (fg g^{-1}), n and λ (cm^{-1}) are constants resulting from the gradient and intercept of the fit for all data (Blelham tarn, Fell Foot).

A)

Sample	**sampling depth**/cm
B1	10 ± 1.7
B2	8 ± 1.3
B3	15 ± 2.5
B4	10 ± 1.7
B5	15 ± 2.5
B6	13 ± 2.2
B7	7 ± 1.2
B8	13 ± 2.2
B9	15 ± 2.5

Sample	**sampling depth**/cm
F1	11 ± 1.8
F2	10 ± 1.7
F3	9 ±1.7
F4	12 ± 2.0
F5	11 ± 1.8
F6	8 ± 1.3
F7	8 ± 1.3
F8	13 ± 2.2
F9	8 ± 1.3
F10	12 ± 2.0
F11	12 ± 2.0
F12	14 ± 2.3
F13	25 ± 4.2
F14	8 ± 1.3
F15	12 ± 2.0

B)

Data	**Coefficients/ power law**		
	$\boldsymbol{m_0}$ / fg g^{-1}	$\boldsymbol{n}$	$\boldsymbol{\chi_v^2}$
Combined	1317 ± 232	1.13±0.06	0.53
Blelham Tarn	1846 ± 965	1.2 ± 0.2	0.52
Fell Foot	1157 ± 309	1.1 ± 0.09	0.43

C)

Data	**Coefficients/ exponential**		
	m_0 / fg g^{-1}	λ /cm^{-1}	χ_v^2
Combined	506 ±26	0.170±0.001	0.57
Blelham Tarn	794 ± 169	0.23 ± 0.01	0.57
Fell Foot	430 ± 28	0.160 ± 0.002	0.44

Table 17: A) Sample number and depth (d), where d is defined as the mid-point of the length of each sample. The uncertainty Δd in d has been determined assuming a Gaussian distribution of depth across a sample, as $\Delta d = d/6$ since the whole of each sample was used in the experimental preparation. B) Fitting data using equation (4.4.1) and C) fitting data using equation (4.4.2).

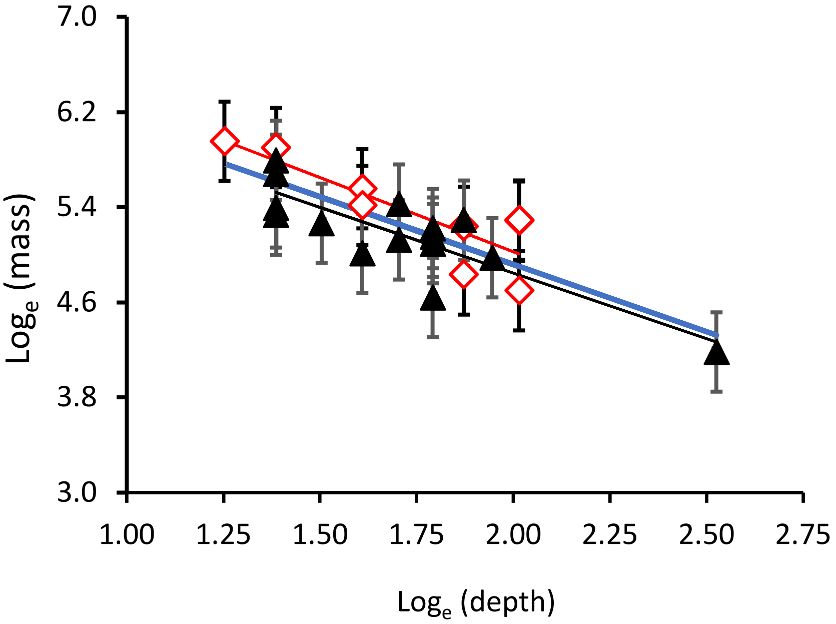

Figure 46: Log$_e$ mass concentration of ^{239}Pu/fg g^{-1} versus Log$_e$ depth/cm of Blelham Tarn (diamond and red line for fitting data), Fell Foot (triangle and black line for fitting data) and combined data fitting (blue line).

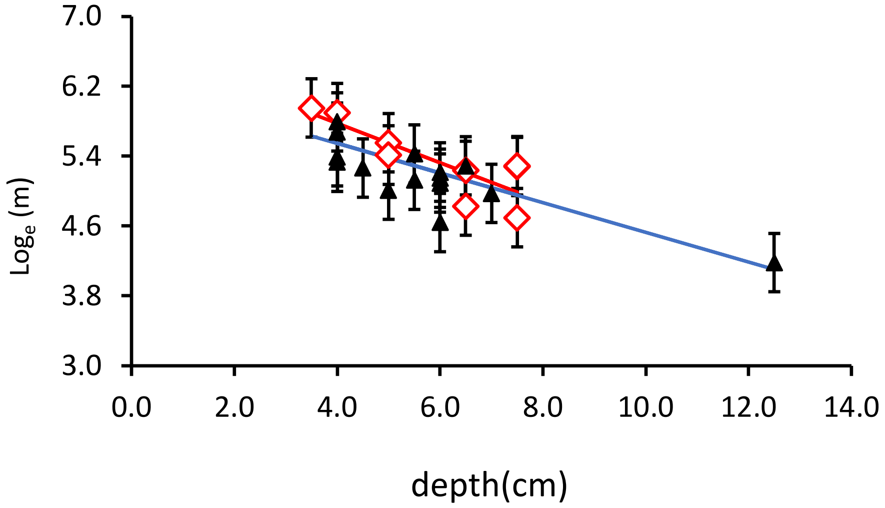

Figure 47: Log$_e$ mass concentration of ^{239}Pu/fg g^{-1} versus depth/cm of Blelham Tarn (diamond and the red line for fitting data), Fell Foot (triangle and black line for fitting data) and combined data fitting (blue line).

Overall, the differences regarding the uncertainties in the mass concentration data show that not all the Blelham Tarn and Fell Foot samples are comprised of the same sample group. In specific, samples (B2, B6, B7 and B9) from Blelham Tarn and samples (F9, F13, F14 and F15) are outliers compared to the mean of these data. Additionally, it also is noticed that similar trends appear for all observed isotopes (^{239}Pu,^{240}Pu and ^{244}Pu).

4.5 Local Proportion to Plutonium in the Lake District Area

Plutonium levels in the environment could be affected by soil qualities that can differ at a localised level. The plutonium isotopes ratios, such as ^{240}Pu/^{239}Pu and ^{244}Pu/^{239}Pu for both Blelham Tarn and Fell Foot samples, can provide additional data to that obtained from the isotopic mass. In this approach, there are three hypothetical scenarios that merit consideration [83]:

1. The total amount of the Pu in Blelham Tarn and Fell Foot comes from global fallout without any local contribution, such as from Sellafield.
2. The distribution of the Pu in the Blelham Tarn and Fell Foot comes from both global fallout and local releases.
3. Most of the Pu in both Blelham Tarn and Fell Foot samples originates from local operations.

In the case of the global fallout contribution (M_G) and local contribution (M_L), as mentioned in scenario 2, the total plutonium mass denoted M can be generated:

$$M = M_G + M_L \tag{4.5.1}$$

For cases 1 and 3 as mentioned above, $M_L = 0$ *and* $M_G = 0$, respectively. Where $M_L \neq 0$ *and* $M_G \neq 0$, each component will have a specific isotopic composition, as shown in equations (4.5. 2) and (4.5.3),

$$M_G = m_{G239} + m_{G240} + m_{G241} + m_{G242} + m_{G244} \tag{4.5.2}$$

$$M_L = m_{L239} + m_{L240} + m_{L241} + m_{L242} + m_{L244} \tag{4.5. 3}$$

It can be said that it cannot be distinguished between the global fallout and local sources of Pu, due to the unknown isotope compositions of the various sources. However, the isotopic ratios provided by previous studies can be used to approximate this. The

^{240}Pu/^{239}Pu can be labelled in this approach as $R_{240/239}$ and respectively, given case 2 has been as follows in terms of $R_{240/239}$ [83].

$$R_{240/239} = \left[\frac{m_{G240} + m_{G240}}{m_{G239} + m_{G239}}\right] \tag{4.5.4}$$

Regarding samples B2, B7, F9 and F15, the proportion of ^{239}Pu isotope excess abundance is lower at samples B6, B7, F13 and F14. Equations (4.5.4) could be adjusted to produce an estimate for the proportion of the overall ^{239}Pu abundance that comes from local sources, in terms of the $^{\mathrm{Minor}}$Pu/^{239}Pu isotopic ratio where the local proportion of plutonium is, F_{L239} as shown in equation (4.5.6 and 4.5.7):

$$F_{L239} = 100 \times \left[\frac{R_{Minor/239} - R_{G\_Minor/239}}{R_{L\_Minor/239} - R_{G\_Minor/239}}\right] \tag{4.5.5}$$

$$F_{L_{239}} = 100 \times \left[\frac{R_{240/239} - R_{G240/239}}{R_{L240/239} - R_{G240/239}}\right] \tag{4.7.6}$$

$$F_{L_{239}} = 100 \times \left[\frac{R_{244/239} - R_{G244/239}}{R_{L244/239} - R_{G244/239}}\right] \tag{4.7.7}$$

In terms of ^{244}Pu/^{239}Pu: the average of combination data for Blelham Tarn and Fell Foot at $(11.8 \pm 1.0) \times 10^{-5}$ is consistent with a global fallout average for the Northern Temperate Zone reported by Wendel et al at $(14.4 \pm 1.5) \times 10^{-5}$ [4]; this value was derived from averaging the peak weapons test between 1963-1964 that were collected from Erie Lake. Although, the measurement of this work is high compared to the Sellafield average at (3.5×10^{-5}) and Salzburg measurement at $(5.7 \pm 1) \times 10^{-5}$ reported by Steier et al. [5], thus significantly supports the argument made by Steier that material that derived from the reactor could be low in ^{244}Pu. In the instance of Salzburg, Chernobyl may explain the decreased ^{244}Pu/^{239}Pu compared to Erie Lake measurement and Ivy Mike debris.

The relationship between local and global measurements to trace Pu in the environmental samples in terms of the ^{244}Pu/^{239}Pu isotopic ratio where the local proportion of plutonium is given in the equation. 4.5.7.

Where, $R_{244/239}$ is the combined average of ^{244}Pu/^{239}Pu ratio measured in this work for Blelham Tarn and Fell Foot at $(11.8 \pm 1.0) \times 10^{-5}$, $R_{G\_244/239}$ is the global average of ^{244}Pu/^{239}Pu at $(14.4 \pm 1.5) \times 10^{-5}$, reported by Wendel [4], and for the local contribution $R_{L\_244/239}$ has been estimated from Sellafield by Steier at (3×10^{-6}) [5]. Furthermore, three measurements for comparison have been considered: Salzburg (Steier) measurements, Runit Island at Enewetak Atoll [84] and Bikar Atoll [85]. The local contributions of $F_{L_{239}}$ are shown in Table 18.

Location	$\boldsymbol{R_{244/239}}$	$\boldsymbol{R_{G\_244/239}}$	$\boldsymbol{R_{L\_244/239}}$	$\boldsymbol{F_{L_{239}}}$ /%
Lake District / This work	$(11.8 \pm 1.0) \times 10^{-5}$	$(14.4 \pm 1.5) \times 10^{-5}$	3×10^{-6}	18 ± 13
Salzburg /Steier	$(5.7 \pm 1) \times 10^{-5}$	$(14.4 \pm 1.5) \times 10^{-5}$	~0	60 ± 12
Runit Island /Hamilton	3.2×10^{-5}	$(11.8 \pm 0.7) \times 10^{-5}$	~0	73 ± 16
Bikar Atoll /Carcho	$(28 \pm 6) \times 10^{-5}$	$(11.8 \pm 0.7) \times 10^{-5}$	4.25×10^{-4}	53 ± 21

Table 18: $F_{L_{239}}$ /% measurements derived from (4.7.1) equation for a comparison of this work result with Salzburg, Runit Island, and Bikar [5], [84] and [85]. Observed that the contribution increased locally.

CHAPTER 5: DISCUSSION

Introduction

This chapter discusses the interpretation of the results obtained from all the measurements and calculations, followed by an overall discussion of the main findings of the thesis.

The main findings of the overall thesis show that the soil samples taken from Blelham Tarn and Fell Foot are consistent with global fallout abundances of radionuclides of ^{241}Am and ^{241}Pu (Bq per g) by using HRGS and Pu isotopes (fg per g) and Pu isotopes ratio (at/at). The levels of actinides in the soil samples and the differences between these and the global fallout samples and project samples are discussed in the research literature from different sites across the southern and northern hemispheres. This study has discussed many factors, such as estimating the local contributions to trace plutonium in soils from Blelham Tarn and Fell Foot.

5.1 Gamma-ray Spectrometry

This study compared ^{241}Am and ^{241}Pu in soil gathered from the shores of Blelham Tarn and Windermere, and through HRGS, the concentration of radioactivity in samples was estimated in the samples; ^{241}Am is typically an indicator of nuclear contamination. ^{241}Am was generated from the radioactive decay of ^{241}Pu as an activation product in nuclear fuel and atmospheric weapons tests. Since ^{241}Pu is also a frequent component of the fallout of ^{241}Am, so ^{241}Am can be employed to assess the particular amount of ^{241}Pu that has been deposited, as shown in this section.

In Figure 48, a graph is provided for γ-ray spectrometry measurements using a high-resolution BEGe detector to obtain estimates of ^{241}Am abundance from Blelham Tarn samples. Gamma spectrometry has shown that the measurements of CCFE samples $(26 \pm 1) \times 10^{-5}$ Bq g^{-1} were consistent with the results achieved from BEGe measurements of each sample carried out at the University of Liverpool data $(27 \pm 1) \times 10^{-5}$ Bq g^{-1}. For comparison with the literature $(25 \pm 3) \times 10^{-5}$ Bq g^{-1} [1], the significant difference indicated in the ^{241}Am level that measured by α spectrometry of sample 6 is $(12 \pm 1) \times 10^{-5}$ Bq g^{-1} was lower in the Michel result than in CCFE and Liverpool data; this suggests that sample 6 is very close to the pathways as seen in Figure 11, or that it is specifically minimal radiation emitting material in the soil. The original data for Liverpool, CCFE and Michel can be provided in the appendix (F) with the graph showing the average for this comparison.

The ^{241}Am abundance was also investigated in soil samples obtained at the regions of Fell Foot in the CCFE measurements via the BEGe system are also consistent with Liverpool measurements. The level of ^{241}Am is very similar between the samples except for samples (F13 and F15). The level of ^{241}Am in these samples is the lowest compared to the rest of the samples. The reason might be due to the sample location being close to the road and perhaps the most sheltered in terms of radionuclides deposition. The increased concentration of ^{241}Am at the Fell Foot site shows that there might have been more ^{241}Pu fallout in this area than in the Blelham Tarn. Furthermore, the measurements from Liverpool are a bit higher than the CCFE data when identifying the ^{241}Am level due to the size of the sample. This has also been explained earlier in Chapter 3; (each sample within this research was transferred into 250 ml Marinelli beaker containers for the Liverpool detector and 9cm Petrie dishes for the CCFE detector).

Since ^{241}Am and ^{241}Pu are correlated, with about 99.7% of ^{241}Pu decaying to ^{241}Am, the quantity of ^{241}Pu present in each spectrum can be calculated using the assessed quantities of ^{241}Am through the 59.5 keV ^{241}Am peak and this can be done using the Bateman equation [69]. The results revealed that the data of ^{241}Pu abundance at Blelham Tarn and Fell Foot is (11 ± 0.5) Bq kg^{-1}, (n=9) and (10.5 ± 0.4) Bq kg^{-1}, (n=15), these data were carried out at University of Liverpool and CCFE, respectively.

When comparing these results to previously reported sample measurements of ^{241}Am levels, the measurements of this research are higher than the previous study, such the contents of ^{241}Am of soil samples at Copepoda (North Sea) were (0.020 ± 0.0026) Bq kg^{-1} / (0.158 ± 0.021) fg g^{-1} and Gironde River sediment (France) range was from (0.16 ± 0.03 to 0.19 ± 0.03) Bq kg^{-1}/ (1.27 ± 0.23 to 1.50 ± 0.23) fg g^{-1}. Also, soil just 5 cm from the surface at (Ibaraki pref, Japan) is (0.34 Bq Kg^{-1})/ (2.69) fg g^{-1}, which is higher than the results of this project [86]. Furthermore, ^{241}Am of this work is lower than the range of the calculations that have been taken out by C. K. Kim et al (1992) on the samples of soil from the Irish Sea that follow the levels of ^{241}Am with a standard of (2.6 to 1894) Bq Kg^{-1} / (20.6 to 14981) fg g^{-1} [87]. A summary of the comparison between the ^{241}Am results of this work and previous studies is shown in Figure 48.

The concentrations of ^{241}Pu were distributed over a wide range in this research. (11 ± 0.5 to 10.5 ± 0.4) Bq kg^{-1} and (11 ± 0.5 to 11 ± 0.4) Bq kg^{-1} of Blelham Tarn and Fell Foot samples, respectively. Additionally, these ranges of calculations fall within the range of the statement by T. Ikäheimonen (2000) of < 0.5 to 27 Bq kg^{-1} in the samples taken from the Baltic Sea [88]. Further, ^{241}Pu activity measurements in this research were lower than the lowest level of ^{241}Pu identified in the sediment samples collected from the Irish Sea (approximately 700 Bq Kg^{-1}) [89] [90]. Moreover, the ^{241}Pu level in this research is also lower than the activity concentrations of ^{241}Pu identified in the Mururoa Atoll that were reported by J. A. Corcho Alvarado (2011) of (19 ± 4) Bq kg^{-1} [91].

^{241}Am/ $^{239+240}$Pu ratio was investigated in soil samples obtained at the regions of Blelham Tarn via the BEGe system. Also, ^{239}Pu and ^{240}Pu data were obtained from AMS (where these data were converted from fg per g to Bq per g), for comparing this ratio with Michel data. The ^{241}Am/ $^{239+240}$Pu activity ratio of this work (0.35 ± 0.04) is consistent with the previous literature (0.36 ± 0.02) [1].

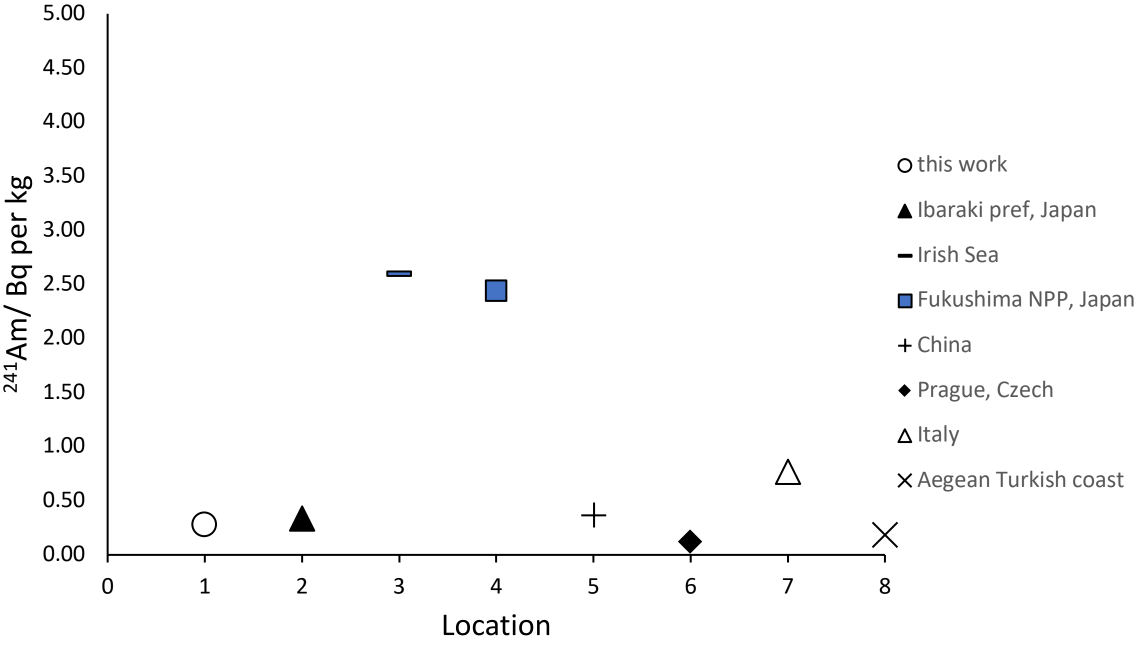

Figure 48: A comparison of ^{241}Am of this work with the previously reported measurements of ^{241}Am concentrations in the environmental samples [86] [87] [88] [89] [90].

5.2 Accelerator Mass Spectrometry Measurements

The isotopic mass abundances (^{239}Pu, ^{240}Pu, ^{244}Pu) are shown in Figures 39,40,41,42 and 43 for Blelham Tarn and Fell Foot, and similarly, the isotopic ratios (^{240}Pu/ ^{239}Pu and ^{244}Pu/^{239}Pu) are shown in Figures 44 and 45. The isotopic mass abundances (^{239}Pu, ^{240}Pu, ^{244}Pu) were determined in terms of femtogram levels per gram (fg/g) and comparing these quantities with previously reported sample measurements of ^{239}Pu and ^{240}Pu background levels, the measurements of this research agreed with the prior art, such as the global average mass ratio (0.182 ± 0.01) of ^{240}Pu/^{239}Pu reported by Kelley et al [2] is consistent with Blelham Tarn and Fell Foot averages ratios.

5.2.1 ^{239}Pu

The average mass concentration of ^{239}Pu was investigated in the soil sample set obtained at Blelham Tarn is (228 ± 32) fg g^{-1} (n = 9), and the average ^{239}Pu, excluding the outliers' samples (B2, B6, B7, B9) relative to this data is (213 ± 13) fg g^{-1} (n = 5). Sample B2 (365.3 ± 5.5) fg g^{-1} and sample B7 (385 ± 9.2) fg g^{-1} are significantly higher in mass concentrations of ^{239}Pu for the other sample, although, samples B6 (125 ± 3.8) fg g^{-1} and B9 (109 ± 3.2) fg g^{-1} have a lower abundance of ^{239}Pu than the set of samples.

The ^{239}Pu abundance in Fell Foot was (188 ± 17) fg g^{-1} (n = 15) in the set of the sample, and the average abundance of ^{239}Pu, excluding outlier's samples (F9, F13, F14 and F15) is (184 ± 8) fg g^{-1} (n =11). Sample F9 (292 ± 5.4) fg g^{-1} and sample F14 (328.1 ± 4.9) fg g^{-1} are greater of ^{239}Pu concentrations than the average of the sample set, while samples F13 and F15 are significantly lower of ^{239}Pu than most Fell Foot samples at the level of (65 ± 1.1) fg g^{-1} and (103 ± 2.3) fg g^{-1}, respectively.

In summary, it can be said that all samples from Blelham Tarn and Fell Foot exhibit levels of ^{239}Pu abundance and the average level of ^{239}Pu for Blelham Tarn samples and Fell Foot samples is (203 ± 16) fg g^{-1}.

The depth dependence of mass concentration for Blelham and Fell Foot suggests an association for ^{239}Pu with depth as per equation (5.1), further, the abundance of ^{239}Pu in samples B6, B9, and F13 and F15 was lower because they are deeper (12 to 25 cm). In addition, the mass concentration of ^{239}Pu in samples B2, B7, F9 and F14 were higher due to the depth of these samples being shallower at approximately (7 - 8 cm). Showing the overall pattern: shallow samples have a higher concentration of ^{239}Pu, and deeper samples have a lower level of mass concentration of ^{239}Pu, as per Equation (5.1).

The statistics in Figure 49, indicate that, despite being derived from various locations, there is no analytical proof that suggests that the depth dependence differs for either site, therefore employing the whole set of data to obtain the coefficient values described in Equations (4.4.1) and (4.4. 2) is supported. The relevant data for the fits and coefficients are provided in Table. B15 from Equation (4.4. 1) and Table. C15 from Equation (4. 4. 2). Significantly, the negative power indicates a consistent level of dispersion with depth. However, it is possible that in this situation the deeper ground reduces the ability to identify maximum mass concentrations at a specific depth.

$$\text{mass} \propto \frac{1}{\text{depth}} \tag{5.1}$$

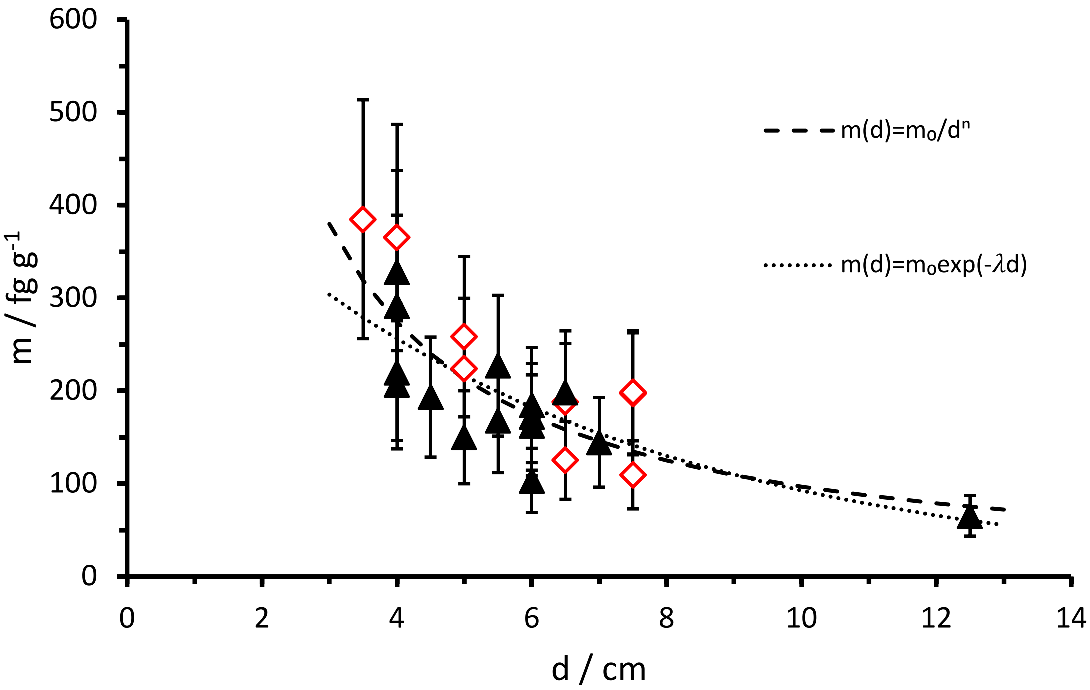

Figure 49. Mass concentration of ^{239} Pu (fg g^{-1}) against the depth of sample (cm) for Blelham Tarn (red diamond) and Fell Foot site (black triangle) included inverse-proportional (broken line) and exponential empirical dependencies (dotted line) fits of the combined data set.

Previous research on Pu, ^{241}Am, and ^{137}Cs in Belarusian soils, reported by Boulyga et al. [92], indicated an exponential relationship such as (equation. 4.4.2) across comparable depth from 0 to 10 cm, while the relatively low altitude Austrian soil sample reported by Srncik et al. [86], shows a depth dependence more reliable with (equation. 4.4.1). It is also in line with the hypothesis that soil strength increases with depth due to gravitationally induced compaction (it is produced from heavy equipment and tillage tools), and corresponding changes in pore size distribution, reported by Lwan Wästerlund [93].

However, considering the acknowledged limits of the empirical studies mentioned above, regarding prediction and their unphysical nature at surface levels, an approach based on convection and dispersion (the convection and dispersion equation, CDE) is instructive, recommended by Bossew and Zhang [95][96], as per,

$$m(d) = \frac{C_0}{2\sqrt{\pi D t_1}} e^{-\frac{(d-vt_1)^2}{4Dt_1}} \tag{5.2}$$

Where C_0 is the amount of mass per unit mass deposited at the surface a ‘t’ (peak deposit 1963 ~57 years), it should be estimated by integrating the average mass concentration for each sample and added together, D and v are the effective dispersion constant. There are hypothetically two distributions in our data – a local one (Sellafield) and a global one (fallout) deposited at different times, so, combining two components in a modified CDE gives:

$$m(d) = \frac{C_0}{2\sqrt{\pi D}} \left(\frac{(1-F_{L_{239}})}{\sqrt{t_1}} e^{-\frac{(d-vt_1)^2}{4Dt_1}} + \frac{F_{L_{239}}}{\sqrt{t_2}} e^{-\frac{(d-vt_2)^2}{4Dt_2}} \right) \tag{5.3}$$

Where t_2 is the amount of time that has passed between sampling and the occurrence of a second deposit, and the relative proportions of local contributions to C_0 are reflected by $F_{L_{239}}$.

For the purpose of reducing equations (5.2) and (5.3), t_1 can be tried on the sampling time since 1963 ~57 years, and C_0 can be calculated using the average of the concentrations at each depth and summed together, which results in (2.2± 0.2) pg g^{-1}. Subsequently, a generalised reduction gradient approach was employed to reduce χ_v^2 for equation (5.2) to generate estimates for D and v, as shown in Table 19. These values are then applied in a similar minimization of equation (5.3) to yield t_2, assuming that the soil must have the same characteristics in both scenarios. These parameters' uncertainties have been calculated using the minimization of a random, non-linear function [97].

Furthermore, both the dispersion coefficient (D and v) have been shown to be in agreement with recent investigations of trace plutonium transfer in grassland in China [95}. The optimisation of equation (5.3) results in a time elapsed of t_2 ~ 30 years since the local plutonium deposition (date of the Magnox deposit), which has no special correlation on any reported, high-stack proceedings from that period. Figure 50 illustrates the mass concentration against depth, utilising the power law, exponential, CDE, and modified CDE fits.

Coefficient	**Zhang et al.**	**This work**	
		Modified CDE data	**Standard CDE**
C_0	(134 ± 10) Bq m^{-2}	(2.2 ± 0.2) pg g^{-1}	(2.2 ± 0.2) pg g^{-1}
D (cm^2 y^{-1})	0.33 ± 0.08	0.19 ± 0.03	0.19 ± 0.03
v (cm y^{-1})	0.08 ± 0.01	0.07 ± 0.01	0.07 ± 0.01
t_1 (y)	57	57 ± 10	57 ± 10
t_2 (y)	-	30 ± 12	-
χ_v^2	-	0.81	0.86

Table 19 The fit data of CDE indicated in Figure 50 and contrasted to the previous study [96].

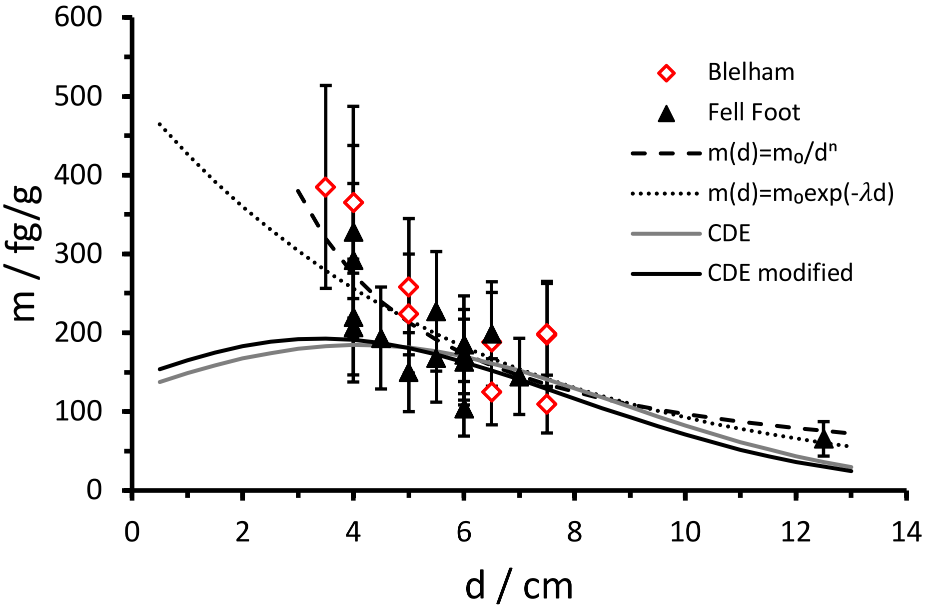

Figure 50. Mass concentration of ^{239}Pu (fg g^{-1}) against the depth of sample (cm) for Blelham Tarn (red diamond) and Fell Foot site (black triangle) included inverse-proportional (broken line), exponential dependence (dotted line) fits of the combined data, CDE data from the equation. 5.2 (grey line) and CDE modified data from the equation.5.3 (black line).

Another factor that can be taken into consideration is the location of the samples. The Blelham Tarn samples have a high ^{239}Pu abundance, sample B7 may be gathered from an area with great dispersion (away from the pathway or lake as seen on the map of Blelham Tarn Figure 11). While the location of sample B9 was close to a tree (tree covering), so this might also be a reason that ^{239}Pu was low in this sample.

The same thing can be considered for Fell foot samples. Sample F15 location was close to the road and wall, so it is perhaps the most sheltered in terms of atmospheric deposition. Further, sample 13 indicated that there is little concentration due to the location of the sample near the trees or the reduced level of ^{239}Pu abundance by farming activities (associated changes in pore size distribution with depth) [93]. Clearly, ^{239}Pu penetration from atmospheric deposition depends on the nature of the soil, which varies with site elevation.

Overall, the differences in mass concentration of ^{239}Pu between Blelham Tarn and Fell Foot are probably because of the environments and elevations in each site. In the Fell Foot site, there is likely to be an alluvial deposit influence due to flooding or transportation in a stream or river, and it is plausible that these alluvial deposits affect the sub-surface flow pathways through the lake (more sheltered) from Grapes et al. [98].

In comparison with previous studies, as indicated in Figure. 48: the average mass concentration of ^{239}Pu for the Blelham Tarn was (228 ± 32) fg g^{-1}, for Fell Foot was (188 ± 17) fg g^{-1}, and the combined data (with outliers samples) of this work (203± 16) fg g^{-1} are consistent with Curtis et al. report [99], they have taken out the calculations on the samples of soil from the Cigar Lake in the region of Australia that follows the levels of ^{239}Pu in range of (2 – 6200) fg g^{-1} of ^{239}Pu [99]. Furthermore, the average of ^{239}Pu abundance of this work falls nicely inside the range of global fallout of (7 – 1600) fg g^{-1}, given in the review of Harley [44]. The combined data of ^{239}Pu abundance is also consistent with those indicated by the sediments in Ontario Lake that have been calculated by Green et al from (2 to 200) fg g^{1} [100].

Other masses of ^{239}Pu have been quantified in an extremely lower level in the southern hemisphere literature reported by S. Salmani-Ghabeshi et al. from (6 -20) fg g^{-1} [101] to the greatest value of 6700 fg g^{-1} at the test location of Semipalatinsk in the region of Kazakhstan reported by Buesseler [27]. The Blelham Tarn, Fell Foot and combined averages of the ^{239}Pu abundance fall within the range of (100 – 500) fg g^{-1}, consistent with the site of River Savannah as reported by C. R. Armstrong et al. [102]. However, ^{239}Pu assessments in this work are lower than those measurements reported by Kelley et al (1999) of soil samples collected from Wick regain, Scotland of 1290 fg g^{-1} [2].

In summary, the measurements of ^{239}Pu for this work fall within the levels of ^{239}Pu assessment produced by nuclear fallout, as shown in Figure 51, by several instances in the literature.

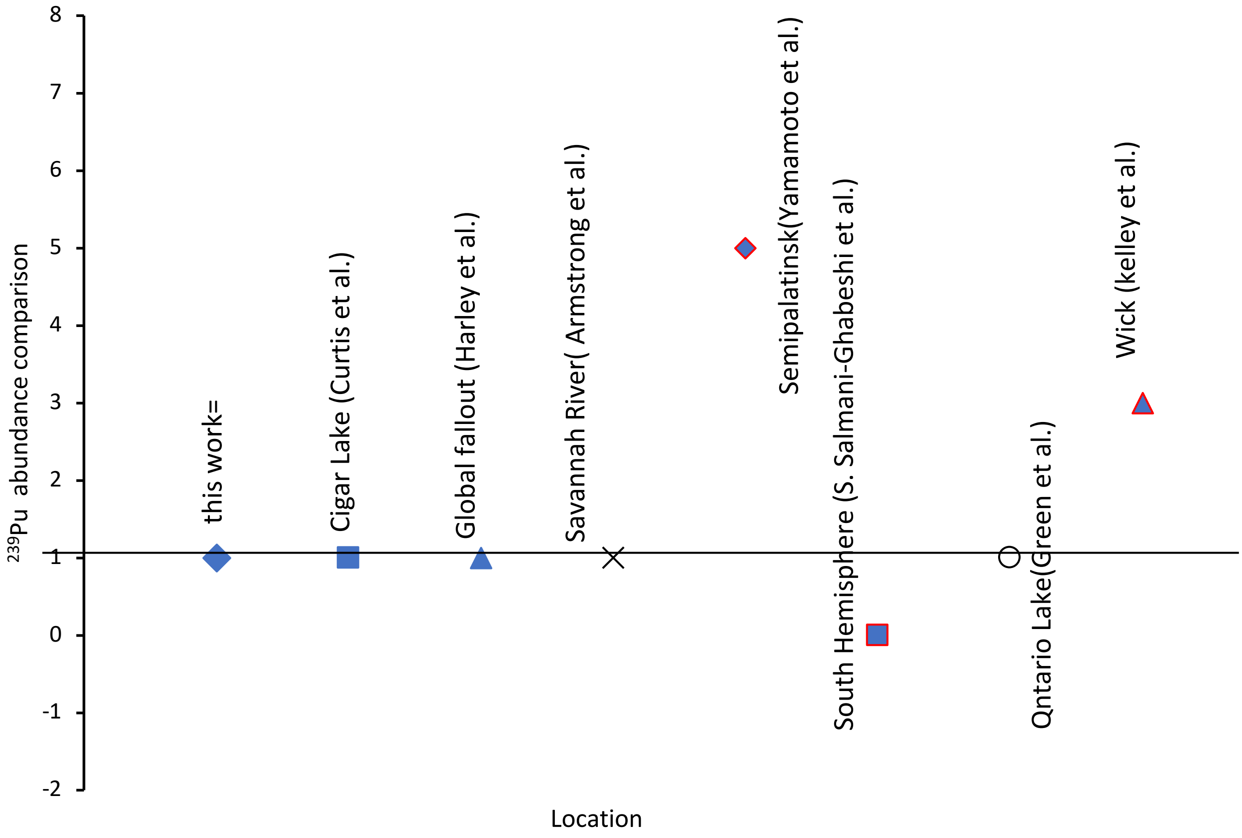

Figure 51: Comparison index of ^{239}Pu abundance for this work with Cigar Lake, Global Fallout, Savanah River, south hemisphere, Ontario Lake Wick and Semipalatinsk [2] [3] [44] [99] [100] [101] [102] [103].

5.2.2 ^{240}Pu

The average mass concentration of ^{240}Pu considered in the soil samples set taken at regions of Blelham Tarn is (41 ± 5) fg g^{-1} (n = 9), and the average ^{240}Pu, excluding the outliers' samples

(B2, B6, B7, B9) relative to these data is (39 ± 2) fg g^{-1} (n = 5). Samples B2 and B7 are significantly higher in mass concentrations of ^{240}Pu for the other sample of (56 ± 1) fg g^{-1} and (69.3 ± 2.1) fg g^{-1} respectively, while samples B6 and B9 have lower abundances of ^{240}Pu than the set of samples of (22.7 ± 0.9) fg g^{-1} and (19.1 ± 3.2) fg g^{-1}, respectively.

The ^{240}Pu abundances in Fell Foot is (34 ± 3) fg/g (n = 15) in the set of the sample, and the average abundance of ^{240}Pu, excluding outlier's samples (F9, F13, F14 and F15) was (33 ± 2) fg g^{-1} (n = 11). Samples F9 and F14 are greater for ^{240}Pu concentration than the average of the sample set, whereas samples F13 and F15 are significantly lower for ^{240}Pu than most Fell Foot samples at the level of (11.4 ± 0.3) fg g^{1} and (20 ± 0.7) fg g^{-1}, respectively.

In summary, it can be said that all samples from Blelham Tarn and Fell Foot are detection levels of ^{240}Pu concentration and the combined data of ^{240}Pu for Blelham Tarn samples and Fell Foot samples are (37 ± 3) fg g^{-1}. A discussion has been made of why some samples are high in ^{240}Pu concentration and some are low, as explained in the previous section (^{239}Pu) in terms of depth dependence and location of samples.

In comparison with previous studies, ^{240}Pu assessments of this work are lower than those measurements reported by Y. Muramatsu et al. (1996) of soil sampled from the Semipalatinsk Nuclear Test location of (0.246 ± 0.001 to 6.74 ± 0.01) pg g^{-1} [103]. Furthermore, Blelham Tarn, Fell Foot of the ^{240}Pu level are lower than the measurements have been made by Tighe et al. (2021) in the range of (93 ±3) fg g^{-1}, on the Dounreay site [83]. The ^{240}Pu abundance in this research is more consistent with those indicated by the sediments in Ontario Lake that have been assessed by Quinto et al., at range (10-100) fg g^{-1}[104].

5.2.3 ^{244}Pu

The mass concentration of ^{244}Pu measured in the soil sample set of Blelham Tarn is $(4 \pm 1) \times 10^{-2}$ fg g^{-1} (n = 3), and the average mass of ^{244}Pu abundance for Fell Foot samples is $(2.2 \pm 3)\times 10^{-2}$ fg g^{1} (n = 13). Further, it can be said that not all the samples from Blelham Tarn and Fell Foot are expressing levels of ^{244}Pu (this can be seen in Figure 43 in the 4.3.3 section) and the combined data of ^{244}Pu for Blelham Tarn and Fell Foot samples at $(2.6 \pm 3)\ 10^{-2}$ fg g^{1}. It can be noted that results for samples B5-B9, F3 and F15 are not shown because AMS did not get a single count for ^{244}Pu, so we could instead show an upper limit for ^{244}Pu in those samples using the estimate by Feldman and Cousins (1998) [82].

Overall, the upper limits in samples (B4 - B9, F3 and F15) are higher than the other samples' results because they generally had low output. Comparison of ^{244}Pu to the prior art, and the combined data of ^{244}Pu abundance for Blelham and Fell Foot at (0.058 ± 0.011) fg g^{1}, this value is lower than those indicated by the soil collected from the Savannah River Site (USA) that has been assessed by C. R. Armstrong et al. (2016) at range (0.31- 44) fg g^{1} [105]. Furthermore, the combined average of the ^{244}Pu level for this work is higher than the measurements have been made by Tighe et al (2021) in the range of $(3.9 \pm 0.8) \times 10^{-2}$ fg g^{-1}, on the Dounreay site [83].

Overall, the ^{239}Pu, ^{240}Pu and abundances for Blelham Tarn and Fell Foot samples were (228 ± 32) fg g^{-1}, (188 ± 17) fg g^{-1}, (41 ± 5) fg g^{-1}, (34 ± 3), respectively, and the combined data of ^{244}Pu is (2.6 ± 0.4), respectively. It should be highlighted that the uncertainty mass of each average mass concentration mentioned above was calculated using the standard error of the mean instead of the propagated analytical uncertainties because there is some additional scatter ("geological" scatter) in the samples that is not reflected by the analytical uncertainties (AMS errors).

The differences regarding the uncertainties in the mass concentration data show that not all the Blelham Tarn and Fell Foot samples are comprised of the same sample group. Specifically, it also is noticed that similar trends appear for all observed isotopic (^{239}Pu,^{240}Pu and ^{244}Pu) in Blelham Tarn and Fell Foot.

5.3 Pu Isotopic Ratios

The Pu ratios can be used to determine the source of radioactive material at a study site. It is common to describe the correlation among actinide isotope quantities as a ratio, and these proportions were estimated across various investigations to obtain global fallout average estimates. This section discusses the results of ^{240}Pu/^{239}Pu and ^{244}Pu/ ^{239}Pu isotopic ratios obtained from Blelham Tarn and Fell Foot samples, and further comparison of these data with previous studies.

5.3.1 ^{240}Pu/ ^{239}Pu isotopic ratio

The average ratio of ^{240}Pu/^{239}Pu isotopic measured in the soil sample set of Blelham Tarn is (0.181 ± 0.003) (n = 9), and the average ratio of ^{240} Pu/^{239}Pu isotopic for Fell Foot samples is (0.181± 0.002) (n =15). Further, the combined data of ^{240}Pu/^{239}Pu for Blelham Tarn and Fell Foot samples is (0.181 ± 0.002).

In comparison with earlier reports, the ^{240}Pu/^{239}Pu ratios for Blelham Tarn and Fell Foot identified in this work are consistent with the global average reported by Kelley (1999) in the range of (0.181± 0.014) [2]. Further, the ^{240}Pu/^{239}Pu average of this work is consistent with the suggested sediments in Ontario Lake that have been estimated by Green et al. [100]. The Blelham Tarn, Fell Foot and combined averages of the ^{240}Pu/^{239}Pu ratios are low relative to the measurements have been made by Steier et al. (2013) in the range of (0.183 ±0.001 to 0.226 ± 0.001) from Irish Sea site (Sellafield site) [5]. However, this measurement is a little high relative to the global average reported by Krey (0.176 ±0.014) [12].

Additionally, measurements were taken from Enewetak soil as the first thermonuclear test Ivy Mike weapons test in 1952, reported by Diamond et al (1960) of (0.36 ± 0.004) is extremely high than the measurement of this work [24]. Also, the measurement of this work is lower than reported by Ketterer et al. at 0.41 [45] and thus gives a clear explanation that there is no link with Chernobyl material. All these comparisons can be shown in Figure 52.

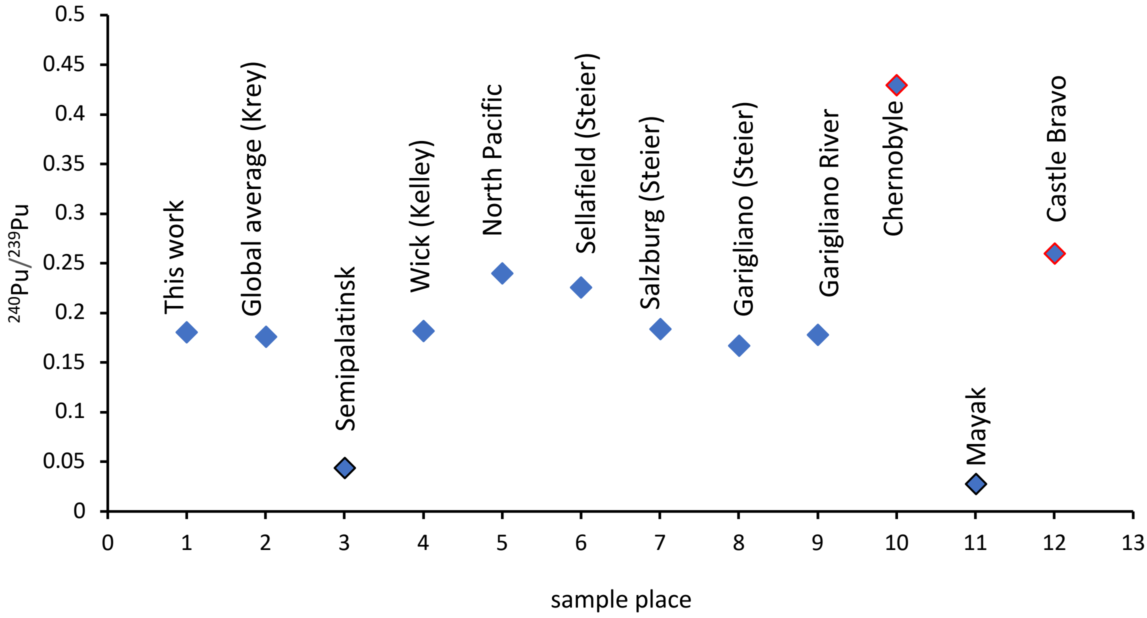

Figure 52: Comparison index of $^{240}Pu/^{239}Pu$ isotopic ratio for this work with previous studies [2] [5] [14] [12] [24] [27][45] [52] [56] [100] [103][109].

5.3.2 $^{244}Pu/^{239}Pu$ isotopic ratio

The average isotopic ratio of $^{244}Pu/^{239}Pu$ measured in the soil sample set of Blelham Tarn is $(14.8 \pm 1.9) \times 10^{-5}$ (n =3), and the average isotopic ratio of $^{244}Pu/^{239}Pu$ for Fell Foot samples is

(11.1 ± 1.1) × 10^{-5} (n=13). Also, the combined data of ^{244}Pu/^{239}Pu for Blelham Tarn and Fell Foot samples is (11.8 ± 1.0) × 10^{-5}.

Additionally, it can be said that not all the samples from Blelham Tarn and Fell foot express levels of ^{244}Pu/^{239}Pu (this can be seen in Figure 45), as explained in the ^{244}Pu, 4.3.3 section that is using the estimate by Feldmann and Cousins (1998) [82]; to calculate the calculate the upper limit for ^{244}Pu in these sample that have 0 count, and then calculate the ^{244}Pu/ ^{239}Pu ratios.

Comparisons between this research and previous studies show that the combined average of ^{244}Pu/^{239}Pu for this work (11.8 ± 1.0) × 10^{-5}, is consistent with Wendel et al (2013) [4] average at (14.4 ± 1.5) × 10^{-5} (this average based on samples collected from Lake Erie during 1963-1964 by Winkler). Further, an average of ^{244}Pu/^{239}Pu in this work is higher than the measurements have been reported by Steier et al (2013) for the Sellafield site at (<3.5× 10^{-6}), and Salzburg samples measurement at (5.7 ± 1) × 10^{-5}, based on the average of ^{244}Pu/^{239}Pu for Sellafield and Salzburg sites that materials are local resources and there is no ^{244}Pu scattered more than 100 km from Chernobyl [5].

In summary, the mass concentration averages of ^{239}Pu for the Blelham Tarn and Fell Foot data of this work are consistent with Curtis et al, Green et al and Armstrong et al studies [99][100][102]. Further, the Blelham and Fell Foot data of ^{240}Pu abundance is more consistent with those indicated by the Ontario Lake sediments assessed by Quinto et al. [104].

The averages of ^{240}Pu/^{239}Pu for Blelham Tarn and Fell Foot samples are consistent with the global fallout average stated by Kelley [2]. Furthermore, the ^{244}Pu/^{239}Pu average is consistent with Wendel's average [4].

5.4 On the local contribution to plutonium in the English Lake District

In terms of ^{240}Pu/^{239}Pu: The isotopic ratio averages of ^{240}Pu /^{239}Pu for Blelham Tarn and Fell Foot determined within this investigation (also combined data at 0.181 ± 0.002) are consistent with the global averages reported by Green et al and Kelley et al [100][2]. However, compared to the calculation obtained of ^{240}Pu/^{239}Pu isotope ratio from the Windscale reactor (Pile 1 = 0.0218) reported by Pomfret [112], this work is high relative to Pile 1 fallout, which might indicate that material in Lake District could be high in ^{240}Pu.

In terms of ^{244}Pu/^{239}Pu: the average of combining the data for Blelham Tarn and Fell Foot at $(11.8 \pm 1.0) \times 10^{-5}$ is consistent with a global average derived from averaging the peak weapons test between 1963-1964 years of samples that were collected from Erie Lake region reported by Wendel et al at $(14.4 \pm 1.5) \times 10^{-5}$ [4]. The measurement of this work is high compared to the Sellafield average at ($<3 \times 10^{-5}$) and Salzburg measurement at $(5.7 \pm 1) \times 10^{-5}$ reported by Steier et al. [5], thus significantly supports the argument made by Steier as the material derived from the reactor would be low in ^{244}Pu. In the instance of Salzburg, Chernobyl may explain the decrease as expected of ^{244}Pu/^{239}Pu in comparison to Erie Lake measurement and in comparison, to Ivy Mike debris.

The relationship between local and global measurements to trace Pu in the environmental samples in terms of the ^{244}Pu/^{239}Pu isotopic ratio is given below [83]

$$F_L = 100 \times \left[\frac{R_{244/239} - R_{G\_244/239}}{R_{L\_244/239} - R_{G\_244/239}}\right] \tag{5.4}$$

Where, $R_{244/239}$ is the combined average of ^{244}Pu/^{239}Pu ratio measured in this work for Blelham Tarn and Fell Foot at $(11.8 \pm 1.0) \times 10^{-5}$, $R_{G\_244/239}$ is the global average of

^{244}Pu/^{239}Pu at (14.4 ± 1.5) × 10^{-5}, reported by Wendel, and for the local contribution $R_{L\_244/239}$ has been estimated from Sellafield by Steier at (3× 10^{-6}). the local contributions of ^{239}Pu ($F_{L_{239}}/\%$) are shown in Table. 20:

$\boldsymbol{R_{244/239}}$		$\boldsymbol{R_{G\_244/239}}$	$\boldsymbol{R_{L\_244/239}}$	$\boldsymbol{F_{L_{239}}/\%}$
This work	(11.8 ± 1.0) × 10^{-5}	(14.4 ±1.5) × 10^{-5}	3× 10^{-6}	18 ± 13
Salzburg (Steier)	(5.7 ± 1) × 10^{-5}	(14.4 ±1.5) × 10^{-5}	~0	60 ± 12
Runit Island (Hamilton)	3.2 × 10^{-5}	(14.4 ±1.5) × 10^{-5}	~0	73 ± 61
Bikar (Carcho)	(28 ± 6) × 10^{-5}	(14.4 ±1.5) × 10^{-5}	4.25× 10^{-4}	53 ± 21

Table 20: $F_{L_{239}}/\%$ measurements derived from (5.4) equation.

Discounting the estimates for F_L based on the ^{240}Pu/^{239}Pu, this can be folded back into the equation above (5.4) to give the $R_{L\_240/239}$ for the local material based on F_L derived via the ^{244}Pu route, as per:

$$R_{L_{240}/239} = \frac{R_{240/239} - R_{G\_240/239}}{F_L} + R_{G\_240/239} \qquad (5.5)$$

Where, $R_{240/239}$ is the average of ^{240}Pu/^{239}Pu ratio measured in this work for Blelham Tarn and Fell Foot at (0.181± 0.002), $R_{G\_240/239}$ is the global average of ^{240}Pu/^{239}Pu at (0.176 ± 0.01), reported by Krey, and the local contribution $F_{L_{239}}$ has been estimated in

Table 20. The $R_{L_{240/239}}$ are shown in Table. 21 for this work, Salzburg, Runit Island and Bikar:

Source	$\boldsymbol{R_{240/239}}$	$\boldsymbol{R_{G\_240/239}}$	$\boldsymbol{F_{L_{239}}}$ /%	$R_{L_{240/239}}$
This work	0.181±0.002	0.176±0.014	18±13	0.21±0.08
Salzburg (Steier)	0.179 ± 0.002	0.176 ±0.014	60±12	0.18±0.03
Runit Island (Hamilton)	0.062 ±0.008	0.176 ±0.014	73 ±16	0.02±0.04
Bikar (Carcho)	0.26 ±0.01	0.176±0.014	53±21	0.34± 0.07

Table 21: $R_{L_{240/239}}$ measurements derived from equation. 5.5.

The data in Table. 18 displays the proportions of ^{239}Pu assessed to arise locally; in this work, $\boldsymbol{F_{L_{239}}}$ was (18 ± 13) % for Blelham Tarn and Fell Foot samples, by using the ^{244}Pu/^{239}Pu Erie Lake global average of Wendell (14.4 ±1.5) × 10^{-5}. (60 ± 12) % for the Salzburg samples [5], the ^{244}Pu/^{239}Pu Erie Lake global average of Wendel was also used in this calculation. (73 ±16) % for the Runit Island sample by Hamilton [84], the ^{244}Pu/^{239}Pu Erie Lake global fallout was used again in this calculation. (53 ± 21) % for the Bikar by Corcho [85].

The data in Table 19 show the local contribution of ^{240}Pu /^{239}Pu ($R_{L_{240/239}}$) in the Blelham Tarn and Fell Foot is (0.21 ±0.08), which is in reasonable agreement with the average for Sellafield (Magnox reactor): (^{240}Pu/^{239}P=0.226 ± 0.001). For Salzburg, the ^{240}Pu/^{239}Pu average at (0.18 ± 0.003) is consistent with global fallout, further, this does not indicate to Chernobyl content as per the value of ^{240}Pu /^{239}Pu at 0.43 and is supported by Y. Murumatsu et al. (2000) and M. E. Ketterer et al (2004) [85]. The local proportion $R_{L_{240/239}}$ in the Runit Island is (0.02 ± 0.04) consistent with Mayak at (0.012 ± 0.02) and the value of

^{240}Pu /^{239}Pu in Bikar is (0.34 ± 0.07) is high, relative to the value reported by Corcho (0.225±0.003).

Overall, the local contribution to trace Pu in Blelham Tarn and Fell foot is given at 18%, with the isotopic ratio of ^{240}Pu/ ^{239}Pu at 0.21, this value of ^{240}Pu/^{239}Pu was above normal compared to global fallout, however, this value is consistent with the average for Sellafield materials by Steier et al. (^{240}Pu/^{239}P = 0.20). On the other hand, this fails to indicate a connection to the Windscale reactor (Pile 1 = 0.0218) reported by Pomfret (Airborne fallout). It was also identified 60% of the Salzburg materials [Steier] are locally that derived by ^{244}Pu/^{239}Pu, no proof exists that materials could be Chernobyl resources.

CHAPTER 6: Optimising the extraction of the refractory component

6.1 Introduction

This chapter aims to describe the research done to extract the refractory component in a subset of the samples studied earlier in the thesis (six of the soil samples collected from Blelham Tarn and Fell Foot Park in the Lake District). This was undertaken because the experimental methods adopted in the earlier research may not have extracted the refractory phase in these samples to the same degree as the non-refractory phase which may then have biased the isotopic fraction towards the lighter Pu isotopes, as ^{244}Pu is anticipated to reside in the refractory component (the majority being spawned in nuclear weapons tests) and thus has not ruled in a proportion of the anthropogenic ^{244}Pu present in the refractory phase to the same degree. The nitric acid leaching approach that was explained in Chapter 3 is effective for the analysis of non-refractory phases. So, for the refractory fraction, dissolution (i.e., with hydrofluoric acid) is considered necessary, as described in this chapter.

6.2 Plutonium preparation method

The mass of samples were supplied to Southampton University (approx. 1g) and were transferred into porcelain and dried at 105°C for a minimum of 4 hrs. The dry masses of the samples were recorded and further calcined at 450 °C for a minimum of 12 hours.

The calcined samples were transferred to PTFE pots and spiked with a ^{242}Pu recovery tracer. The spiked samples were digested using a conc. HF solution (10 ml) and evaporated to dryness (repeated 2 times). The dry residue was dissolved in conc. nitric acid and evaporated to dryness (15 ml, repeated thrice). Following the nitric acid digestion, the solid residue was dissolved in 20 ml of conc. Hydrochloric acid and boiled undercover at approx. 105°C for approx. 1 hour. Approx. 1g of solid boric acid was added to the hot HCl solution, and the solution was allowed to boil for another hour and finally evaporated to dryness. The solid residue was re-dissolved in 20 ml of 1M nitric acid, boiled undercover for approx. 1 hour and allowed to cool to room temperature.

The sample solutions were transferred to 50 ml centrifuge tubes and 10 mg of Fe carrier (as $FeCl_3$ solution) was added (the samples had enough Fe on their own but was kept this step to keep it consistent with the blank samples, which had no Fe initially). To each sample, ammonia solution was added to form a $Fe(OH)_3$ precipitate (pH 8-9). This was separated by centrifuging, the supernatant discarded, and the Fe hydroxide was re-dissolved in HCl to form approx. 25 ml of 9M HCl solution. To each sample, 0.2 g of sodium nitrite ($NaNO_2$, in the form of an aqueous solution, 0.5 ml/sample) was added and the tubes were placed in a hot water bath (ca. 80°C) for a128 approx. 1 hr to allow the $NaNO_2$ to decompose. Following this step, the samples were allowed to cool to room temperature.

A set of anion exchange columns was prepared (1 × 8, 200 mesh, 0.8 × 5 cm), the columns were conditioned with 9M HCl and the sample was loaded onto the columns. When the sample solutions passed the columns, they were washed with 2×20ml of 9M HCl, followed by 2×25 ml of 8M HNO_3 and again 10 ml of 9M HCl. All the solutions so far were rejected, and the Pu fraction was eluted to clean beakers using 40 ml of 9M HCl/ammonium iodide solution.

To collect fractions, 5 ml of conc. nitric acid was added, and they were evaporated to dryness. The residue was transferred into 1.5 ml Eppendorf vials using 3% HNO_3 solution spiked with approx. 2-3 mg of Fe in the form of Fe solution (ca. 100µl of $Fe(NO_3)_3$ solution in water). Ammonia was added to form $Fe(OH)_3$ precipitate (0.4 ml of conc. ammonia solution) and the samples were centrifuged using a micro-centrifuge. The supernatant was rejected, and the precipitate was washed with water and centrifuged again. The washed precipitate was dried at 80°C for a minimum of 4 hours, and the dry residue was transferred from the Eppendorf vials to porcelain or quartz crucibles and ignited at 800°C (approx. 100°C/hr ramp was used) for another 4 hours to form final Fe_2O_3. The produced Fe_2O_3 was transferred into clean Eppendorf vials and passed for AMS analysis at Lancaster University [113] [114].

6.3 Accelerator mass spectrometry results

The methods described above resulted in a measurement of the $^{244}Pu/^{239}Pu$ isotopic ratio of $(12.7 \pm 3.3) \times 10^{-5}$ for the 6 samples assessed in this stage of the research. This is statistically consistent with the global average taken from Lake Erie data of $(14.4 \pm 1.5) \times 10^{-5}$ and the measurement obtained of the entire sample set with the non-HF preparation, of $(11.8 \pm 1.0) \times 10^{-5}$. We note that the revised measurement is low relative to the global average as for the original measurement, indicating an excess of ^{239}Pu over ^{244}Pu in the ground relative to the global average and, whilst not statistically significant, the magnitude of the revised measurement is greater than that obtained with the non-HF preparation, i.e., $(11.8 \pm 1.0) \times 10^{-5} < (12.7 \pm 3.3) \times 10^{-5}$ which, is consistent with the hypothesis that a stubborn component of excess ^{244}Pu relative to ^{239}Pu was residing in the refractory phase, which the revised preparation has extracted.

6.4 Estimates of the local contribution to trace plutonium using the refractory-adjusted data

The relationship between local and global measurements to trace Pu in the environmental samples in terms of the $^{244}Pu/^{239}Pu$ isotopic ratio is given in the equation 5.4 as per:

$$F_L = 100 \times \left[\frac{R_{244/239} - R_{G\_244/239}}{R_{L\_244/239} - R_{G\_244/239}}\right] \tag{5.4}$$

where $R_{244/239}$ is the combined average of ^{244}Pu/^{239}Pu ratio measured in this work for Blelham Tarn and Fell Foot without the refractory adjustment at (11.8± 1.0) × 10^{-5}, $R_{G\_244/239}$ is the global average of ^{244}Pu/^{239}Pu at (14.4 ± 1.5) × 10^{-5}, reported by Wendel [4], and for the local contribution $R_{L\_244/239}$ as estimated for Sellafield by Steier at (3 × 10^{-6}) [5]. Furthermore, the local contributions of $F_{L_{239}}$ are shown in Table 22.

$\boldsymbol{R_{244/239}}$	$\boldsymbol{R_{L_{244/239}}}$	$\boldsymbol{F_{L_{239}}}$ **/ %**	$\boldsymbol{R_{240/239}}$	$\boldsymbol{R_{L_{240/239}}}$
$(11.8 \pm 1.0) \times 10^{-5}$	3×10^{-6}	18 ± 13	0.1813 ± 0.002	0.21 ± 0.03
$(13.6 \pm 6.5) \times 10^{-5}$	3×10^{-6}	6 ± 47	0.389 ± 0.006	0.27 ± 0.13
$(12.7 \pm 3.3) \times 10^{-5}$	3×10^{-6}	12 ± 14	0.389 ± 0.006	0.22 ± 0.03

Table 22: ^{244}Pu/^{239}Pu isotopic ratios for the original data as shown in the first row, refractory-adjusted data as shown in the second row, and the average of both.

6.5 Summary of the Revised Local Contribution Measurements

In the previous measurements we obtained 11.8 x 10^{-5} to give a local ^{239}Pu contribution of 18% and hence a $\boldsymbol{R_{L_{240/239}}}$estimate of 21%, that is higher than the global average.

The revised analysis with our MILEA has yielded a $\boldsymbol{R_{244/239}}$measurement of 13.6x 10^{-5} (therefore consistent with better extraction from the refractory residues although large errors) to yield 6% local contribution and an increase in $\boldsymbol{R_{L_{240/239}}}$ to 27% (strengthening the Magnox hypothesis). The large error derives from fewer samples being prepared with the HF), with the errors suggest consistency between with 11.8 and 13.6 measurements. The average of the two preparations yields a $\boldsymbol{R_{244/239}}$ measurement of 12.7x 10^{-5}, although they are effectively different samples, i.e., one with and one without the refractory contribution.

CHAPTER 7: CONCLUSIONS AND FUTURE WORK

7.1 Conclusion

This research has used the application of high resolution γ-ray Spectroscopy (HRGS). The investigation achieved useful information on ^{241}Am data for Blelham Tarn and Fell Foot samples, which was ^{241}Am peaks apparent across all samples and supported the calculation of the ^{241}Pu concentration.

Based on AMS, ^{239}Pu, ^{240}Pu, and ^{244}Pu abundances for the Blelham Tarn and Fell Foot samples are generally consistent with global fallout averages. The ^{240}Pu/^{239}Pu and ^{244}Pu/^{239}Pu isotopes ratio for both sides are consistent with the global fallout averages as well.

The results from this work show that a local source that contains 20% ^{240}Pu contributes to 18% of the trace plutonium in the environment at the study locations in the English Lake District. Based on ^{244}Pu and with no refractory extraction the percentage of ^{240}Pu is higher than the fallout average, but it is consistent with thermal spectrum fuel materials represented at Sellafield such as Magnox deposit (^{240}Pu/^{239}P=0.226 ± 0.001)

The proportions of ^{239}Pu were assessed to arise locally; in this work, 60% for the Salzburg samples by using the ^{244}Pu/^{239}Pu Erie Lake global average of Wendell $(14.4 \pm 1.5) \times 10^{-5}$. 73% for the Runit Island sample, this value is used for the local proportion $(R_{L_{240/239}})$ calculation with $R_{G_{240/239}}$= (0.176 ± 0.014), given ^{240}Pu/^{239}Pu = 0.02 ± 0.04 that is consistent with Pu weapons production range from (0.01 to 0.07) [115].

The depth dependence of trace environmental plutonium in English Lake District soils is consistent with the convection dispersion equation (CDE application), determined by a deposition era that corresponds with peak fallout in 1963. Two deposition components with distinct periods indicate the probability of local (Sellafield, Magnox deposit) and global fallout (nuclear weapons fallout in 1963) proportions of deposition at various times are found. The sampling times since dispersion are 30 years and 57 years. Furthermore, the dispersion and velocity coefficients are consistent with trace Pu in grassland by Zhang [96].

The revised analysis with our MILEA has yielded a $\boldsymbol{R_{244/239}}$ measurement of 13.6x 10^{-5} (therefore consistent with better extraction from the refractory residues although large errors) to yield a 6% local contribution and an increase in $\boldsymbol{R_{L_{240/239}}}$ to 27%. Whilst the errors suggest consistency between 11.8 and 13.6 measurements. The average of the two preparations has yielded a $\boldsymbol{R_{244/239}}$ measurement of 12.7x 10^{-5}.

Future work

Numerous investigations on soil sampling have shown that actinide abundance decreases with depth, but the literature is less comprehensive regarding the behaviour of actinides on soil surface . Further, increasing the number of samples would be better to understand the impact of the surrounding environment on the abundance of actinides.

Continue to modify our paper that was started in 2023 and includes the results that were obtained using HF dissolution and compare that with the HNO3 leaching data, to clarify that HNO3 leaching only gets "volatile" Pu in organic matter and on the surface of refractory particles, whereas the HF dissolution breaks down those refractory particles thereby liberating Pu from inside them as well as the volatile component.

Appendix (A)

1. Samples location Blelham Tarn and Fell Foot

Sample number	Blelham Tarn	Lake Windermere
Sample 1	54°24.006´N, -02°58.325´ W	54°16.271′ N, -02°57.398′ W
Sample 2	54°23.993´N, -02°58.421´ W	54°16.291′ N, -02°57.361′ W
Sample 3	54°23.960´N, -02°58.528´ W	54°16.318′ N, -02°57.321′ W
Sample 4	54°23.913´N, -02°58.607´ W	54°16.364′ N, -02°57.289′ W
Sample 5	54°23.882´N, -02 58.664´ W	54°16.454′ N, -02°57.202′ W
Sample 6	54°23.827´N, -02°58.954´ W	54°16.493′ N, -02°57.177′ W
Sample 7	54°23.801´N, -02 58.926´ W	54°16.544′ N, -02°57.121′ W
Sample 8	54°23.767´N, -02°58.991´ W	54°16.525′ N, -02°57.119′ W
Sample 9	54°23.627´N, -02°59.033´ W	54°16.499′ N, -02°57.110′ W
Sample 10		54°16.460′ N, -02°57.140′ W
Sample 11		54°16.448′ N, -02°57.118′ W
Sample 12		54°16.424′ N, -02°57.137′ W
Sample 13		54°16.409′ N, -02°57.139′ W
Sample 14		54°16.391′ N, -02°57.192′ W
Sample 15		54°16.369′ N, -02°57.182′ W

Table. 23: Location of the soil cores used in this study from Blelham Tarn and Lake Windermere (Cumbria UK).

Appendix (B)

2. BEGe detector characteristics used at the University of Liverpool

Specification of this detector

Model	BE2825
Cryostat model	7500SL
Preamplifier model	2002 CSI

Physical characteristics

Active Diameter	61 mm	Distance from window (outside)	5 mm
Active area	2800 mm²	window thickness	0.6 mm
Thickness	25.5 mm	window material	carbon Epoxy

Electrical characteristics

Depletion voltage	(+) 3500	Vdc
Recommended bias voltage vdc	(+) 4000	Vdc
Reset rate at recommended bias	/	sec (PO preamp only)
Preamplifier test point voltage at recommended bias	-0.3	vdc (RC preamp only)

Resolution and Efficiency

With amp time constant of 4 µs - 7.2 µs Rise time 0.8 µs flat Top

Isotope	**Fe-55**	**Co-57**	**Co-60**
Energy (KeV)	5.9	122	1332.5
FWHM (ev)	348	579	1723
FWTM (ev)			3172

Appendix (C)

3.Marinelli calibration resource NPRL 664

COMPOSITION OF MULTINUCLEAR SOURCE [16]

Etalon Multi-Gamma in Resin 250ml Marinelli flask

(TYPE 12ML01EGRM15 REFERENCE NO. 82361B/1)

Reference Date: 13th November 2019 at 12h UTC

Radioisotope	**Gamma-ray energy KeV)**	**Activity (K Bq)**	**Gamma Fraction**
Am-241	59.5	0.887	35.9
Cd-109	88.0	8.35	3.7
Co-57	122.1	0.433	85.6
Ce-139	165.9	0.543	80.0
Cr-51	320.1	9.28	9.9
Sn-113	391.7	0.856	65.0
Sr-85	514.0	1.378	96.0
Cs-137	661.7	2.131	85.1
Mn-54	834.8	2.200	100
y-88	898.0	2.57	93.7
Zn-65	1115.5	6.19	50.0
Co-60	1173.2	3.34	99.9
Co-60	1332.5	3.34	100
Y-88	1836.1	2.57	99.2

Table 24: The energy range of the Marinelli calibration source NPRL 664 between 59.5 keV (^{241}Am) and 1835.9 keV (^{88}Y).

Appendix (D)

4.Output file of detector efficiency in different energy regions from Liverpool University using LabSOCS

```
keV_eff_%err_effw_%cnvrg(i)_%cnvrg(i-1) _pntsN:   45.00  3.04702e-02  15.0  1.22845e+01
0.078043  -0.364877    2993
keV_eff_%err_effw_%cnvrg(i)_%cnvrg(i-1) _pntsN:   60.00  3.37142e-02  10.0  1.35924e+01
0.073627  -0.342858    2993
keV_eff_%err_effw_%cnvrg(i)_%cnvrg(i-1) _pntsN:   80.00  3.81706e-02  10.0  1.53891e+01
0.089168  -0.304347    2993
keV_eff_%err_effw_%cnvrg(i)_%cnvrg(i-1) _pntsN:  129.00  4.16385e-02  10.0  1.67872e+01
0.112394  -0.239322    2993
keV_eff_%err_effw_%cnvrg(i)_%cnvrg(i-1) _pntsN:  150.00  3.97147e-02  10.0  1.60116e+01
0.118738  -0.226279    2993
keV_eff_%err_effw_%cnvrg(i)_%cnvrg(i-1) _pntsN:  200.00  3.31804e-02   8.0  1.33772e+01
0.121367  -0.200230    2993
keV_eff_%err_effw_%cnvrg(i)_%cnvrg(i-1) _pntsN:  300.00  2.25977e-02   8.0  9.11061e+00
0.122181  -0.180135    2993
keV_eff_%err_effw_%cnvrg(i)_%cnvrg(i-1) _pntsN:  500.00  1.34094e-02   6.0  5.40623e+00
0.130340  -0.168160    2993
keV_eff_%err_effw_%cnvrg(i)_%cnvrg(i-1) _pntsN:  700.00  9.74139e-03   6.0  3.92739e+00
0.122897  -0.155551    2993
keV_eff_%err_effw_%cnvrg(i)_%cnvrg(i-1) _pntsN: 1000.00  7.07617e-03   4.0  2.85287e+00
0.120035  -0.148076    2993
keV_eff_%err_effw_%cnvrg(i)_%cnvrg(i-1) _pntsN: 1400.00  5.29801e-03   4.0  2.13597e+00
0.126808  -0.140598    2993
keV_eff_%err_effw_%cnvrg(i)_%cnvrg(i-1) _pntsN: 2000.00  3.85357e-03   4.0  1.55363e+00
0.119382  -0.137136    2993
```

Appendix (E)

5.Output file of detector efficiency in different energy regens from CCFE

SGI_template: CIRCULAR_PLANE						
ISOCS_file_name: SoilSample.gis						
Detector_name: B13135						
Collimator_name: no_collimator						
Convrgence_ [%]: 1.0000						
Test_description: SOIL_SAMPLE						
Comment:						
Date_Time: Tue_Feb__8_11:57:57_2022						
Source_area_cm2: 5.66116e+1						
Source_grams: 7.24628e+1						
keV_eff_%err_effw_%cnvrg(i)_%cnvrg(i-1) _pntsN: 45.00 1.03579e-1 15.0						
keV_eff_%err_effw_%cnvrg(i)_%cnvrg(i-1) _pntsN: 60.00 1.30236e-1 10.0						
keV_eff_%err_effw_%cnvrg(i)_%cnvrg(i-1) _pntsN: 80.00 1.41241e-1 10.0						
keV_eff_%err_effw_%cnvrg(i)_%cnvrg(i-1) _pntsN: 100.00 1.41528e-1 10.						
keV_eff_%err_effw_%cnvrg(i)_%cnvrg(i-1) _pntsN: 150.00 1.23030e-1 10.0						
keV_eff_%err_effw_%cnvrg(i)_%cnvrg(i-1) _pntsN: 200.00 9.86801e-2 8.						
keV_eff_%err_effw_%cnvrg(i)_%cnvrg(i-1) _pntsN: 300.00 6.53970e-2 8.0						
keV_eff_%err_effw_%cnvrg(i)_%cnvrg(i-1) _pntsN: 500.00 3.81339e-2 6.0						
keV_eff_%err_effw_%cnvrg(i)_%cnvrg(i-1) _pntsN: 700.00 2.73367e-2 6.						
keV_eff_%err_effw_%cnvrg(i)_%cnvrg(i-1) _pntsN: 1000.00 1.96143e-2 4.						
keV_eff_%err_effw_%cnvrg(i)_%cnvrg(i-1) _pntsN: 1400.00 1.45066e-2 4.						
keV_eff_%err_effw_%cnvrg(i)_%cnvrg(i-1) _pntsN: 2000.00 1.04401e-2 4.0						

Appendix (F)

6.Liverpool, CCFE and Michel activities data in terms of Bq per g

A)

Liverpool data	Net Area Count	Error	Activity (Bq/g)	Error
1	2152	80	0.00028	1E-05
2	1455	75	0.00030	1E-05
3	1797	77	0.00030	1E-05
4	2602	82	0.00031	2E-05
5	2763	83	0.00025	2E-05
6	1288	74	0.00024	1E-05
7	3004	85	0.00025	2E-05
8	2455	82	0.00030	2E-05
9	1588	76	0.00019	1E-05
Average			0.00027	5E-06
Uncertainty			0.00001	

B)

Culham data	Net counts	Error	Activity (Bq/g)	Error
1	499	27	0.00027	2E-05
2	474	26	0.00028	2E-05
3	451	26	0.00024	2E-05
4	549	28	0.00030	2E-05
5	569	28	0.00028	2E-05
6	402	25	0.00019	2E-05
7	472	26	0.00030	2E-05
8	655	30	0.00027	2E-05
9	471	26	0.00023	2E-05
Average			0.00026	6E-06
Uncertainty			0.00001	

C)

Michel data				
	Activity (Bq/m2)	Error	Activity (Bq/g)	
1	33	3	0.00022	2E-05
2	29	3	0.00019	2E-05
3	27	3	0.00018	2E-05
4	49	4	0.00033	3E-05
5	50	4	0.00033	3E-05
6	18	2	0.00012	1E-05
7	52	4	0.00035	3E-05
Average			0.00025	7E-06
Uncertainty			0.00003	

Table 25: ^{241}Am activity (Bq/g) in Blelham Tarn cores for Liverpool University (A), Culham Science Centre (B) and Michel data (C).

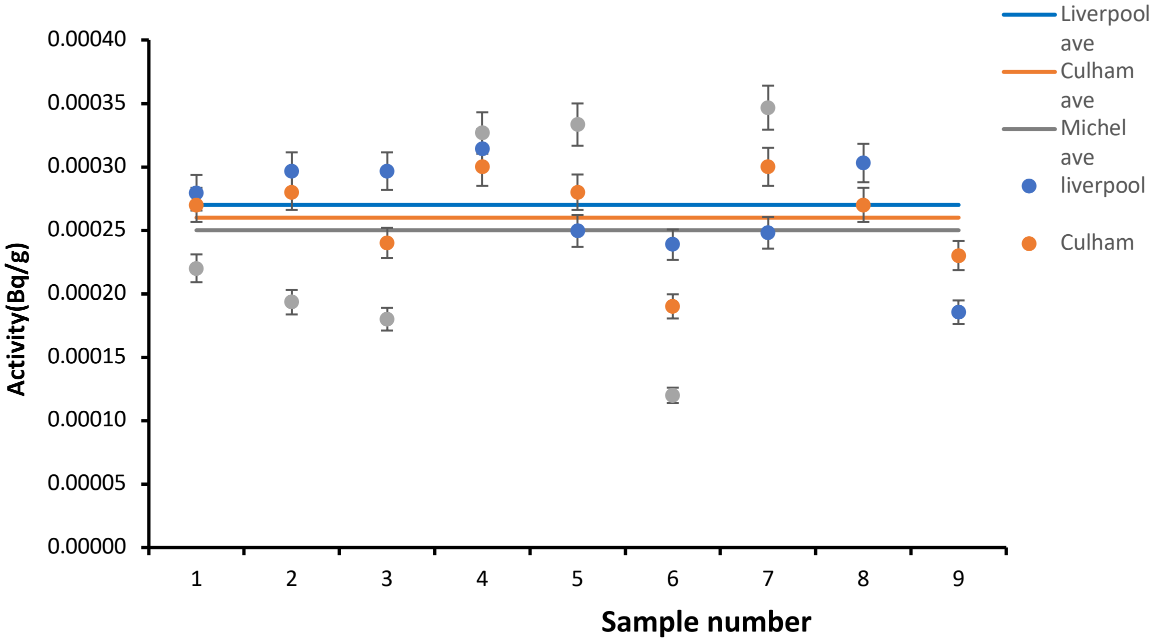

Figure 53: Comparison of ^{241}Am abundance for this work with Michel's study.

Appendix (G)

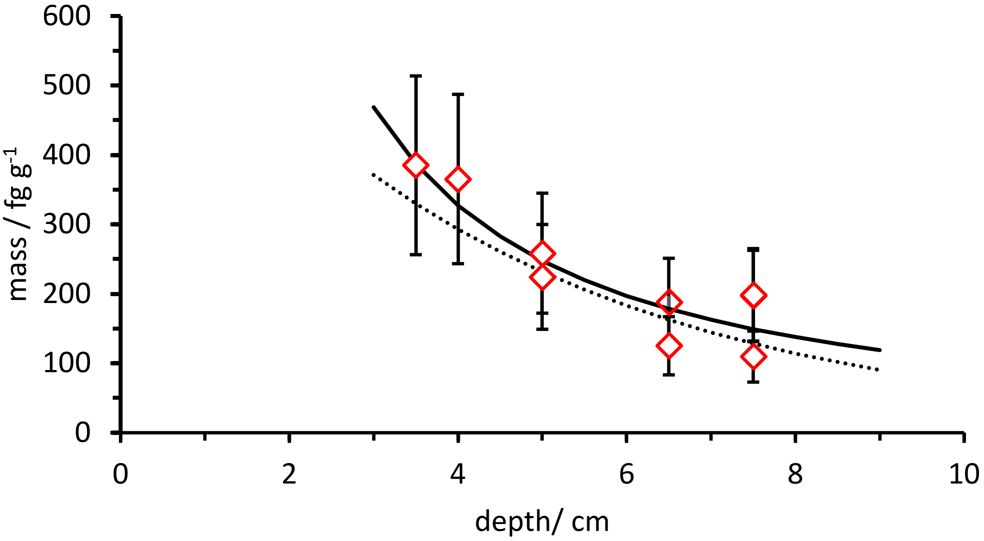

Figure 54: Mass concentration of ^{239}Pu/fg g^{-1} versus depth/cm for Blelham Tarn (red diamond) with corresponding fits to Blelham Tarn from the equation. 4.1 (solid black line) and from the equation.4.4.2 (dotted black line).

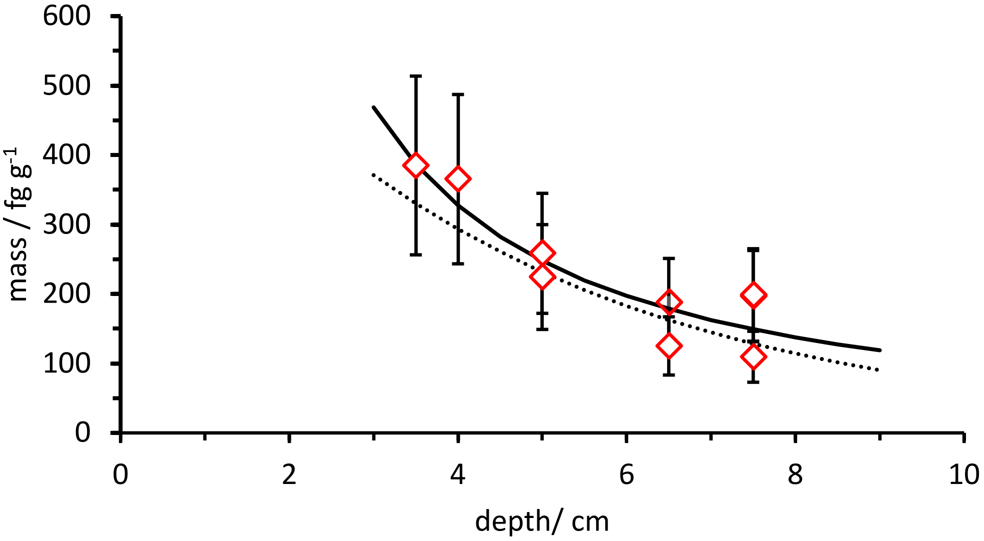

Figure 55: Mass concentration of ^{239}Pu/fg g^{-1} versus depth/cm for Blelham Tarn (red diamond) with corresponding fits to Blelham Tarn from the equation. 4.1 (solid black line) and from the equation.4.4.2 (dotted black line).

REFERENCES

[1] H. Michel et al., “Plutonium and americium inventories in atmospheric fallout and sediment cores from Blelham Tarn, Cumbria (UK)”. Journal of Environmental Radioactivity, 59(2), 127-137, 2002. https://doi.org/10.1016/S0265-931X(01)00039-X

[2] J. M. Kelley et al., “Global distribution of Pu isotopes and 237Np”, *Sci. Total Environ.* 237/238, pp. 483-500, 1999. doi.org/10.1016/S0048-9697(99)00160-6

[3] L. W. Green, F. C. Miller, J. A. Sparling, and S. R. Joshi, “Determination of plutonium 240/239 ratios in Lake Ontario sediments,” *J. Am. Soc. Mass Spectrom.*, vol. 2, no. 3, pp. 240–244, May 1991, doi: 10.1016/1044-0305(91)80050-H.

[4] C. C. Wendel et al., “Long-range tropospheric transport of uranium and plutonium weapons fallout from Semipalatinsk nuclear test site to Norway”. Environ Int. Sep; 59. pp. 92-102, 2013.

[5] P. Steier et al. “Ams of the minor plutonium isotopes”. Nuclear inst and methods in physics research b.:160-164. doi: 10.1016/j.nimb.2012.06.017.

[6] T. Hamilton et al. "Frequency distribution, isotopic composition and physical characterization of plutonium-bearing particles from the Fig-Quince zone on Runit Island, Enewetak Atoll." *Journal of radioanalytical and nuclear chemistry* 242 (2022).

[7] JA. Corcho, et al. "Isotopic signatures of plutonium and uranium at Bikar atoll, northern Marshall Islands." *Journal of Environmental Radioactivity* 242 (2022): 106795.

[8] BBC News, 9th July 2017, ‘Unesco awards Lake District World Heritage site status’, https://www.bbc.co.uk/news/uk-england-cumbria-40547691

[9] Sites of Special Scientific Interest (SSSIs), UK Environmental Law Association 2008-2017. http://www.environmentlaw.org.uk/rte.asp?id=303.

[10] S.C. Maberly et al., “From Ecological Informatics to the Generation of Ecological Knowledge: Long-Term Research in the English Lake District”. In: Recknagel, F., Michener, W. (eds) Ecological Informatics. Springer, Cham, 2018 https://doi.org/10.1007/978-3-319-59928-1_21

[11] M. J Joyce et al., “Searching for zero plutonium in the far north of Scotland. Actinide Research Quarterly”, (Third Quarter), 27-31, 2019.

[12] J. Gray et al., “Discharges to the Environment from the Sellafield Site”. Journal of Radiological Protection, vol. 2.: pp. 99–131, 1995.

[13] W. L Masterton et al., “Chemistry: Principles and Reactions”, 2 Edition, Saunders College Publishing, New York, 1993.

[14] J. J. Katz et al., “The Chemistry of Actinide Elements & Co. Ltd., London” 1957. https://doi.org/10.1002/ange.19590710318

[15] J. Westrum et al., "The Preparation and Some Properties of Americium Metal1" Journal of the American Chemical Society, vol. 73, no. 7, PP: 3396-3398, 1951.

[16] C. Scheib et al., "Geological controls on radon potential in England", Proceedings of the Geologists' Association, vol. 124, no. 6, pp: 910-928, 2013.

[17] British Geological Survey., “Mineral Profile: Uranium”, Mar. 2010.

[18] E.P. Hardy., “Global inventory and distribution of fallout plutonium”, *Nature* 241, pp. 444-445, 1973.

[19] W. Thorsten., "High-Precision isotope ratio measurements of Uranium and Plutonium in the environment", PhD thesis, University of Southampton, 2002.

[20] Nuclear Forensic Search Project., http://metadata.berkeley.edu/nuclear-forensics/ from Wikimedia Common.

[21] B. Oleg., "Securing Russia's HEU stocks", Science & Global Security, 7:3, pp. 311-331, 1998. DOI: 10.1080/08929889808426464

[22] C. C. Wendel et al., "Long-range tropospheric transport of uranium and plutonium weapons fallout from Semipalatinsk nuclear test site to Norway". Environ Int. Sep; 59. pp. 92-102, 2013.

[23] S. Winkler., "Accelerator mass spectrometry of heavy radionuclides with special focus on 182Hf", [PhD-thesis. Canberra] 2007.

[24] H. Diamond et al., "Heavy Isotope Abundance in the Mike Thermonuclear Device". *Ph\s. Rev.,* 119(6): pp. 2000-2004, 1960.

[25] A. Burrows et al., "A new mechanism for core-collapse supernova explosions". *Ap. J.,* 640: pp. 878-890, 2006.

[26] M.R. Scott et al., "Transport and deposition of plutonium in the ocean: evidence from Gulf of Mexico sediments", Earth Planet. Sci. Lett. 63, pp. 202-222, 1983.

[27] K. O. Buesseler et al., "The isotopic signature of fallout plutonium in the North Pacific", J. Environ. Radioactivity 36, pp. 69-83, 1997.

[28] P.W. Krey et al., "Atmospheric burnup of the Cosmos-954 reactor", *Science* 105, pp. 583-585, 1979.

[29] A. Makhijani et al., Nuclear Wastelands, The MIT Press, Cambridge, Massachusetts, USA, 1995.

[30] W. Thorsten. “High-Precision isotope ratio measurements of Uranium and Plutonium in the environment”. PhD thesis, University of Southampton, 2002.

[31] J. S. Oh. “The migration and accumulation of radionuclides in the Ravenglass saltmarsh”, University of Southampton, [PhD-thesis, Cumbria], 1999.

[32] K.E Sampson et al., “The determination of ^{240}Pu/^{239}Pu atomic ratios and 237Np concentrations within marine sediments”, Radionuclides in the study of marine processes, pp. 177-186, 1991.

[33] N. Momoshima et al., “Identification of the contamination source of plutonium in environmental samples with isotopic ratios determined by inductively coupled plasma mass spectrometry and alpha spectrometry”, J. Radioanal. Nucl. Chem. 221, pp. 213-217, 1997.

[34] DEEML, “Surface Air Sampling Program",2000 Available from: *http://www.eml.doe.gov/databases/sasp/*.

[35] D. Arnold D et al., “Die $^{(239+240)}$ Pu Aktivitäetskonzentrationen in der bodennahen Luft Norddeutschlands von 1963 bis 1997”, Strahlenschutz Praxis 2, pp. 25-27, 1999.

[36] K. Irlweck. And J. Wicke., “Isotopic composition of plutonium immissions in Austria after the Chernobyl accident”. Journal of radioanalytical and nuclear chemistry, 227(1-2), pp.133-136, 1998

[37] M. Clark, F. Smith., “Wet and dry deposition of Chernobyl releases”. Nature **332**, 245–249, 1988, https://doi.org/10.1038/332245a0

[38] The Nuclear Energy Agency (NEA), “Chernobyl Ten years on”, Radiological and Health Impact, 1995.

[39] G. H Hall et al., “A survey of the limnological characteristics of the lakes of the English Lake District: The Lakes Tour 1995. Report to the Environment Agency”, Northwest Region, 1996.

[40] P. A. Cawse., 1983. Ecological Aspects of Radionuclides Release. Blackwell, Oxford, p.47, 1983.

[41] T. O&rsquo., "The depositional environments and structures of the Borrowdale Volcanic Group and the Windermere Supergroup in the Southern Lake District, England", Hdl.handle.net.

[42] H.L Moorhouse et al., Regional versus local drivers of water quality in the Windermere catchment, Lake District, United Kingdom: The dominant influence of wastewater pollution over the past 200 years. Global change biology, 24(9), pp.4009-4022, 2018.

[43] A. M. Müller et al., “Competitive 10be Measurements below 1 Mev with the Upgraded Eth-Tandy Ams Facility.” Nuclear Inst. and Methods in Physics Research B 2010 pp. 2801–2807. https://doi.org/10.1016/j.nimb.2010.05.104

[44] J. H. Harley., “Plutonium in the environment-a review”, J. Radiation Res. Vol. 21, pp. 83-104, 1980.

[45] M. E. Ketterer et al. “Resolving Chernobyl Vs. Global Fallout Contributions in Soils from Poland Using Plutonium Atom Ratios Measured by Inductively Coupled Plasma Mass Spectrometry.” Journal of Environmental Radioactivity pp. 183–201. 2003, https://doi.org/10.1016/j.jenvrad

[46} M. Srncik., et al. "Vertical distribution of ^{238}Pu, $^{239(40)}$ Pu, ^{241}Am, ^{90}Sr and ^{137}Cs in Austrian soil profiles" *Radiochemical Acta*, vol. 96, no. 9-11, 2008, pp. 733-738. https://doi.org/10.1524/ract.2008.1559

[47] S. F. Boulyga., et al. "Depth profiling of Pu, 241 Am and 137 Cs in soils from southern Belarus measured by ICP-MS and α and γ spectrometry." *Journal of Environmental Monitoring* 5.4 (2003): 661-666. https://doi.org/10.1039/B303621A

[48] H. Zhang et al., "Determination of ^{241}Am in Environmental Samples": A Review. *Molecules***2022**, *27*, 4536. https://doi.org/10.3390/molecules27144536

[49] J. A. Corcho Alvarado., et al. "Determining ^{241}Pu in environmental samples: case studies in alpine soils" Radiochemical Acta, vol. 99, no. 2, 2011, pp. 121-129. https://doi.org/10.1524/ract.2011.1803

[50] D. Ray et al. "Controls on anthropogenic radionuclide distribution in the Sellafield-impacted Eastern Irish Sea", Science of The Total Environment, Volume 743,2020, 140765, ISSN 0048-9697, https://doi.org/10.1016/j.scitotenv.2020.140765.

[51] T. Ikäheimonen., "Measurement of 241 Pu in environmental samples." Journal of Radioanalytical and Nuclear Chemistry243.2 (2000): 535-541.

[52] M. Yamamoto., et al. "Plutonium Isotopies Composition in Soil from the Former Semipalatinsk Nuclear Test Site." *Radiochimica Acta* 72.4 (1996): 209-216. https://doi.org/10.1524/ract.1996.72.4.209

[53] J. Lachner and Marcus Christl et al. "Isotopic signature of plutonium at Bikini Atoll, Applied Radiation and Isotopes", Volume 68, Issue 6,2010, Pages 979-983, ISSN 0969-8043, https://doi.org/10.1016/j.apradiso.2010.01.043.

[54] Sites of Special Scientific Interest (SSSIs), UK Environmental Law Association 2008-2017. http://www.environmentlaw.org.uk/rte.asp?id=303.

[55] J. Soares da Silva Burato et al., "Recent advances and trends in miniaturized sample preparation techniques", Journal of Separation Science, vol. 43, no. 1, pp. 202-225, 2019. Available: 10.1002/jssc.201900776.

[56] S. Cengiz et al., “SEM-EDS analysis and discrimination of forensic soil”. Forensic Science International, 141(1),33-37,2004. https://doi.org/10.1016/j.forsciint.2003.12.006

[57] Atlas TM Manual 15Ton (15T) and 25Ton (25T) Hydraulic Press User Manual from Specac. MANUALLY OPERATED HYDRAULIC PRESS, (15 AND 25 TON). www.specac.com.

[58] JEOLO(UK), (SEM) of JEOL 6010-LV (JEOL (UK) Ltd., Herts, UK) applications training for a wide variety of scanning electron microscopes (SEM), scanning probe microscopes. https: www.jeoluk.com.

[59] H. Khan et al., "Experimental methods in chemical engineering: X-ray diffraction spectroscopty— XRD", The Canadian Journal of Chemical Engineering, vol. 98, no. 6, pp. 1255-1266, 2020.

[60] M. Khandaker, "High purity germanium detector in gamma-ray spectrometry", International Journal of Fundamental Physical Sciences, vol. 1, no. 2, pp. 42-46, 2011. Available: 10.14331/ijfps.2011.330011.

[61] MIRION TECHNOLOGIES, “Gamma Spectroscopy Software”, 2020.

[62] High-Resolution Gamma Spectroscopy Section. MSc Radiometric Development recourse, Liverpool University, 2015.

[63] MIRION TECHNOLOGIES., “Broad Energy Germanium Detectors from Canberra, (BEGe). 2020.

[64] M. Korun et al., ‘Evaluation of gamma-ray spectrometric results near the decision threshold’, App. Rad. Isot. 73 pp. 1 (2013).

[65] MIRION TECHNOLOGIES., “LabSOCS correction software for efficiency calibration”, 2020.

[66] T. E. Sampson., “Plutonium isotopic composition by gamma-ray spectroscopy”: a review, Los Alamos National Laboratory, 1986.

[67] B. Denecke., “Measurement of the 59.5-keV gamma-ray emission probability in the decay of ^{241}Am with a 4π-CsI(T1) - sandwich spectrometer”. Volume 38, issue 10,1987, pages 823-830, (2002).

[68] H. Bateman., “The solution of a system of differential equations occurring in the theory of radioactive transformations. In Proc”. Cambridge Philos. Soc (Vol. 15, No. pt V, pp. 423–427), 1910.

[69] J. Cetnar., 2006. “General solution of Bateman equations for nuclear transmutations. Annals of Nuclear Energy, 33(7), pp.640-645, 2006. https://doi.org/10.1016/j.anucene.2006.02.004.

[70] H. Bateman, “Solution of a system of differential equations occurring in the theory of radioactive transformation,” Proc. Cambridge Philos. Soc. **15**, 423–427 (1910).

[71] M. Joyce.,” Nuclear Engineering: A Conceptual Introduction to Nuclear Power”., Netherlands: Elsevier Science, (2017).

[72] L. John., “Erring with high-level nuclear waste disposal: a case study of the precautionary principle, International Journal of Environmental Studies”,58:5, 549-583, 2001, DOI: 10.1080/00207230108711351

[73] S. Liu, "Radiocarbon Sample Preparation Based on The Flam-Sealed Zn/Fe Reduction Method in Accelerator Mass Spectrometry Analysis", Atomic Spectroscopy, vol. 43, no. 05, 2022.

[74] C. Tighe et al., 'Bespoke analysis of soil in a high uranium background for identification of trace plutonium in decommissioning applications', PhD, Lancaster University: Lancaster University, 2020. 141 p. https://doi.org/10.17635/lancaster/thesis/918

[75] E. Chamizo et al., "Analysis of 236U and plutonium isotopes, 239,240Pu, on the 1 MV AMS system at the Centro Nacional de Accelerators, as a potential tool in oceanography". Nuclear Instruments and Methods in Physics Research Section B: Beam Interactions with Materials and Atoms, 361, 535-540, 2015. https://doi.org/10.1016/j.nimb.2015.02.066.

[76] A. Sekiguchi et al., "First results on 236U levels in global fallout. Science of The Total Environment", 407(14),4238-4242,2009. https://doi.org/10.1016/j.scitotenv.2009.01.058

[78] T. Semkow et al., "Chi-Square Distribution: New Derivations and Environmental Application", Journal of Applied Mathematics and Physics, vol. 07, no. 08, pp. 1786-1799, 2019.

[79] A. Kadhim and A. Abdalhameed, "A hybrid feature selection technique using chi-square with genetic algorithm", 2022 Muthanna International Conference on Engineering Science and Technology (MICEST), 2022.

[80] Y. Yuan et al., "Calculation of deception probability of netted radar based on non-central chi-square distribution", International Journal of Distributed Sensor Networks, vol. 17, no. 7, p. 155014772110337, 2021.

[81] raystuckey1., “Chi-Squared Distribution Calculator-GeoGebra : https://www.geogebra.org/, 2021.

[82] G.J. Feldman and R.D Cousins., “Unified approach to the classical statistical analysis of small signals”. *Physical Review D*, *57*(7), p.3873. (1998).

[83] C. Tighe et al. Local and global trace plutonium contributions in fast breeder legacy soils. Nat Commun. 2021 Mar 19;12(1):1381. doi: 10.1038/s41467-021-21575-9. PMID: 33741911; PMCID: PMC7979690.

[84] T. Hamilton et al. "Frequency distribution, isotopic composition and physical characterization of plutonium-bearing particles from the Fig-Quince zone on Runit Island, Enewetak Atoll." *Journal of radioanalytical and nuclear chemistry* 242 (2022).

[85] JA. Corcho, et al. "Isotopic signatures of plutonium and uranium at Bikar atoll, northern Marshall Islands." *Journal of Environmental Radioactivity* 242 (2022): 106795.

[86] M. Srncik., et al. "Vertical distribution of ^{238}Pu, $^{239(40)}$ Pu, ^{241}Am, ^{90}Sr and ^{137}Cs in Austrian soil profiles" *Radiochemical Acta*, vol. 96, no. 9-11, 2008, pp. 733-738. https://doi.org/10.1524/ract.2008.1559

[87] C. Kim., et al. "Distribution and behaviour of 99 Tc, 237 Np, 239,240 Pu, and 241 Am in the coastal and estuarine sediments of the Irish Sea." Journal of radioanalytical and nuclear chemistry 156.1 (1992): 201-213.

[88] T. Ikäheimonen., "Measurement of 241 Pu in environmental samples." Journal of Radioanalytical and Nuclear Chemistry243.2 (2000): 535-541.

[89] P.J. Kershaw, et al., The measurement of the isotopic composition of plutonium in an Irish Sea sediment by mass spectrometry. Journal of Radioanalytical and Nuclear Chemistry, Articles **198**, 113–124 (1995). https://doi.org/10.1007/BF02038249

[90] F. Livens., “Controls on anthropogenic radionuclide distribution in the Sellafield-impacted Eastern Irish Sea”. Science of The Total Environment, 743, 140765 (2020). https://doi.org/10.1016/j.scitotenv.2020.140765

[91] J. A. Corcho Alvarado., et al. "Determining ^{241}Pu in environmental samples: case studies in alpine soils" Radiochemical Acta, vol. 99, no. 2, 2011, pp. 121-129. https://doi.org/10.1524/ract.2011.1803

[92] S. F. Boulyga., et al. "Depth profiling of Pu, 241 Am and 137 Cs in soils from southern Belarus measured by ICP-MS and α and γ spectrometry." *Journal of Environmental Monitoring* 5.4 (2003): 661-666. https://doi.org/10.1039/B303621A

[93] I. Wästerlund., “Impacts of soil disturbance on forest and forest soils”, Soil and root damage in forestry, Ch. 2 (2020) 23-45, Elsevier, ISBN: 978-0-12-822070-2.

[94] H. Zhang et al., “Determination of ^{241}Am in Environmental Samples”: A Review. *Molecules***2022**, *27*, 4536. https://doi.org/10.3390/molecules27144536

[95] P. Bossew P, Kirchner G. Modelling the vertical distribution of radionuclides in soil. Part 1: the convection-dispersion equation revisited. J Environ Radioact. 2004;73(2):127-50. PMID: 15023444. doi: 10.1016/j.jenvrad.2003.08.006

[96] W. Zhang., et al. "Distribution and migration of 239,240 Pu in soil profiles in North China." *Science of the Total Environment* 857 (2023): https://doi.org/10.1016/j.scitotenv.2022.159471

[97] P. R. Bevington and D. K. Robinson., “Data reduction and error analysis for the Physical Sciences”, McGraw-Hill Education.2nd Ed., ***ISBN*** 13: ***9780079112439***.

[98] T. R. Grapes et al., (2006) Hydrodynamics of flood plain wetlands in a chalk catchment: The River Lambourn, UK. J. Hydro. 320(3–4), (2006) 324–341.

[99] D. Curtis, J, “Nature’s uncommon elements: Plutonium and technetium,” 1999.

[100] L. W. Green et al , “Determination of plutonium 240/239 ratios in Lake Ontario sediments,” *J. Am. Soc. Mass Spectrom.*, vol. 2, no. 3, pp. 240–244, May 1991, doi: 10.1016/1044-0305(91)80050-H.

[101] S. Salmani-Ghabeshi et al, “Presence of 236 U and 239,240 Pu in soils from Southern Hemisphere,” *J. Environ. Radioact.*, vol. 192, pp. 478–484, 2018, doi: 10.1016/j.jenvrad.2018.08.003.

[102] C. R. Armstrong et al , “Plutonium Isotopes in the Terrestrial Environment at the Savannah River Site, USA: A Long-Term Study,” *Environ. Sci. Technol.*, vol. 49, no. 3, pp. 1286–1293, 2015, doi: 10.1021/es504147d.

[103] Y. Muramatsu et al., "Plutonium Isotopies Composition in Soil from the Former Semipalatinsk Nuclear Test Site" *Radiochemical Acta*, vol. 72, no. 4, 1996, pp. 209-216. https://doi.org/10.1524/ract.1996.72.4.209F.

[104] F. Quinto et al., “Determination of 239Pu, 240Pu, 241Pu and 242Pu at femtogram and attogram levels – evidence for the migration of fallout plutonium in an ombrotrophic peat bog profile,” *Environ. Sci. Process. Impacts*, vol. 15, no. 4, p. 839, 2013, doi: 10.1039/c3em30910j.

[105] Y. Muramatsu et al., “Measurement of 240Pu/239Pu isotopic ratios in soils from the Marshall Islands using ICP-MS”. Sci Total Environ. 2001 Oct 20;278(1-3):151-9. doi: 10.1016/s0048-9697(01)00644-1. PMID: 11669263.

[106] C. R Armstrong., et al. "Anthropogenic plutonium-244 in the environment: Insights into plutonium’s longest-lived isotope." *Scientific Reports* 6.1 (2016): 1-8.

[107] Y. Muramatsu et al. "Determination of plutonium concentration and its isotopic ratio in environmental materials by ICP-MS after separation using and extraction chromatography." Journal of Analytical Atomic Spectrometry14.5 (1999): 859-865

[108] L. W. Cooper., et al. "Sources of the transuranic elements plutonium and neptunium in arctic marine sediments." Marine Chemistry 69.3-4 (2000): 253-276.

[109] M. Srncik et al., “Determination of U, Pu and Am isotopes in Irish Sea sediment by a combination of AMS and radiometric methods”. *Journal of environmental radioactivity*, *102*(4), 331–335 (2011). https://doi.org/10.1016/j.jenvrad.2011.01.004

[110] K. O. Buesseler. "The isotopic signature of fallout plutonium in the North Pacific." *Journal of Environmental Radioactivity*36.1 (1997): 69-83.

[111] T. M. Beasley., et al. "Isotopic Pu, U, and Np signatures in soils from Semipalatinsk-21, Kazakh Republic and the southern Urals, Russia." *Journal of environmental radioactivity*39.2 (1998): 215-230.

[112] D. G. Pomfret., "Safety and dose management during decommissioning of a fire damaged nuclear reactor." *Safety*2.2 (2000): 5-299.

[113] J. W. Mietelski, P. Gaca, M.A. Olech Radioactive contamination of lichens and mosses collected in South Shetlands and Antarctic Peninsula, Journal of Radioanalytical and Nuclear Chemistry, Vol. 245, No.3 (2000) 527-537,

[114] P. E. Warwick, I. W. Croudace, J.- S. Oh Radiochemical determination of ^{241}Am and Pu(α) in environmental materials, Anal. Chem. 2001, 73, 3410-3416.

[115] W. Thorsten Warneke et al., “A new ground-level fallout record of uranium and plutonium isotopes for northern temperate latitudes Earth and Planetary Science Letters, Volume 203, Issues 3–4,2002, Pages 1047-1057, ISSN 0012-821X, https://doi.org/10.1016/S0012-821X(02)00930-5.